Universidade do Minho
Escola de Engenharia

Salomé Carneiro Neto de Nóbrega Luís

Using elastin-like recombinamers as scaffolds for tissue engineering and regenerative medicine in the context of skin regeneration

outubro 2022

Using elastin-like recombinamers as scaffolds for tissue engineering and regenerative medicine in the context of skin regeneration

Salomé Carneiro Neto de Nóbrega Luís

UMINHO | 2022

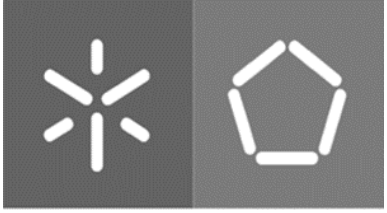

Universidade do Minho
Escola de Engenharia

Salomé Carneiro Neto de Nóbrega Luís

Using elastin-like recombinamers as scaffolds for tissue engineering and regenerative medicine in the context of skin regeneration

Dissertação de Mestrado

Mestrado Integrado em Engenharia Biomédica

Ramo de Biomateriais, Reabilitação e Biomecânica

Trabalho realizado sob a orientação do

Doutor Artur Jorge Araújo Magalhães Ribeiro

outubro 2022

COPYRIGHTS AND TERMS OF USE OF WORK BY THIRD PARTIES

ACKNOWLEDGEMENTS

This dissertation could not have been completed without the cooperation and assistance of several entities, which I will highlight below.

First and foremost, I would like to thank my supervisor, Doctor Artur Ribeiro for agreeing to join me on this adventure, for aligning my professional goals with an ambitious project, and for motivating me to be a professional of excellence.

I would also like to express my deepest gratitude to Professor José Carlos Rodríguez Cabello for allowing me to develop part of this project at Technical Proteins NanoBiotechnology, S.L. during my ERASMUS traineeship (Financial Agreement 2020-1-PT01-KA103-077707). This adventure would not have been possible without the support of the Bioforge team (Group of Advanced Materials and Nanobiotechnology), particularly of PhD candidate Diana Juanes, who always clarified my doubts and piqued my curiosity, and research assistant Rocío Lera, who not only assisted me but also served as a professional role model for me to emulate.

Furthermore, I acknowledge the Technical Proteins NanoBiotechnology, S.L. team's guidance, particularly PhD candidate Federica Sallustio's teachings and advice, and thank Daniela Guerra, Desiré Bustos and Sara Anzola for all of the laughs and adventures we shared over lunch.

I would also like to express my gratitude to the Bioprocess and Bionanotechnology Research Group team for their sound advice and willingness to teach whenever I needed it. I would especially like to thank Doctor André da Costa for his support, for sharing his knowledge and encouraging me to be more critical.

Furthermore, I want to recognize and thank my parents for their important role in my life's success, not only as a safe haven, but also for constantly challenging me to grow. I thank my brother for his faith in me and the security he has provided.

It is inexplicable how much I needed you to accomplish my goals, Duarte and my friends who make me sun. I applaud you never giving up on me, for always listening and counseling me, and for invariably looking out for my well-being.

My heartfelt gratitude goes out to everyone who contributed to the creation of this dissertation.

"All my certanties are provisional."

- Oki Sato

STATEMENT OF INTEGRITY

I hereby declare having conducted this academic work with integrity. I confirm that I have not used plagiarism or any form of undue use of information or falsification of results along the process leading to its elaboration.

I further declare that I have fully acknowledged the Code of Ethical Conduct of the University of Minho.

RESUMO

As lesões crónicas resultam do comprometimento do processo de cicatrização. O envelhecimento da população e o aparecimento de comorbidades que prejudicam a regeneração da pele contribuem para o aumento da incidência de lesões crónicas, sendo agora considerado uma epidemia. Como as terapias atuais apresentam desvantagens relevantes no tratamento de lesões crónicas, existe a necessidade clínica para o desenvolvimento de soluções eficazes que tratem as lesões crónicas a curto prazo, reduzindo a falha e a carga económica destas terapias. Assim, esta dissertação visava a criação de um *scaffold* de acordo com os princípios da Engenharia de Tecidos (TE) para promover a regeneração da pele utilizando *elastin-like recombinamers* (ELRs). Estas proteínas são polímeros geneticamente modificados com base na sequência natural da elastina, a qual é uma importante proteína estrutural da pele. Como este biomaterial combina as vantagens das proteínas recombinantes e as propriedades da elastina, foram criados dois polímeros recombinantes, SKS-IKVAV e SKS-PPFLM, os quais resultam de duas modificações diferentes da proteína SKS.

Os ELRs foram concebidos e expressos na Technical Proteins Nanobiotechnology (TPNBT) S.L., como parte de um estágio ERASMUS (Contrato Financeiro 2020-1-PT01-KA103-077707). Apesar dos resultados favoráveis em relação à expressão proteica, não foi possível desenvolver um protocolo de purificação destes polímeros durante o estágio ERASMUS na TPNBT, o que inviabilizou a construção de *scaffolds* e concluir se o SKS-IKVAV e/ou o SKS-PPFLM podem ser utilizados na TE da pele.

Uma vez que as proteínas SKS-IKVAV e SKS-PPFLM não puderam ser utilizadas para a construção de *scaffolds*, uma nova abordagem, utilizando a proteína STAR, foi testada no Centro de Engenharia Biológica da Universidade do Minho para o desenvolvimento de soluções de TE da pele. Esta proteína demonstra características semelhantes às dos ELRs, e foi utilizada para a criação de filmes à base de proteínas. Estes materiais baseados na proteína STAR foram caracterizados fisicamente, quimicamente e *in vitro* e a potencial utilização dos mesmos na regeneração da pele foi favoravelmente concluída.

As perspetivas futuras dos filmes à base de STAR incluem aprofundar o conhecimento do seu comportamento *in vitro* e a incorporação de substâncias bioativas com propriedades anti-inflamatórias, anti-oxidantes e antibacterianas, para combater as principais causas do desenvolvimentos de lesões crónicas.

Palavras-chaves: Cicatrização de lesões, *Elastin-like-recombinamers*, Filmes à base de proteínas, Regeneração da pele.

ABSTRACT

Chronic wounds result from a disruption in the wound healing process. The aging of population and the appearance of comorbidities that jeopardize skin regeneration contribute for an increase on chronic wounds incidence being now considered as an epidemic. Since current therapies present significant drawbacks in the treatment of chronic wounds, there is a clinical need to develop effective solutions that treat chronic wounds in the short term, reducing failure and the economic burden of these therapies. As a result, the goal of this dissertation was to design a scaffold based on Tissue Engineering (TE) principles to promote skin regeneration using elastin-like recombinamers (ELRs). These proteins are genetically modified polymers based on the sequence of natural elastin, which is a structural protein found in the skin. Since this biomaterial combines the benefits of recombinant proteins with the properties of elastin, two recombinant polymers, SKS-IKVAV and SKS-PPFLM, were created from two different modifications of the SKS protein.

The elastin-like recombinamers were designed and expressed at Technical Proteins Nanobiotechnology (TPNBT) S.L., as part of an ERASMUS traineeship (Financial Agreement 2020-1-PT01-KA103-077707). Despite the promising results regarding protein expression, it was not possible to develop a purification protocol for these polymers during the ERASMUS trainee in TPNBT, making the construction of the scaffolds and determining whether SKS-IKVAV and/or SKS-PPFLM can be used in skin TE impossible.

Since the SKS-IKVAV and SKS-PPFLM proteins could not be used for scaffold design, a new approach, using the STAR protein, was tested at the University of Minho's Centre of Biological Engineering, for the development of solutions for skin TE. This protein shows similar properties to ELRs and was used to create protein-based films. These STAR-based materials were physically, chemically, and *in vitro* characterized, and their potential use in skin regeneration was concluded favorably.

The future prospects for STAR-based films will include greater understanding of their *in vitro* behavior, as well as the incorporation of bioactive substances with anti-inflammatory, antioxidant, and antibacterial properties to combat the primary causes of chronic injury development.

Keywords: Elastin-like recombinamers, Protein-based films, Skin regeneration, Wound healing.

GRAPHICAL ABSTRACT

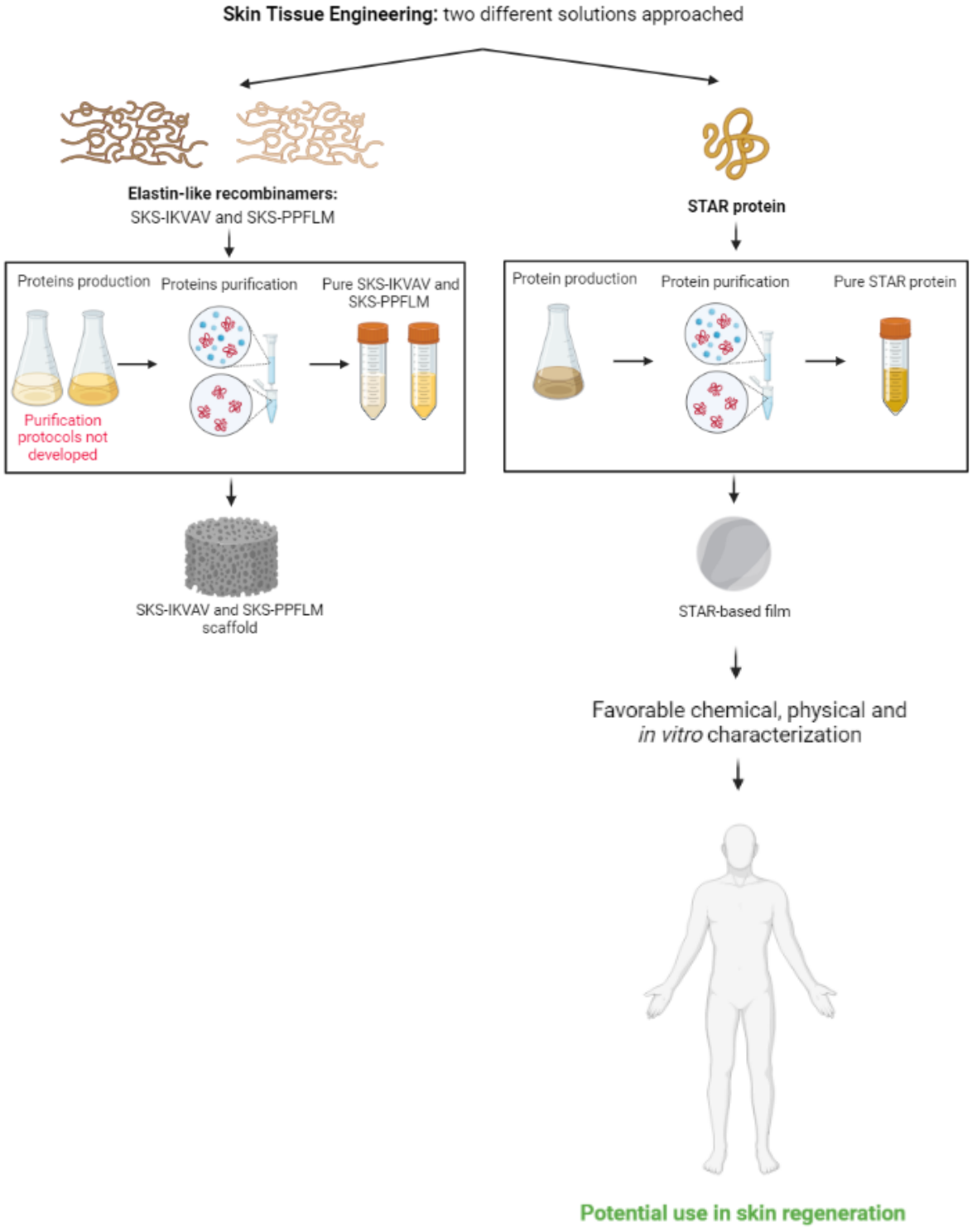

Scheme created with Biorender.com

TABLE OF CONTENTS

LIST OF FIGURES

LIST OF TABLES

LIST OF ABBREVIATIONS AND ACRONYMS

A

aa Amino acid

APS Ammonium persulfate

ATCC American Type Culture Collection

B

BBRG Bioprocess and Bionanotechnology Research Group

bp Base pairs

BPB Bromophenol blue

C

CEAs Cultured epidermal autographs

CEB Centre of Biological Engineering

D

DMEM Dulbecco's modified Eagle's medium

DMSO Dimethyl sulfoxide

DTT Dithiothreitol

E

ECM Extracellular matrix

E. coli *Escherichia coli*

EDS Energy-dispersive X-ray spectroscopy

EDTA Ethylenediamine tetraacetic acid

EFT Elapsed fermentation time

ELPs Elastin-Like polypeptides

ELRs Elastin-like recombinamers

F

FBS Fetal bovine serum

FTIR Fourier-Transform Infrared Spectroscopy

G

GAGs Glycosaminoglycans

GFs Growth factors

I

ITT Inverse temperature transition

L

LB Luria-Broth

LCST Lower critical solution temperature

M

mf final dry mass

mi initial dry mass

MTS 3-(4,5-dimethylthiazol-2-yl)-2,5-diphenyltetrazoliumbromide

MW Molecular weight marker

N

NDA Non-disclosure agreement

O

OD_{600nm} Optical density of a sample measured at a wavelength of 600 nm

P

p7 p7RARE

PBS Phosphate buffered saline

PCL Polycaprolactone

pD pDrive All

PLA Polylactic acid

R

RM Regenerative Medicine

ROS Reactive oxygen species

S

S.A.P. Shrimp alkaline phosphatase

SD Standard deviation

SDS Sodium dodecyl sulphate

SDS-PAGE Sodium dodecyl sulfate polyacrylamide gel electrophoresis

SELPs Silk-elastin-based polypeptides

SEM Scanning electron microscope

SKS Serine-Lysine-Serine

T

TAE Tris acetate ethylenediamine tetraacetice acid

TB Terrific Broth

TB AIM Terrific Broth Autoinduction

TE Tissue Engineering

TEDTA Tris ethylenediamine tetraacetic acid

TEMED Tetramethylethylenediamine

TPNBT Technical Proteins Nanobiotechnology S.L.

Tris Tris(hydroxymethyl)aminomethane

Tt Transition temperature

U

UV Ultraviolet

V

VPGVG Valine, proline, glycine, valine, glycine

W

Wd Initial dry mass

Ws Mass of the swollen material

1. INTRODUCTION

As the skin protects the human body from external agents and maintains homeostasis, one of its most important properties is wound healing, whereby various molecular and cellular factors enable the recovery of the integrity and function of this organ [1-4].

Despite skin's high regenerative capacity, chronic wounds result in inadequate repair [3,5]. These injuries disrupt one or more phases of the normal healing process, most commonly because of prolonged inflammation and/or infection, the formation of drug-resistant microbial biofilms, and the inability of skin cells to respond to restorative stimuli [5,6]. Hence, these wounds do not recover fully in the expected time, and their treatment usually includes surgical intervention [3,7].

Because of the global epidemic of chronic wounds, research efforts have been focused on developing Tissue Engineering (TE) solutions, which involve cultivating cells on three-dimensional support structures capable of serving as temporary molds for the extracellular matrix (ECM), allowing regeneration of a final functional tissue [8]. These constructs can have antibacterial properties and aid wound healing in one or more layers of affected skin by providing an appropriate mechanical support for cell growth, allowing this organ to regenerate at the same rate as these structures degrade [9,10]. To that end, their design must consider healthy skin's ECM characteristics, such as architecture, fibrous constitution, high water content, and physical, chemical, and mechanical properties [8].

Polymers are the most commonly used materials to create biodegradable structures, and natural polymers, specifically proteins, are widely used in skin TE because they are the main constituents of human tissues, and the organism has established metabolic pathways to process them [11]. Recombinant proteins, in particular, stand out, as it is possible to design natural-like proteins with target characteristics [12].

1.1. Context and motivation

It is estimated that (1 – 2) % of the population in developed countries will suffer from chronic wounds at any given time [6]. Specifically, in Portugal, a study in a continuing care unit

demonstrated that 82 % of all wounds identified among their patients were chronic [13]. The worldwide incidence of chronic wounds has been increasing globally in recent years, owing to an ageing population, i.e., an increase in people suffering from diseases and comorbidities that impair wound healing, such as diabetes, obesity, venous hypertension, and peripheral vascular diseases [6].

Furthermore, due to the high rate of cell proliferation in epithelial tissue and frequent exposure to physical and chemical damage, skin cancer is one of the most common cancers in humans and, as the standard treatment consists in the excision of the affected area, the resulting lesions are similar to chronic wounds [1,14].

Because of the numerous types of chronic wounds, existing solutions are developed for specific injuries. However, the most common treatment for chronic wounds is skin graft transplant, which consists of transferring healthy skin from one site to the wounded area [15,16]. Skin grafts are distinguished in autografts (the host is the donor), allografts (harvested from a cadaver), or xenografts (the donor is not of the same species as the host), being the first the current gold standard treatment [16].

Whilst autografts are less likely to provoke an immune response than heterologous ones, they are not exempt from disadvantages, the most relevant being the creation of a deep wound in the donor site that could become chronic [15,17]. There may also be a shortage of suitable donor tissue and/or the patient may not be fit for this treatment due to the presence of diseases/comorbidities that impair wound healing [17]. Additionally, skin grafts show inefficiency or ineffectiveness to completely heal some of these lesions due to the incapacity of overcoming the increase of bacterial resistance inherent to the infiltration of external pathological agents [18].

In addition, the continuous professional care required in these treatments has become a challenge in the COVID-19 pandemic [19]. This sudden change in daily life has reinforced the need to find solutions that effectively treat chronic injuries in the short term, reducing the overall economic/clinical burden of these therapies and the creation of multi-resistant bacterial biofilms, minimizing the failure of the treatment [6,20].

Hence, new skin regeneration therapies are focused on TE solutions, as the technology employed allows the development of off-the-shelf regenerative models customized for each patient with similar shape and function to the healthy native tissue [20,21].

Regarding the choice of material for the scaffolds, elastin is widely emphasized, as it is one of the most important structural and functional proteins of the skin's ECM [21].

Therefore, elastin-like recombinamers (ELRs) and similar recombinant polymers have a high potential for the construction of support structures as they combine natural polymers properties with the tailoring ability of recombinant proteins. Moreover, ELRs usually exhibit excellent biocompatibility since the host immune system is unable to distinguish between endogenous elastin and ELRs, as they are based on the natural elastin sequence. In addition, the tunable properties of ELRs, as well as their highly predictable and versatile sequence, enables them to be altered according to a specific end application [22].

1.2. Objectives

This dissertation in Biomedical Engineering, in the branch of Biomaterials, Rehabilitation and Biomechanics, aimed to create a recombinant polymeric scaffold and evaluate its use in the context of skin regeneration. For this purpose, two distinct ELRs – SKS-IKVAV and SKS-PPFLM - were designed using molecular biology tools and expressed at Technical Proteins Nanobiotechnology S.L. (TPNBT), a Spanish spin-off company of the University of Valladolid whose main goal is the development of "protein polymer-based materials for biomedical applications" [23]. This internship was integrated within the scope of an ERASMUS project (Financial Agreement 2020-1-PT01-KA103-077707).

However, after facing the impossibility of developing an optimized protocol for the purification of ELRs before returning from the ERASMUS, another class of polymers were applied on the development of protein-based films at the Centre of Biological Engineering (CEB), in the Bioprocess and Bionanotechnology Research Group (BBRG). CEB is located at the University of Minho (Braga, Portugal) and is a research center with projects in various areas, particularly within the Biotechnology, Bioengineering, Biomaterials, Biomedical and Life Sciences, Environmental and Agricultural Sciences [24]. Specifically, the BBRG consolidates renowned work in the areas of fiber bioprocesses, enzyme technology, molecular dynamics, nano and micro-formulations, and hair research [25].

The protein chosen for the protein-based films shares the overall characteristics of ELRs and will be henceforth named STAR due to intellectual property protection. Hence, it was necessary to

optimize the expression process of STAR, using a combination of different culture media. After the purification of this polymer and creation of the protein-based films, these were modified with the reducing agent dithiothreitol (DTT) and with methanol in order to discern the most favorable composition for the mentioned purpose.

Subsequently, film engineering, physicochemical characterization, and final biological evaluation were performed, which allowed to discern the advantages and disadvantages of the STAR films and their ability to be used as skin regeneration devices.

1.3. Thesis outline

The present thesis is divided into seven chapters, being these structured as follows:

Chapter 1 discusses the introduction to this dissertation, indicating the context and motivation for which the exposed thesis is being developed. Likewise, it presents the objectives achieved.

Chapter 2 has a detailed exposition of the anatomy, physiology, functions, and biomechanics of the skin. Subsequently, it presents a brief description of the wound healing process.

Chapter 3 includes a concise exposition of the history of skin wound treatments and a subchapter focused on skin TE, containing a general reflection of the characteristics, materials and methods used in regenerative constructs.

Chapter 4 presents the context of the work, indicating the modifications made to the initial plan for the production of ELRs for scaffold construction in the context of TE and Regenerative Medicine (RM) of the skin.

Chapter 5 includes the materials and methods associated with the ELRs design and expression, as well the related results and their discussion.

Chapter 6 includes the materials and methods associated with the STAR polymer expression, purification and development and characterization of STAR-based films.

Finally, **chapter 7** presents the main conclusions and future prospects of the work developed in this dissertation.

2. SKIN

The integumentary system includes sweat glands, hair follicles, nails as well as the largest organ in the human body, the skin, which accounts for (15 – 16) % of an adult's total body weight [1,26]. The epidermis, dermis, and subcutaneous tissue/hypodermis — which primarily consists of fat, connective tissue and is in contact with muscles — make up the skin (**Figure 2-1**) [1,26-28]. The dermo-epidermal junction, a basement membrane, is also present to support the epidermis and anchor it to the dermis [27].

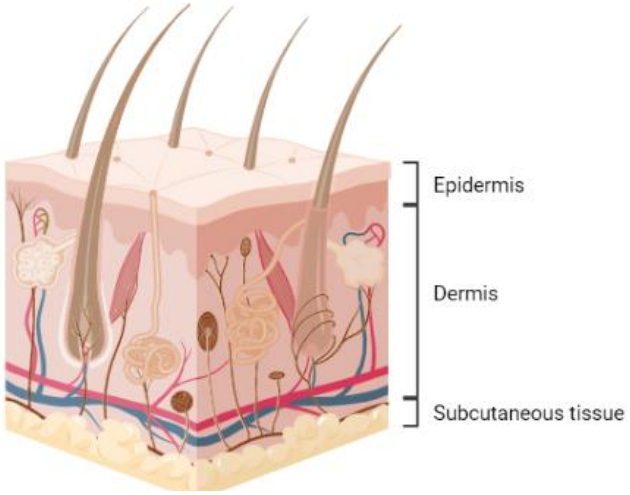

Figure 2-1 — General structure of the skin. Created with Biorender.com and adapted from [29].

Because of skin's continuity, its thickness varies considerably depending on the anatomical location. Nonetheless, it is, on average, between 1 to 3 mm and aside from acting as an effective barrier to the external environment, ensuring protection against pathological agents and other environmental threats, the skin allows sensory information to be transmitted because it is a sense-of-touch organ, triggering a physiological response based on the sensation felt [1,30]. Furthermore, it displays structures, cells, and chemical messengers involved in the immune surveillance process and plays a vital part in maintaining bodily homeostasis, through the regulation of moisture and the loss of biological substances, thermoregulation, and protection from dangerous environmental factors like ultraviolet (UV) radiation exposure [1,27,31].

Additionally, skin serves social and sexual purposes since the condition, color, shine, and ornamentation of this organ are a significant component of how individuals view beauty [27].

2.1. Epidermis

The epidermis is the thinnest and outermost layer of skin defined as a stratified squamous epithelium, whose most common cells are keratinocytes (up to 95 % of the epidermis) [27]. These cells are characterized by their large size, ample intercellular connections, and abundant cytoplasm when compared to other cell populations in this layer [32].

Nonetheless, the importance of keratinocytes is not limited to their incidence, as they also synthesize cytokines, chemical messengers involved in immune processes, in the case of a wound and produce the protein keratin, the main constituent of skin, hair, and nails [26,27].

Additionally, the renewal of the epidermis continuously throughout life is enabled by the maturation of keratinocytes during the keratinization process, where they undergo differentiation and migrate from the basal layer to the most superficial layer of the skin. Depending on the type and incidence of cells and the maturation phase of keratinocytes, it is possible to divide the epidermis into five internal layers [28,30]. From top to bottom, they are designated *stratum corneum*, *stratum lucidum*, *stratum granulosum*, *stratum spinosum*, and *stratum germinativum* [30]. As the lower three layers are all composed of living (nucleated) cells and have a similar columnar structure, they are collectively referred to as *stratum/ rete* Malpighi [1,28]. Hence, in the *stratum granulosum* occurs the process in which keratinocytes undergo a type of apoptosis denominated terminal differentiation and begin to become longer and horizontally flattened [28,30].

The *stratum germinativum* consists of mitotically active and inactive keratinocytes, the former being the first responsible for populating the entire epidermis. Thus, these epidermal stem cells present a delayed cell cycle [1,26]. **Figure 2-2** depicts the epidermal layers.

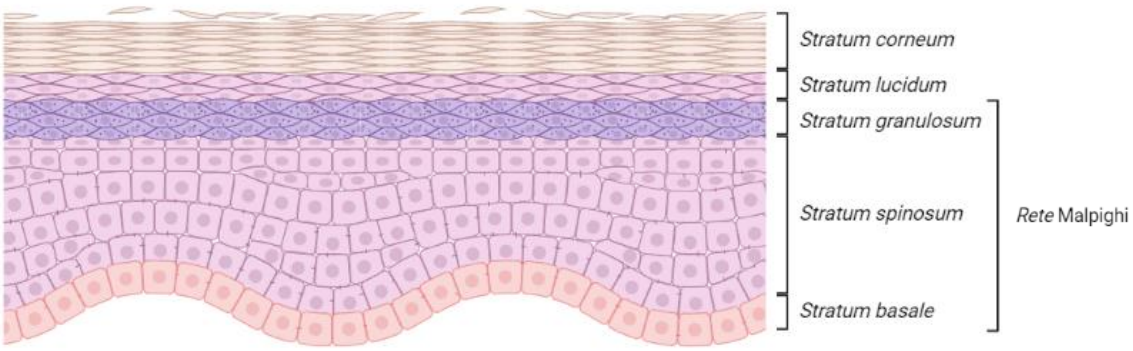

Figure 2-2 — Structure of the epidermal layers. Created with Biorender.com and adapted from [27].

Shedding takes place in the *stratum corneum*, in a 28-day cycle entitled desquamation [27]. The purpose of this phenomenon is to replace the current corneocytes (fully differentiated, flattened dead keratinocytes without nucleus and cytoplasmatic organelles [27]) with newer cells [26,30]. To assist this process, desmosomes (intercellular keratin filaments complexes in the plasma membrane) undergo proteolytic degradation as the corneocytes progress outward [1]. Hence, these complexes are responsible for controlling shearing forces in the epithelium as they enable the adhesion of keratinocytes to each other and of surface proteins to the keratin filaments [28].

Additionally, prevention of excessive water loss and resistance to physical stresses are possible due to the lamellar lipidic barrier present between the corneocytes, consisting of ceramides, fatty acids, and cholesterol. Hence, the swelling of the corneocytes is a consequence of their high-water content, endowing the *stratum corneum* with pliability and elasticity, which prevents the formation of clefts [27].

Epidermal thickness varies regionally because of the different prevalence of keratinocytes and the length of folds and ridges present in that area. Consequently, only in areas where the skin is thicker is presented the *stratum lucidum* that is composed of dead nucleated cells with thickened plasma membranes which endow the skin with greater capability to stretch and lower the effects of friction [28,30,33].

Since the epidermis is avascular, it relies on the diffusion of nutrients, gases, and the elimination of waste from the underlying dermis [27,28]. Therefore, the dermis participates in the regulation of epidermal proliferation and differentiation, intending to maintain a constant thickness of each inner layer of the epidermis. Hence, it is important to remark the existence of gap junctions, intercellular pores across the epidermis, which enable communication between cells of different *strata* and this non-mechanical interconnectivity is essential for the regulation of cell metabolism, growth, and differentiation [1].

The non-keratinocytic cells of the epidermis are melanocytes, Merkel cells, and Langerhans cells [30]. Melanocytes constitute 5 – 10 % of the cells in the *stratum germinativum* and can extend to another *strata*, being characterized by the production of melanin, a pigment that absorbs UV radiation and is synthetized from the amino acid (aa) tyrosine in the melanogenesis process. After synthesis, melanin is transferred to the nucleus of keratinocytes via melanosomes

(cellular vesicles) making it responsible for skin color and protection against photodamage [21,27,28].

Another type of cells presents in the *stratum germinativum*, although with a lower incidence, is the Merkel cells [27]. These cells are oval-shaped, slow-adapting, and are involved in sensory processes of touch, as they are in contact with sensory neurons grouped in Merkel discs. Therefore, these structures jointly detect touch, being most evident in areas of high tactile sensitivity [1,30].

Langerhans cells can be particularly found in the *stratum spinosum* and these specialized cells participate in various processes of the immune system, having a recognition purpose which allows evoking phagocytosing microbes and T lymphocytes to the affected area [30]. An illustrative image of all the cell populations mentioned is present in **Figure 2-3**.

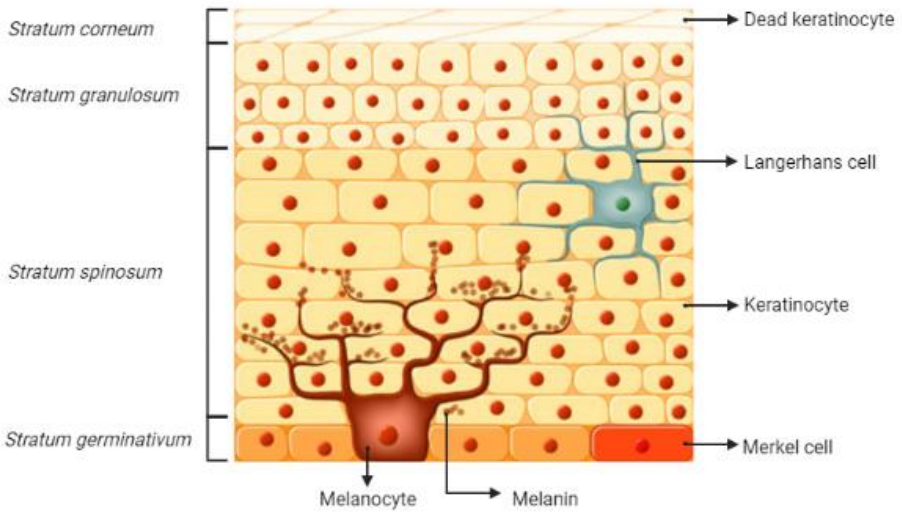

Figure 2-3 — Non-keratinocytic epidermal cells. Adapted from [34].

2.2. Dermis

The dermis is the thickest and central layer of the skin and is essentially an interconnected fibrous network of collagen and elastin. This network composes the skin's ECM, which can be defined as a three-dimensional acellularized structure that supports and controls cell growth, adhesion, differentiation, and proliferation through several chemical factors. This cell-secreted and regulated matrix is largely enriched in water, proteoglycans, and other fibrous proteins, such as laminin and fibronectin [1,30].

Collagen is a structural protein that presents variations as it consists of three polypeptide subunits and has a fibrillar appearance due to the highly frequent glycine-proline-hydroxyproline tripeptide, also referred to as α chain, which lacks intrachain hydrogen bonds in its triple helix arrangement [35-37]. Hence, collagen protects the dermis against stress and strain due to the combination of its high tensile strength and woven architecture, making up to 70 % of dermis dry weight [28,30].

Elastin is an amorphous protein that endows the skin with its characteristic elasticity, allowing it to stretch and compress to a certain limit without deformation [30]. Thus, this protein is presented in the center of the elastic fibers, which have a fibrillary structure since they consist of microfibrils intertwine in crosslinked tropoelastin [31,38]. **Figure 2-4** shows the elastin and collagen network in the ECM of the dermis.

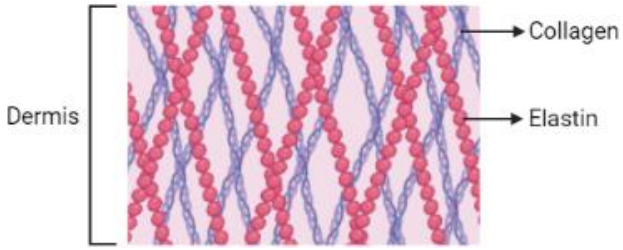

Figure 2-4 — Schematic representation of the dermis. Created with Biorender.com and adapted from [39].

Tropoelastin is defined as a polypeptide with two domains, the hydrophobic region with of any duo up to quintets of glycine, valine, proline, and alanine repeats and the hydrophilic consists of intermittent lysine in alanine or enriched proline domains [40,41].

Hence, the constitution of tropoelastin is responsible for its characteristics, as proline residues enable the stabilization of this protein secondary structures, such as β-turns and β-sheets, and the glycine content favors hydrogen bonds with water. The latter increases hydration, flexibility, and the adoption of organized structures by the focus protein [42].

The production of elastic fibers (elastogenesis) is complex, starting with the secretion and coacervation (self-aggregation by liquid-liquid phase separation due temperature increase [43]) of tropoelastin on the cell surface. After these microstructures' growth, they migrate into the intercellular space, being covalently crosslinked by enzymes and, with the repetition of this

process, the elastic fibers mature. Thus, the flexibility and elasticity displayed by elastin is conferred by its precursor, tropoelastin [44,45].

Similarly, laminin participates in the formation of tissue's ordered networks and in signaling, laminin 5 or 332 being essential for the anchoring of epidermal keratinocytes in the dermo-epidermal junction. Additionally, laminin accelerates the assembly of basement membranes, which hastens the recovery of injured skin [46-48].

Another protein mentioned is fibronectin, which consist of long fibrils of ECM stabilized by disulfide bonds, turning into fibers by self-assembly. In interaction with other ECM proteins, fibronectin participates in cell adhesion, migration, and differentiation via integrin receptors [49-51].

The stated proteins are continuously broken down and replaced, however age and intensive UV exposition affect this process, resulting in loss of skin flexibility [27].

Additionally, the dermis has salts, water, and a viscous gel constituted mainly by proteoglycans (glycosaminoglycans – GAGs - associated with a protein backbone [31]), which are negatively charged macromolecules that intervene in cellular adhesion, migration, differentiation, and proliferation [1,51-53]. Specifically, the proteoglycans-based gel, also referred to as ground substance, allows nutrients, waste products, hormones, and other specialized molecules pass through the dermis, lubricating the collagen and elastin network. Moreover, being a dense bulk, the ground substance also acts as a shock absorber [27,31].

The dermis is divided into two, the papillary dermis and the deeper reticular dermis (**Figure 2-5**) [26,27].

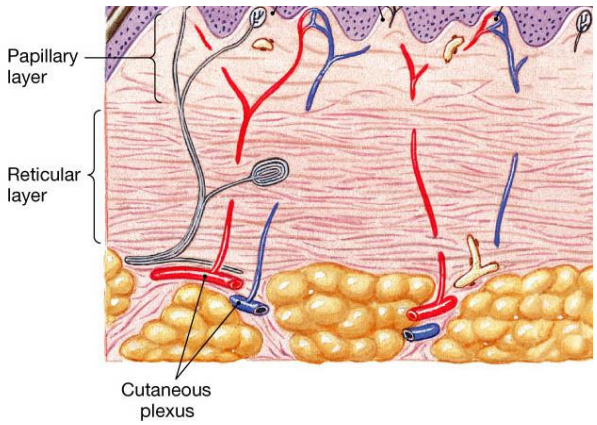

Figure 2-5 — Schematic representation of the internal dermal layers. Adapted from [54].

The papillary dermis is the more superficial and the thinner of the two, while the reticular is internally bounded to subcutaneous fat, has denser connective tissue, larger capillary vessels, more interwoven elastic fibers, ticker collagen bundles and fewer cells. Nonetheless, as the papillary dermis presents a more random collagen and elastic fibers network and has a higher quantity of gel, withstands greater frictional forces [26-28].

The types of cells present in the dermis are mast cells, immune system cells, Langerhans cells, and fibroblasts. Mast cells have an oval or spindle shape and are scattered throughout the connective tissues of the human body, being particularly present in the papillary layer of the dermis since they detect pain, itch, and temperature [1,55].

Immune system cells, such as leukocytes, can enter the structure of the dermis in response to several stimuli, such as the formation of a wound [1,55]. Moreover, fibroblasts are a relevant constituent of the dermis since in their mature state (as fibrocytes [31]) synthesize elastin, collagen, and the constituents of the viscous gel, playing a crucial role in the wound healing process [27].

Due to its anatomical location and anchorage to the epidermis, one of the main functions of the dermis is to sustain and support nutritionally and physically the epidermis, also having a protective role giving its pliability and tensile strength, preventing mechanical trauma to the underlying structures. However, excessive friction or shearing forces can separate these two layers [27,30].

2.3. Subcutaneous tissue

The subcutaneous tissue (**Figure 2-6**), also known as the *panniculus* or hypodermis, is considered the deepest layer of the skin and contains aggregates of lipid cells known as lipocytes, which are separated by fibrous septa of collagen and sizeable capillary vessels. Hence, lipocytes have an insulating effect and are intertwined with blood vessels and nerves to further influence thermoregulation and synthesize leptin, a body weight regulating hormone. This layer also includes mast cells, although in less quantity than the papillary layer of the dermis [1].

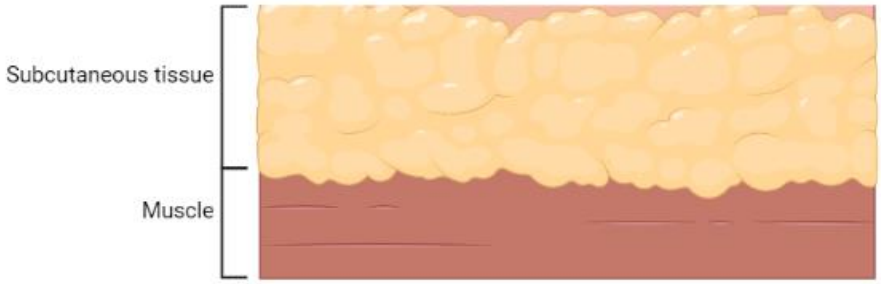

Figure 2-6 — Schematic representation of the subcutaneous tissue. Created with Biorender.com and adapted from [56].

Therefore, the *panniculus* serves not only to store energy, absorb shock, as it also provides buoyancy to the skin and supports the dermal and epidermal layers [1,27].

2.4. Biomechanical properties of skin

The biomechanical properties of the skin are defined by its cellular and molecular components, as well as the architectural organization they take. Although each individual layer endows the skin with different properties and its characteristics subtly change between different anatomical sites, the overall arrangement of this organ can be interpreted as a multi fibrillary and vacuolar system with a balance of tension-compression forces, having the dermis as its main mechanical component [26,31].

Therefore, this complex organ demonstrates anisotropy, indicating that its mechanical properties change depending on the orientation in which the tissue is being analyzed. Specifically, the rich constitution of collagen, elastic fibers, and the presence of the ground substance capacitate the skin with extraordinary elasticity and flexibility, which varies depending on the direction in which the force is applied [26]. This natural behavior was recognized by Langer in the 19th century, who first mapped the naturally occurring tension lines in the skin [57].

Skin exhibits viscoelastic behavior when deformed, usually under stretch, thus its response when stress is applied is non-linear, as represented by its typical stress-strain graph in **Figure 2-7** [26]. This graph shows skin's behavior under an executed force (stress) plotted against the change in length (strain).

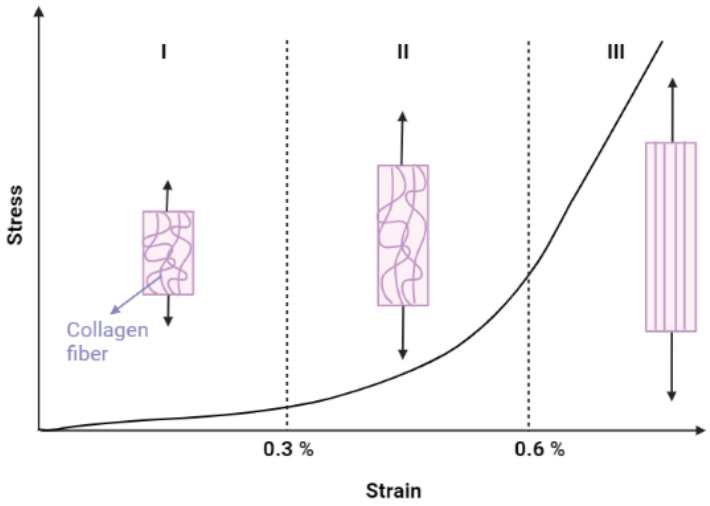

Figure 2-7 — Typical skin stress-strain curve. Created with Biorender.com and adapted from [58].

Skin deformation is a dynamic process characterized by three phases. In the first phase, also referred to as the "loading phase", the smallest force produces the largest alteration in length, meaning that at a strain of up to 0.3 %, the skin does not offer great resistance. This limited isotropic behavior is due to the alignment of elastic fibers and the entanglement of collagen in the dermis, which enables a linear relationship between stress and strain. Thus, the skin behaves as an elastic material, which is also verified by its low Young's Modulus (0.1 - 2) MPa [26,57,58].

In the second phase, a greater force is required to deform the skin since the collagen fibers are reoriented and some of skin ECM are forced between them. Accordingly, as the collagen fibers begin to stretch, a non-linear behavior in the stress-strain curve is presented [26,58].

Ultimately, in phase three, for strains higher than 0.6 %, a return to the linear stress-strain relationship can be verified, as the dermis fibers are at maximal length due to the disappearance of their characteristic spindle architecture. The collagen fibers are responsible for this effect since they are stiffer than the elastic. Thus, the force required to produce more strain increases notably, with collagen fibers breaking down on application of a deformation equal to or greater than 0.7 % [26,57,58].

In conclusion, it is possible to classify skin as a quasi-incompressible material since its volume changes are negligible when considerable deformation is applied. However, the effect of deformation on the skin depends on the duration of its application since a hyperplastic response

can be verified when a slowly constant stress is applied, this property being named creep. The phenomenon described occurs due to the decrease in the force required to maintain the skin with a certain length over time [26,57].

Contrarily, if the stress is applied too rapidly to enforce rapid stretch, rupture of the collagen fibers occurs, resulting in dermal injuries [26].

2.5. Wound healing process

As a result of the important functions of the skin, one of its most crucial features is wound healing, i.e., the regeneration process of the skin after the development of a wound. A wound occurs due to the disruption of the epithelial layer or mucosa of the skin caused by thermal or physical trauma and its regeneration involves four overlapping and well-orchestrated stages [5,20,59], as observed in **Figure 2-8**.

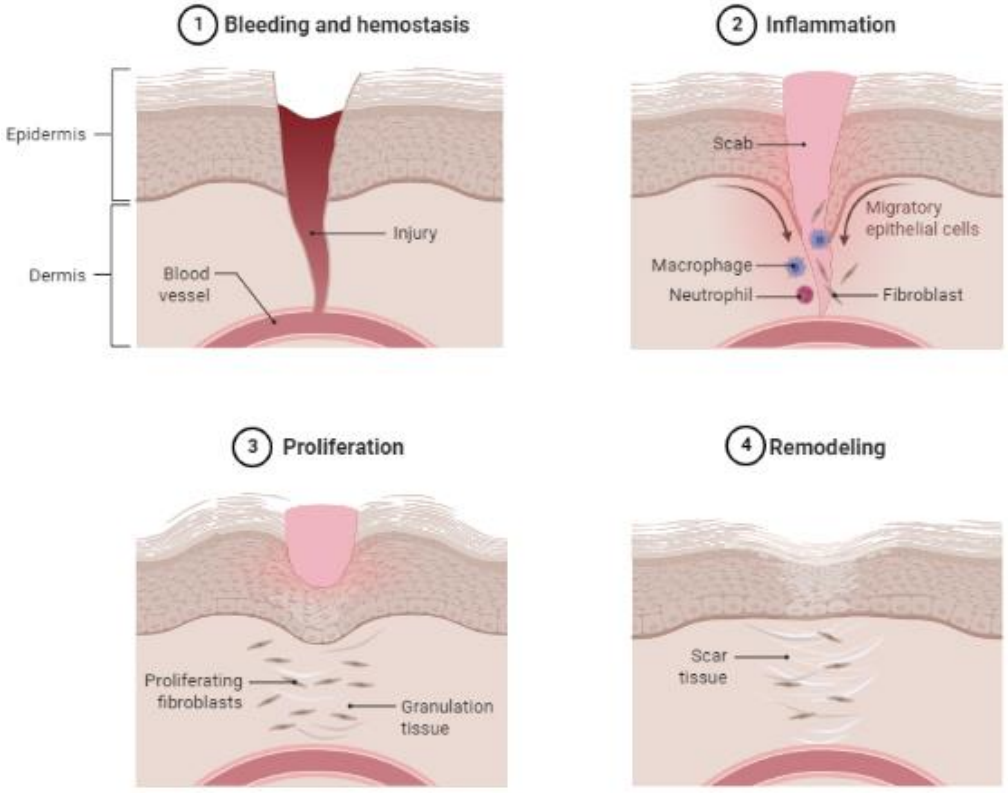

Figure 2-8 — Wound healing process. Created with Biorender.com.

2.5.1. Hemostasis

Hemostasis is immediately triggered by the microvascular disruption and extravasation of blood that occurs from the injury, as vasoconstriction is activated by the endothelium to prevent further blood outflow and the clotting cascade initiates. The latter process aims to form a clot of fibrin, fibronectin, and other proteins with platelets trapped to act as a temporary matrix for cell migration while preventing blood loss [5,20].

Specifically, platelets in the clot and surrounding wound tissue lead to secretion of growth factors and pro-inflammatory cytokines, attracting and activating fibroblasts, endothelial cells and macrophages, key actors of subsequent phases. Additionally, these blood system cells contain vasoactive molecules that heighten microvascular permeability, allowing fluid to pass into the extravascular area [5,20,60].

Furthermore, epidermal cells from the wound edges migrate to the injured area to form a thin cover, this process being known as epiboly [5].

2.5.2. Inflammation

The second phase of the wound healing process has an overall duration of 3 – 5 days. Once the bleeding is under control, an intensive migration of inflammatory cells (chemotaxis) occurs and immune cells such as neutrophils, macrophages, and lymphocytes arrive at the wounded area mainly to cleanse the injured region of external microorganisms, cellular debris, enzymes, and highly reactive species as reactive oxygen species (ROS) that are detrimental to the wound healing process [5,60].

Particularly, macrophages participate in two important roles in this phase. At the beginning, these cells release cytokines, which will recruit and activate leukocytes, inducing further inflammation. Conversely, at the end of this phase, macrophages terminate the induction of apoptotic cells, such as neutrophils, thus promoting the beginning of the proliferative phase [59,60].

Additionally, the inflammatory cells secrete growth factors (GFs) that boost fibroblast migration and proliferation of vascular endothelial cells in the subsequent phase [59,60].

2.5.3. Proliferation

The third phase of the wound healing process initiates 3 days after the wound formation and lasts 2 - 4 weeks. It is characterized by fibroblast migration, deposition of provisional ECM components to reconstruct it, and formation of granulation tissue, the latter consisting of new connective tissue and capillary vessels formed from old ones of the injured area initiated by endothelial progenitor cells [5].

At the beginning, fibroblasts migrate to the wound area, followed by endothelial cells, which are attracted by GFs released previously and the enzymatic conversion of fibrinogen to fibrin by thrombin. Hence, the primary goal of these cells is to synthesize proteins that are used to reconstruct the damaged ECM. Additionally, after ECM reformation, the fibroblasts maintain interactions to regulate its further formation and remodeling [5,59].

As the proliferative phase progresses, the temporary matrix of fibrin and fibronectin is progressively replaced by type III collagen produced by dermal skin fibroblasts accompanied by angiogenesis to create the granulation tissue [5,59].

The end of this phase is marked by the re-epithelization of the wound, process enabled by the migration and proliferation of epithelial cells that requires specific conditions, such as high humidity, nutrition, and control of external organisms, being modulated by several GFs [5,60].

Following a wound, the structures of all skin appendages are also capable of re-epithelialization through the migration of keratinocytes from the epithelium into the *stratum corneum* [1].

2.5.4. Remodeling

The last phase of the wound healing process is the remodeling and further synthesis of the ECM initiated in the previous phase, with scar maturation also occurring [5].

Remodeling can last for years, beginning in week 1 of wound formation, and is characterized by constant cycles of collagen II formation and breakdown and its replacement with collagen type I so that the skins' ECM stabilizes (usually 21 days after injury) and acquires an architecture similar to that of healthy skin. As the scar matures, its tensile strength increases through collagen type I fiber enlargement, accumulation, and cross-liking [5,60].

Moreover, wound contraction may occur, driven by the interaction between fibroblast and the surrounding ECM. This phenomenon happens throughout all healing processes and is regulated by contractile fibroblasts (myofibroblasts), cytokines and growth factors present in the wound area [5,60].

2.5.5. Chronic wounds

Notwithstanding skin's high regenerative capacity, chronic wounds result of inadequate repair. These injuries, by definition, disrupt one or more phases of the normal healing process, most commonly because of prolonged inflammation and/or infection, the formation of drug-resistant microbial biofilms, or the inability of skin cells to respond to restorative stimuli, healing in an unpredictable or long-time frame. Thus, chronic wounds treatment usually includes surgical intervention [3,5,6,59].

As chronic wounds fail to progress beyond the inflammatory phase, they are often characterized by an imbalance of pro- and anti-inflammatory cytokines and GFs, which impedes the proliferation of vascular endothelial cells, fibroblasts, and collagen matrix deposition. Additionally, high levels of proteases and excessive ROS release by inflammatory cells affect the wound healing process by damaging the cells or the ECM and degrading the GFs [59]. Other characteristics that are commonly associated with chronic injuries and hinder their regeneration process are present in **Figure 2-9**.

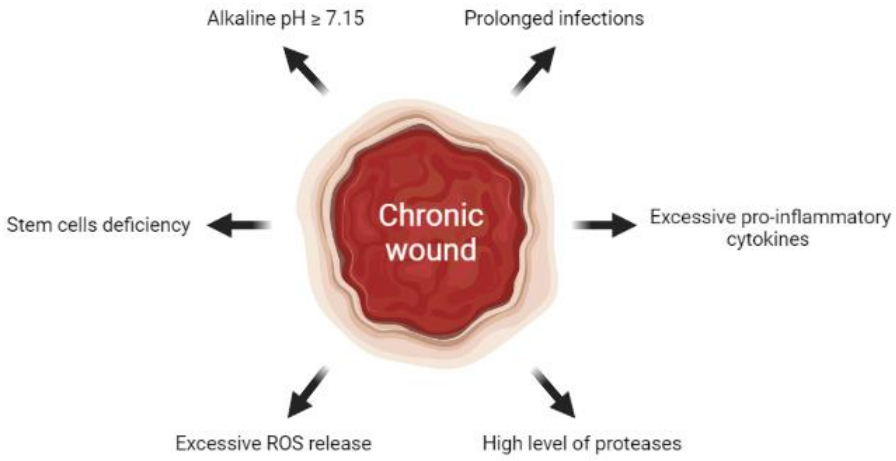

Figure 2-9 — General characteristics of chronic wounds. Created with Biorender.com and adapted from [59].

Chronic wounds can be caused by a variety of factors, including burns, trauma, prolonged pressure (pressure ulcers), venous valve malfunction (venous ulcers), or metabolic diseases such as diabetes (diabetic foot ulcers). Hence, several local or systemic factors hinder or prevent normal skin repair [5,59] and a summary of these influential factors is presented in **Table 2-1**.

Table 2-1 — Summary of local and systemic factors that impair the normal wound healing process, adapted from [5,60]

Local factors	Systemic factors
Inadequate blood supply	Advancing age and general immobility
Increased skin tension	Obesity
Poor venous drainage	Malnutrition
Presence of foreign body reaction and/or elements	Deficiency of proteins, vitamins, and/or trace elements
Presence of slough and/or non-viable tissue	Systemic malignancy and terminal illness
The continued presence of external microorganisms (e.g., formation of bacterial biofilms)	Systemic diseases (e.g., diabetes *mellitus*, rheumatoid arthritis, connective tissue diseases, metabolic diseases)
Infection	Peripheral vascular disease and vasculitis
Excess local mobility	Venous oedema or lymphoedema
Underlying osteomyelitis	Chemotherapy and radiotherapy
Malignant transformation	Impaired macrophage activity

These factors alter cells and their activity, decrease levels of GFs, and/or lead to abnormal alterations in the ECM, increasing the presence of highly reactive molecules, especially ROS [5].

Thus, deficiency/lack of epithelialization or inadequate blood supply are common compromising factors during the wound healing process, as the regeneration process largely depends on them [5].

3. STATE OF THE ART

The existence of healers, people who cared for physical trauma, has been verified since the Paleolithic, with plants being extensively used as dressings for wounds or to produce balsamic ointments to stop hemorrhages, to hasten the healing process and to minimize the risk of infection. Additionally, the use of ice to minimize pain dates back to this era [61,62].

In ancient Greece the importance of cleansing wounds with water and vinegar was advocated and salves were used to stimulate suppuration, diminish inflammation, and remove necrotic tissue. In addition, the syringe was used to inject fluids and to remove pus from wounds. Greek physicians first established the classification of wounds. They classified the injuries into fresh or non-healing wounds. These concepts then evolved to the current acute and chronic wound classification [62-64].

War scenarios were also instrumental in the evolution of wound treatments and therapies, being emphasized the role of the renowned, professional service *Medici* during the Roman Empire. This group of trained physicians allowed on-site wound treatment with the available surgical instruments to rapidly restore function to the injured area. Nonetheless, their treatment did not prevent scarring of the tissue, not only due to the lack of technological knowledge, but also because of the heroic connotation of wounds and scars [61].

This hidden meaning of scars and wounds had a radical change in the Middle Ages, with the treatment of injuries being characterized by the return of incantations and potions. Therefore, it was not until the 18th century, that it was possible to study the anatomical and physiological changes resulting from the formation of a lesion. This allowed the conclusion that all bodies experienced a shock after any injury due to the visible decline that patients underwent after the formation of a wound [61].

The 19th century was marked by the invention of anesthesia, which expanded surgical treatments, increasing the use of skin grafts. Hence, although history indicates the use of skin grafts for more than 2500 years, the first reports of their clinical application were made on a sheep in 1804 by Baronio [61,65].

In 1895, Mangoldt showed that clusters of cells adhered better to the injured site than epidermal skin fragments and Pinkus disclosed that the responsible for the formation of an

epidermal sheet were basal precursor cells from skin fragments. Yet, this favorable result was not achieved with differentiated keratinocytes since they become necrotic during this phase [65].

Nescience regarding the presence of pathogens during wound healing led to the epidemic dissemination of diseases, as gangrene, among postoperative patients. Consequently, skin graft treatments were unsuccessful in numerous cases, making their use less frequent [61].

Nonetheless, at the turn of the 20th century, with the acceptance that microorganisms present in wounds lead to infection, antiseptic techniques were established. Also, the discovery of penicillin and other antibiotics enhanced the success of wound care since therapies were only effective if the infection in the area surrounding the wound was controlled [61,63].

However, it was not until the mid-1950s that the biological processes and biochemical determinants of wound healing began to be understood. Besides the importance to eliminate pathogens, it was disclosed the role of oxygen and nutrients to the regeneration of the affected area promoted by the cells involved in the process. In addition, Medawar successfully isolated proliferating epidermal cells, showing that keratinocytes could be implanted if they were isolated from skin fragments cultured under dynamic conditions. Still, the cell yield obtained was insufficient to treat chronic wounds [61,62,66].

These findings further boosted the research and the application of skin grafts, with these being considered full-thickness if all epidermal and dermal layers were present or split-skin if they only exhibit the epidermis and papillary dermis [65,66].

Artificial skin grafts have been clinically implemented with the goal of assisting the natural regeneration of lesions, either by preventing the development of infections, by having oxygen and water permeability, ensuring hydration of the affected area, or merely by acting as a temporary or permanent matrix for cells [59].

The first clinically applied artificial grafts were cultured epidermal autographs (CEAs), i.e., sheets of keratinocytes cultured in an irradiated fibroblast feeder layer. These were considered the best treatment for chronic wounds, since it was believed in the 1970s that regeneration of these lesions could be effectively achieved only by reconstructing the epidermis [66].

Nonetheless, this type of graft presents several disadvantages, such as a thickness of only 3 – 4 cell layers, making it very fragile to handle and with insufficient mechanical properties to mimic the epidermis, and were unable to regenerate all skin layers since they did not have a substrate that mimicked the dermis. In addition, even if a nondegradable matrix was used to

support the graft, the detachment of this sheet with enzymes caused cell contraction, shrinking the graft by 30 % to 50 %. Moreover, these grafts were prone to infection, presented a success rate that varies from 15 % to 85 % and were associated with high costs and a short shelf life (normally 24 h). However, CEAs have contributed to increased survival rates for burn patients, being Epicel® (**Figure 3-1**) clinically available since 1987, and others developed with fibrin glue, hyaluronan, chitosan, or polycaprolactone (PCL) are also currently marketed [61,66,67].

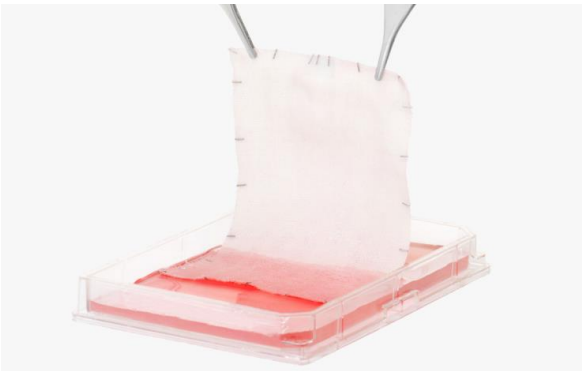

Figure 3-1 — Epicel® graft. Adapted from [68].

Parallel to CEAs, dermal grafts began to be developed by Yannas, Burke, and Bell, these consisting of a three-dimensional scaffold of a natural or synthetic polymer able to support cell attachment, proliferation, and ECM production, being seeded and cultured with allogenic (genetically different from the host) or autogenic (genetically equal to the host) fibroblasts. These scientists are considered the pioneers of matrix-based skin TE, having applied collagen as a cell carrier due to its relevance in dermal constitution and developed Integra™ Artificial Skin, clinically available since 1984 (**Figure 3-2**). This is one of the most well-known artificial skin grafts and consists of an acellular dermal replacement whose matrix material is a polysiloxane membrane for the epidermis and reconstituted bovine tendon and shark GAGs for the dermis [66].

Figure 3-2 — Integra™ Artificial Skin. Adapted from [69].

Despite this graft having a matrix that mimics the epidermis to some extent, the use of a temporary acellular polymeric base does not guarantee adequate regeneration of the basal layer. Hence, dermal grafts also have serious drawbacks, all of which stem from the lack of an epidermal substitute layer [66]. Other clinically available skin grafts are present in **Table 3-1**.

Table 3-1 — Clinically available skin grafts, adapted from [66]

Product	Clinically available since	Type
Alloderm®	2001	Acellular dermal replacement
TransCyte®	1997	Acellular dermal replacement
Dermagraft®	1999	Cellular dermal replacement
Cultured human epidermis	2000	Cultured epidermal autograft
CryoCeal	2000	Cultured epidermal allograft
Cultured epidermis	2002	Cultured epidermal autograft
BioSeed-S®	2001	Autologous epidermal gel
Apligraf	2001	Bilayer skin replacement
HYAFF™ and Laserskin™	2000	Bilayer skin replacement
OrCel™	2001	Bilayer skin replacement

Currently, the gold standard for the treatment of chronic wounds is the use of autologous skin grafts and whilst these are less likely to provoke an immune response than heterologous ones, they are not exempt from disadvantages. The most relevant is the creation of a deep wound in the donor site that could become chronic; there may also be a shortage of suitable donor tissue and/or the patient may not be fit for this treatment due to the presence of diseases/comorbidities that impair wound healing [15-17].

Skin graft therapy is typically supplemented with the use of biological factors involved in the progression of an injury from acute to chronic. As a result, the topical application of anti-inflammatory active agents (such as essential oils), antioxidants, and GFs combined with protease inhibitors stands out since they showed to be effective in chronic wound treatment [59].

Furthermore, because adult stem cells have the ability to migrate to injured tissues and proliferate and differentiate into the required cell type, they have been studied in the chronic wound context. The topical delivery of several adult stem cells has been referred in literature as advantageous for chronic wound treatment, namely bone marrow-derived, adipose tissue-derived, and mesenchymal stem cells [59].

Among other treatments used today, some of them are inspired by ancient techniques, such as negative pressure wound therapy, which aims to apply negative pressure through an electronically controlled pump on an adhesive dressing that protects the wound area. The success of this treatment is due to the draining of the wound exudate, which promotes blood circulation and the formation of granulation tissue [61,70].

Nonetheless, in most chronic wounds there is a need for skin replacement and the limitations listed above could be overcome by a skin equivalent matrix, as it could not only regenerate the epidermis and the dermis, but also the dermo-epidermal junction with the specific architecture and components of each layer. Hence, the currently available therapies usually do not regenerate or restore the skin's integrity/function, instead acting as a substitute with significant functional and visual differences from the healthy tissue [18,66].

The lack of solutions that can be tailored to each specific injury and patient to effectively treat chronic wounds creates a clinical need for the development of new treatments, as off-the-shelf scaffolds seeded with patient cells, since immunity issues could be avoided, and they could be designed to fit the wound area by mimicking the lacking skin layers [15,17].

The present-day approach for the construction of scaffolds for the treatment of chronic wounds is the integration of two distinct layers, one serving as the epidermis and other as the dermis, by combining *in vitro* cultured keratinocytes and fibroblasts into this acellular matrix [17].

Despite contour the aforementioned obstacles of grafts; this TE approach has major challenges, namely the restricted sizes of scaffolds grown *in vitro*, which lead to improper vascularization in the following integration of these scaffolds *in vivo*. Additionally, they induce excessive wound contraction, which may lead to functional limitations. They do not prevent scarring, resulting in the formation of new tissue with a different texture and quality than the surrounding skin. Moreover, some of the scaffolds implanted *in vivo* show poor mechanical integrity, immune rejection, and failure to integrate with the supportive layers, which may be related to the use of different materials and architectures to mimic the two different skin structures. Thus, there is a lack of standardization and reproducibility of these repair constructs and, in spite of the existence of several commercial solutions and research in this area, particularly driven by the cosmetic industry, the currently available TE strategies are limited and do not meet all the specifications and requirements for a proper wound healing process [17,71-73].

Additionally, it is relevant to indicate that TE solutions are very expensive, mainly related to the cost of *in vitro* cell culture and the overall manufacturing process due to the materials and methods used. Thus, nowadays scaffolds are often reserved for cases where conventional methods do not guarantee skin regeneration [71-73].

One way to reduce the cost of scaffold manufacturing is by producing materials through established and easy laboratory protocols, overcoming the expensive techniques used to obtain natural polymers or to manufacture synthetic ones and that can be used to regenerate different skin layers. An example of such materials are recombinant proteins, these macromolecules having provided important advances in biomedical biotechnology since 1982 with the use of recombinant human insulin to treat diabetes. Thus, there are currently more than 130 recombinant proteins approved by health regulatory entities (e.g., Food and Drug Administration) [74].

Is also relevant to mention that research for chronic wounds therapies is increasingly adopting GFs and stem cells, so that scaffolds not only serve as a template for tissue regeneration, but also have biochemical and cellular elements needed to induce repair in native tissues. There are several factors involved in the wound healing process, but the ones that are being investigated and already incorporated in scaffolds are fibroblast, epidermal, transforming beta, and platelet-derived GFs, the latter being very important in the early stages of wound healing [75].

3.1. Wound healing and tissue engineering

RM is a branch of biomedical research that aims to replace, regenerate, or engineer human cells, tissues, and organs to restore normal function [76]. Hence, it employs different regenerative strategies, such as using single cells to replace native ones that no longer provide the required function, or delivering tissue-inducing substances, such as GFs and differentiation factors to targeted sites. While these options individually are appropriate for the treatment of small, well-contained defects, cell growth on three-dimensional scaffolds is the only therapy that can engender scalable tissue, essential for the regeneration of chronic skin wounds [8].

Therefore, TE, a subfield of RM is expected to be used to create an ideal solution for chronic wounds as the technologies involved allow the development of off-the-shelf constructs through

biodegradable biomaterials, whose architecture can be customized to the lesion and the stem cells used can be those of the patient. Additionally, the use of the aforementioned active substances used in parallel with skin grafts can be integrated in these constructs in order to exponentiate the success of the therapy [76-78].

Wound healing TE research has been focused on growing cells in three-dimensional scaffolds or other supporting structures, i.e., as films and hydrogels, to engineer constructions capable of serving as temporary molds to the ECM, allowing the regeneration of a final functional tissue while creating a protective barrier that prevents further infection and fluid loss [8,17]. These constructions can aid wound healing in one or in several skin layers affected in chronic wounds, providing an appropriate mechanical support for cell growth, in a manner that the regeneration of this organ occurs at the same rate at which these structures are degraded [9,10].

Accordingly, a requirement of TE is that the constructive models must be biodegradable since the purpose of the therapy is to assist the organism in the regeneration of a certain tissue and not to definitively replace it [76-78].

3.1.1. General characteristics of regenerative constructs

TE combines the use of stem cells, biomaterials, and bioactive substances to improve the success of tissue regeneration. Hence, only support structures associated with the use of cells are considered TE solutions [79].

There are general well-accepted requirements for regenerative constructs as depicted in **Figure 3-3**.

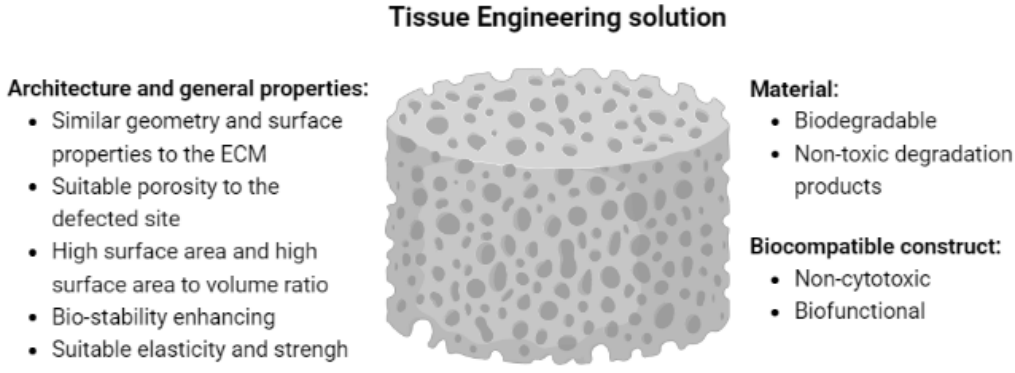

Figure 3-3 — Ideal characteristics of TE solutions. Created with Biorender.com and adapted from [79].

Scaffolds are the most common TE structure because they allow for easier mimicking of the tissue to be regenerated while meeting the above requirements. They should present high porosity, adequate pore size and interconnectivity to enable cell proliferation, migration, adhesion, growth, and differentiation throughout the structure. Also, a high surface area is required to allow easy perfusion of nutrients and gases for the nourishment of the seeded cells or their waste disposal, and biocompatibility [8,11,80], defined as "the ability of a material to perform with an appropriate host response in a specific application" [81]. For the scaffold to be considered biocompatible it should not exhibit cytotoxic response, have good biofunctionality, that can be resumed in the ability to promote ECM deposition, correct gene expression, and not induce changes in cell phenotype [8,11,80].

Moreover, the mechanical properties of the scaffolds should be similar to those of the tissue to be regenerated and the rate of degradation should be adjusted to the rate the new tissue forming, possibly by altering their physical and chemical stability. Also, the degradation products should be non-toxic [8,11,80].

Additionally, these constructs must be efficient, allowing repair of skin structure and function in a timely manner. Moreover, they should be easy to handle, to produce, and obtained using biomaterials that have an unchallenging manufacture to reduce production costs [17].

However, while there are global requirements for a TE solution, it must be developed according to the characteristics of the tissue, such as the specifics of its ECM, cellular content, and biomechanics [81].

3.1.2. Materials for regenerative constructs

Considering the properties of scaffolds, polymeric biomaterials are regarded as ideal for the development of TE devices [82]. This is due to their chemical tunability, which allows scaffolds to be engineered with the properties required for a specific application [11].

Synthetic and natural polymers present different properties and due to their controlled production, synthetic polymers like silicone and polylactic acid (PLA) or PCL are considered more available and tunable than natural ones. These materials are characterized by their carbonic backbone, having identical repeating units, which makes them uniform. Hence, synthetic

polymers have very predictable properties that can be highly engineered to mimic the native tissue [11,67,83].

In particular, the potential of PCL has been underlined since it is already used in sutures and drug delivery devices. Still, materials in this category are prone to more unfavorable biological responses since some of the interveners in their manufacturing process may not be biological and/or environmentally friendly [83].

One of the most commonly used natural polymers are proteins, such as collagen, elastin, or keratin, as they are complex macromolecules with one or more aa chains that are substantially present in all human tissues. Additionally, gelatin, derived from denaturation and partial hydrolysis of collagen, silk, a material endowed with more durability, degradability, and strength than others, and fibrin, an important ECM protein, are also extensively referred. Hence, this type of biomaterial with similar but not identical repeating units is less likely to be cytotoxic as they are easily incorporated and expelled into biological systems since there are established pathways for their metabolic processing [11,66].

Nonetheless, the immunogenicity verified in some natural polymers, the complexity of their monomers and their lower availability are disadvantages that need to be overcome. Additionally, natural polymers evidence batch-to-batch variability and unfavorable biomechanical properties due to their rapid biodegradation and low stability [11,12].

Therefore, recombinant proteins stand out since they are natural-like macromolecules, which can be engineered with target characteristics according to the specific requirements of their application. Hence, they are defined as proteins created via heterologous expression, as a result of genetic engineering and examples of them are human-derived proteins, such as collagen and elastin [12,84].

As the manufacture of these proteins is based on the use of different molecular biology tools to design and obtain recombinant genes, it is possible to control the biomaterial at a molecular level with precise size and sequence control, overcoming the low availability and variability of natural polymers. In addition, bioactive sequences or residues can be incorporated to model the physicochemical properties of these proteins [85,86].

The reference to the complexity of natural polymers as a disadvantage is justified by the associated production costs. Hence, as recombinant proteins allow complexity with a low production cost, this characteristic is a relevant advantage of this class of biomaterials [87].

When designing a scaffold for skin TE, the properties and constitution of the skin have to be considered. Among the constituents of the skin, collagen and elastin stand out, mainly due to their functions. Although in lower concentration than collagen, elastin has many relevant functions in the skin, modulating cells-ECM interactions and, as a signaling macromolecule, induces cell adhesion, differentiation, and proliferation in the skin matrix [87]. Additionally, elastin plays a relevant role in angiogenesis, which is crucial for proper wound healing, as deficient blood supply impairs this process [88].

Furthermore, ELRs are a promising class of biologically inspired proteins, their use being widely referred in TE literature since these recombinamers offer the opportunity to biomimicry one of the most important fibrillar proteins of the ECM [88].

3.1.2.1. Elastin-like recombinamers (ELRs)

Elastin-like polypeptides (ELPs) are genetically engineered proteins based on the natural hydrophobic sequence of elastin, the pentapeptide motif valine, proline, glycine, valine, and glycine (VPGVG) [21,43]. This sequence, responsible for the elastic properties of elastin, was first described by Gray and his team [89] and the first type of ELPs was synthesized by Urry's laboratory [90] aiming to elucidate the characteristics of this unit [43].

Physicochemical studies have demonstrated that ELPs have a smart behavior, such as reversible phase transition in response to temperature [22]. The latter phenomenon, also known as inverse temperature transition (ITT) (**Figure 3-4**), is an inherited feature of elastin/tropoelastin thermoresponsiveness [21]. Hence, ELPs remain soluble below the transition temperature (*Tt*) and aggregate when the temperature is raised above the *Tt*. Above this temperature the polymer chains hydrophobically fold and lose their clathrate water structures [54], leading to phase separation. Thus, *Tt* is also known as the lower critical solution temperature (LCST) [21,43].

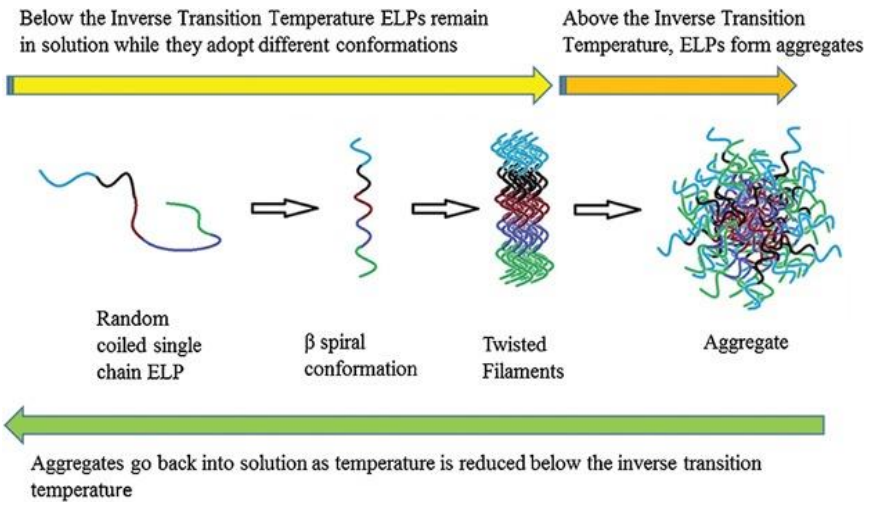

Figure 3-4 — Behavior of ELPs according to temperature. Adapted from [91].

An ELP *Tt* can be tuned by salts present in the medium, pH, and pressure, but also by polypeptide hydrophobicity and length [92]. Specifically, ELPs hydrophobicity can be changed through the modification of the fourth aa of the VPGVG pentapeptide, endowing the ELP design with great flexibility since distinct aa in this domain can endow the final polymer with different properties, making their choice depend on the final application of the polymer [43,93]. Hence, the motif began to be described as VPGXG, where X can be any aa except proline since it destabilizes the secondary conformation of the final protein [21,88,93].

Another advantageous characteristic of the pentapeptide sequence is the inability of the host immune system to distinguish between endogenous elastin and ELPs [21]. **Table 3-2** shows the favorable biological performance of ELPs *in vitro* testing conducted by Urry, which demonstrate their promising use in the field of RM [94].

Table 3-2 — Results of *in vitro* testing of ELPs, adapted from [94]

Test	Result
Ames mutagenicity	Non mutagenic
Cytotoxicity-agarose overlay	Nontoxic
Acute systemic toxicity	Nontoxic
Intracutaneous toxicity	Nontoxic
Muscle implantation	Favorable
Acute intraperitoneal toxicity	Nontoxic
Systemic antigenicity	Non antigenic
Dermal sensitization	Non sensitizing
Pyrogenicity	Nonpyrogenic
Lee-White Clotting	Normal
In vitro hemolysis	Non hemolytic

Initially, ELPs were chemically synthesized, hampering the production of long polypeptides. However, with the 1980s advent of recombinant DNA technology, the production of ELPs has begun to be carried out through its expression in heterologous hosts, mainly *Escherichia coli* (*E. coli*), making also possible to incorporate bioactive sequences into these proteins [43]. Considering the recombinant nature of the ELPs obtained using molecular biology tools, Rodríguez-Cabello *et al.* [95] proposed a new nomenclature to ELPs, elastin-like recombinamers (ELRs).

The use of ELRs in the context of TE is not new. For example, an ELR hydrogel was developed as an experimental model to study and modulate cell behavior in 3D cultures and these recombinamers have already been used in drug delivery systems, vaccines, and gene delivery vectors in the last decades [86,96].

Additionally, other proteins can be recombined with ELRs to alter the properties of the recombinant protein so that they are more suitable for the tissue to be regenerated. An example are silk-elastin-based polypeptides (SELPs) that combine the mentioned advantages of ELRs with additional chemical and thermal stability, mechanical tunability and more physical crosslinking sites due to the tandemly repeated silk units (GAGAGS) [97].

For the design and engineering of ELRs-based scaffolds for skin TE in this dissertation, the final polymer would result from the fusion of different ELRs polymers, these being called SKS, SKS-IKVAV and SKS-PPFLM, the latter two resulting from different modifications of the former [99]. SKS stands for serine-lysine-serine sequence [86] and since a confidentiality agreement has been signed with TPNBT, the complete sequences of the three polymers mentioned will not be presented. Due to intellectual property protection, the STAR protein's aa sequence will also not be disclosed in this dissertation.

3.1.3. Fabrication methods of regenerative constructs

The technologies available for the fabrication of scaffolds in TE are immeasurable, as each specific end application and chosen material requires optimized manufacturing to provide the optimal solution.

Since relevant characteristics of scaffolds are porosity and pore size, traditional technologies focus on the extrusion of fibers to create porous structures. Using electro/melt/wet spinning, solvent casting, and freeze-drying it is possible to obtain 3D structure on the scaffold ideal to cells to adhere and proliferate [99,100].

Technological advances in several areas have allowed the development of other manufacturing tools, in order to mimic the ECM of several tissues more accurately and biologically functionalize the final structure. For example, manufacturing methods such as 3D printing, which comprises inkjet, micro extrusion, stereolithography and bioprinting, are now being employed to obtain scaffolds with precise architecture [99].

Because the goal of this dissertation was to demonstrate the feasibility of using ELRs in a scaffold to promote skin regeneration, the manufacturing method under study for its construction was based on click-chemistry (**Figure 3-5**).

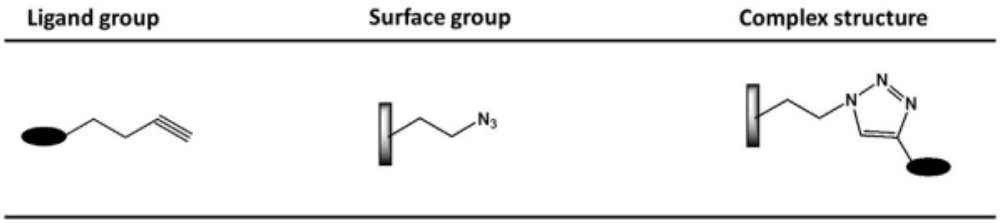

Figure 3-5 — Schematic representation of the chemical groups involved and resulting from click-chemistry. Adapted from [101].

This is a chemical manufacturing mechanism that allows the covalent cross-linking of two ELRs at a liquid-liquid interface to produce micro-scale, bioinspired scaffolds with tunable diffusion properties. This method, which has already been used for the construction of scaffolds with SKS polymer, is simple to implement and does not require specialized technical knowledge [102].

4. CONTEXT OF THE WORK

The construction of SKS-IKVAV and SKS-PPFLM synthetic genes was successfully accomplished at the TPNBT facilities at Valladolid - Spain. However, due to contingencies of time related with the ERASMUS mobility program it was not possible to follow the work with the ELRs, particularly the production and the purification of the polymers.

The second stage of the work with the ELRs was expected to be developed at the BBRG at Centre of Biological Engineering (CEB), in University of Minho. However, since none of the polymers were successfully obtained, a new strategy using a new polymer with similar characteristics to those of ELRs – STAR - was used to obtain protein-based films for skin TE.

For a better comprehension of the work developed in this dissertation, the materials, methods, results, and discussion of each class of proteins will be presented separately. The first one is related to the ELRs and was developed at TPNBT facilities at Valladolid – Spain and the second part is related with the application of STAR polymer, and was developed at BBRG at CEB, University of Minho.

5. ELASTIN-LIKE RECOMBINAMERS: SKS-IKVAV AND SKS-PPFLM FOR SKIN TISSUE ENGINEERING

Since ELRs are elastin-based recombinant polymers, they can be potentially used as a biomaterial in TE solutions to promote skin regeneration.

Thus, this section of the dissertation was focused on the synthesis of the SKS-IKVAV and SKS-PPFLM recombinant genes using genetic engineering tools and bioproduction of the proteins at TPNBT.

5.1. Materials

The materials used for the design and production of the recombinamers are below. Since a confidentiality agreement has been signed with TPNBT, the aa sequences of the SKS-IKVAV and SKS-PPFLM proteins will not be presented.

5.1.1. Chemical reagents

The chemical reagents employed in the making of the ELRs are listed in **Table 5-1**.

Table 5-1 — List of chemical reagents employed

Reagent and Abbreviation	Brand
1 kb Plus Ladder	Invitrogen
Acrylamide	Amresco
Agarose	Sigma Aldrich
Ammonium persulphate (APS)	Sigma Aldrich
Ampicillin	Apollo Scientific
Bromophenol blue (BPB)	Sigma Aldrich
Cooper chloride	Sigma Aldrich
D (+) glucose	Merck
Ethanol	Merck

Ethylenediaminetetraacetic acid (EDTA)	Sigma Aldrich
Glacial Acetic Acid	Sigma Aldrich
Glucose	Sigma Aldrich
Glycerol	Sigma Aldrich
Glycine	Sigma Aldrich
Kanamycin	Apollo Scientific
SYBR™ Safe DNA Gel Stain	Invitrogen
Sodium dodecyl sulfate (SDS)	Sigma Aldrich
Tetramethylethylenediamine (TEMED)	Sigma Aldrich
Tris(hydroxymethyl)aminomethane (Tris)	Sigma Aldrich
Type I water	
β-Mercaptoethanol	Sigma Aldrich

5.1.2. Vectors

In this work, two types of vectors were used. The pDrive All cloning vector with 3938 base pairs (bp) (Quiagen), also referred as pD, was used for the assembly of the final gene sequence. The p7RARE expression vector with 5546 bp (Novagen), further mentioned as p7, for the cloning of the gene constructs to be expressed in *E. coli*. The maps of pD and p7 can be found in **Annex I**, in **Figures Annex I-1** and **Annex I-2**, respectively.

Each monomeric gene fragment of SKS-IKVAV and SKS-PPFLM (Nzytech) had 456 bp and the complete gene corresponded to 6 inserts.

5.1.3. Molecular biology kits

To purify the DNA plasmid from the bacteria, the NucleoSpin® Plasmid kit (Macherey-Nagel) was employed while the PureLink® Quick Gel Extraction kit (Invitrogen) was used for the purification of DNA fragments from agarose gels.

5.1.4. Bacterial strains

The *E. coli* strains used in the work were:

- XL1-Blue, *recA1 endA1 gyrA96 thi-1 hsdR17 supE44 relA1 lac [F´ proAB lacIqZΔM15 Tn10 (Tet)]*.

- BLR (DE3) (Novagen), *F- ompT hsdSB (rB- mB-) gal dcm Δ (srl-recA) 306::Tn10 (Tet) (DE3)*.

5.1.5. Culture media for bacterial growth

The culture media used for *E. coli* growth and transformation were Luria-Broth (LB) (Conda) 25 g/L; LB-Agar: 25 g/L (LB, Conda) and 1.5 % (p/v) (Agar, Fluka); Expression medium: 55.85 g/L Terrific Broth (TB) (Formedium), 8 mL/L glycerol and 100 µL defoamer; Fermenter medium: 1/3 of 25 g/L LB (Conda), 2/3 of 55.85 g/L of TB (Formedium), 8 mL/L glycerol and 100 µL/L defoamer; and SOC I (Sigma Aldrich).

5.1.6. Enzymes

The restriction enzymes used were: *Ear* I (isoschizomer *Eam*I 104I), *EcoR* I, *Nde* I, *Ssp* I (FastDigest enzymes, ThermoFisher Scientific), and *Sap* I (isoschizomer *Lgu*I) (ThermoFisher Scientific). For the cloning of the gene constructs were also used the T4 DNA Ligase, the shrimp alkaline phosphatase (S.A.P.) and the FastAP (ThermoFisher Scientific). All the enzymes were used as per manufacturer protocol.

5.1.7. Buffer solutions

The buffer solutions used are listed in **Table 5-2**.

Table 5-2 — List of buffer solutions

Buffer solution	Composition or supplier
DNA LB 5X loading buffer	30 % (v/v) glycerol, 0.1 % (w/v) SDS, 0.05 % (w/v) BPB, 50 mM tris pH 8, 0.05 mM EDTA
FastAP Buffer 10X	ThermoFisher Scientific
FastDigest buffer 10X	ThermoFisher Scientific
Protein loading buffer 5X	0.3 M tris pH 6.5, 10 % (w/v) SDS, 50 % (v/v) glycerol, 25 % (v/v) β-mercaptoethanol, 2 % (v/v) BPB
S.A.P. buffer 10X	ThermoFisher Scientific
SDS-PAGE running buffer	25 mM tris-base pH 8.3, 192 mM glycine and 0.1 % (w/v) SDS
T4 DNA Ligase buffer 10X	ThermoFisher Scientific
Tris acetate EDTA (TAE) 1X	40 mM tris-base pH 8, 1 mM EDTA, 20 mM glacial acetic acid
Tango buffer 10X	ThermoFisher Scientific

5.2. Methods

The scheme in **Figure 5-1** demonstrates the strategy used to obtain the SKS-IKVAV and SKS-PPFLM polymers using *E. coli* strains. The use of *E. coli* as a bacterial host in the production of recombinant proteins is justified due to its fast growth rate, easiness to manipulate and ability to grow at different temperatures and nutrient sources [103].

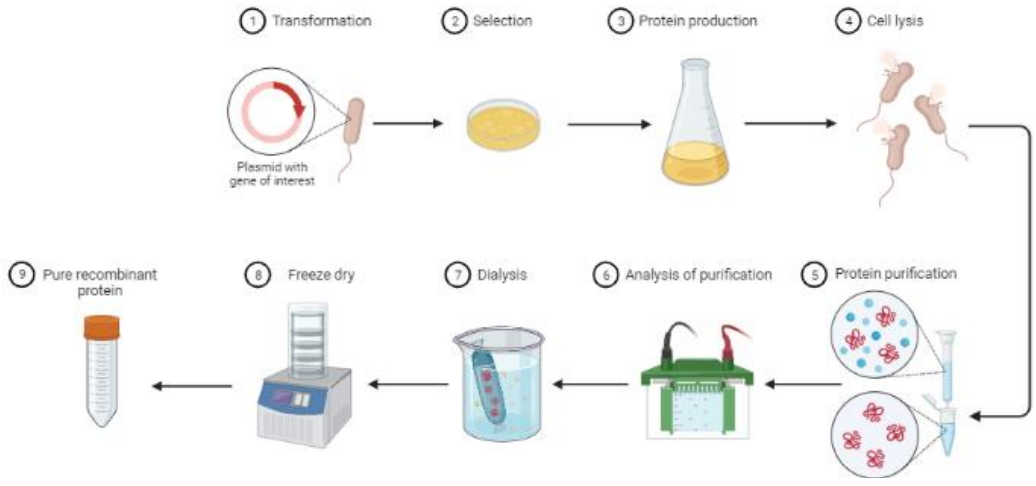

Figure 5-1 — Strategy of production of recombinant proteins using *E. coli*. Created with BioRender.com.

Since the purification protocols of the SKS-IKVAV and SKS-PPFLM proteins were not developed, the steps 5 to 9 were not carried out and, as an NDA was signed with TPNBT, the protocols of the first four phases are described with some details omitted.

5.2.1. Genetic engineering of SKS-IKVAV and SKS-PPFLM genes

In order to obtain SKS-IKVAV and SKS-PPFLM genes it was necessary to resort to genetic engineering approach due to the artificial nature of the ELRs.

As the complete synthetic gene expressing the entire recombinamer is challenging to attain given methodological and technical limitations, the repetitive structure of the recombinamers allows seamless splicing of monomer DNA segments, also referred to as inserts, to create multimerized genes [104].

Hence, the monomeric genes encoding the repetitive sequence of SKS-IKVAV and SKS-PPFLM were obtained, and the iterative-recursive method was applied to construct the polymeric genes, relying on the use of *Ear* I and *Sap* I enzymes, since type IIS endonucleases leave cohesive ends that allow the insertion of DNA fragments into the plasmid of interest [104,105].

Under this strategy, the ELRs genes sequences had to be flanked by two *Ear* I restriction sites for excision of inserts from the cloning vector, and by one *Sap* I restriction site for linearization of the vector. In addition, the cloning vector could not have any endogenous *Sap* I restriction sites [104].

5.2.1.1. DNA digestion with restriction enzymes

DNA digestion with restriction enzymes comprised the fast and preparative digestion protocols and both were performed according to the manufacturer and results were verified by DNA agarose gel electrophoresis.

The enzymes used for fast digestion were *Ear* I, *EcoR* I, *Nde* I, and *Ssp* I from the FastDigest range. Since the ELRs gene sequences were flanked by two *Ear* I restriction sites, *Ear* I was the most commonly used enzyme.

The fast digestion solution with a final volume of 5 µL consisted of type I water, 0.5 µL FastDigest buffer 10X, 200 ng of plasmid containing the ELR gene sequence, and 0.5 µL FastDigest enzyme(s) (1 µL of FastDigest enzyme digests 1 µL of DNA, and more than the minimum volume was used to ensure total digestion). The solution was then centrifuged at 11000 rpm for 1 min at room temperature and incubated for up to 2 h at 37 °C. Afterwards, it was heat shocked at 80 °C for 5 min to inactivate the enzyme.

The preparative digestion solution with a final volume of 20 µL consisted of type I water, 2 µL Tango buffer 10X, 3 µg of plasmid, and 1.2 µL of *Sap* I. The solution was centrifuged at 11000 rpm for 1 min at room temperature and incubated at 37 °C overnight.

5.2.1.2. DNA dephosphorylation

DNA dephosphorylation was conducted with the FastAP enzyme after a preparative digestion and with the S.A.P. following the purification of DNA fragments from an agarose gel.

To 20 µL of preparative digestion solution was added 2.55 µL of FastAP buffer 10X and 3 µL of FastAP. The reaction mixture was then incubated for 10 min at 37 °C and the enzyme was inactivated at 75 °C for 5 min.

Following plasmid retrieval from the agarose gel, 3 µL of S.A.P. buffer 10X and 1 µL of S.A.P. were added to 30 µL of DNA. The reaction was incubated at 37 °C for 1 h and the enzyme inactivated at 80 °C for 5 min.

5.2.1.3. DNA agarose gel electrophoresis

Two DNA agarose gel electrophoresis protocols were used depending on the DNA application. If the objective was to verify the aa sequence of the plasmid, the analytical protocol was used, however, if the aim was to recover DNA fragments after the electrophoresis, the preparative protocol was used.

The agarose concentration in TAE 1X buffer was selected according to the DNA fragment size to be isolated in the gel (**Table 5-3**).

Table 5-3 — Relation between fragment size and agarose final percentage in TAE 1X

Fragment size (bp)	Agarose final % in TAE 1X (w/v)
800 - 1000	0.8
400 - 8000	1
300 - 7000	1.2
200 - 4000	1.5
100 - 2000	2

Each gel was prepared by adding the agarose to 30 mL of TAE 1X buffer in a 250 mL Erlenmeyer flask. The mixture was then melted in a microwave and the concentration was adjusted by adding type I water. After cooling the solution, it was casted in a horizontal mold with a comb of 10 or 15 wells depending on the number of samples.

A variable volume of DNA LB 5X loading buffer was added to the DNA samples (6 µL for samples with FastAP and 5 µL with no FastAP).

Following the formation of the gel, each DNA sample (5 µL in the analytical electrophoresis and the total volume in the preparative) and 4 µL of the molecular weight marker (MW) 1 kb Plus Ladder (**Figure 5-2**), were loaded to the wells and ran at a given voltage, current, and time, which depended on whether the technique was analytical (90 Volts constant, 400 mA for 60 min) or preparative (60 Volts constant, 400 mA for 120 min).

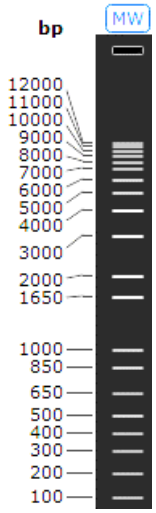

Figure 5-2 — 1 kb Plus Ladder in 1 % agarose gel, retrieved from SnapGene® software.

At the end of the run, the gel was removed from its mold, the DNA bands were stained with a 1X safe DNA stain (40 mL of TAE 1X and 2 µL of SYBR™ Safe DNA Gel Stain) for 30 min at room temperature and visualized on a Bio-Rad Gel Doc EZ Imager, using the Image Lab™ software. The image retrieved was always compared with the theoretical restriction map of the samples obtained with SnapGene® software.

5.2.1.4. DNA fragments purification from an agarose gel

To obtain DNA fragments from an agarose gel, a minimum quantity of agarose gel containing the desired band was removed with a scalpel during UV light visualization rapidly to avoid DNA mutations. Then, the recovered gel bands were weighed, and the DNA was purified using the PureLink® Quick Gel Extraction kit (Invitrogen) as per the manufacturer protocol.

After, the concentration of the samples was measured and their purity assessed with the Nano Drop 2000c Spectrophotometer (ThermoFisher Scientific), using the NanoDrop2000 software. A 260nm/280nm ratio equal or in between 1.80 and 2.00 indicated that the DNA is pure, and no aromatic compounds, RNA, salts, carbohydrates, or phenolic contaminations are present.

5.2.1.5. DNA insert ligation (sticky-end) into vector DNA

The DNA insert ligation (sticky-end) into vector DNA was performed after obtaining the dephosphorylated vector and the gene fragment(s) with compatible sticky ends.

Hence, 70 ng of linear vector and the insert gene fragment(s) - with a molar ratio of 1:5 - were incubated in a solution with a final volume of 10 µL of type I water, 1 µL 10X T4 DNA Ligase buffer, and 1 µL of T4 DNA Ligase enzyme. The solution was centrifuged at 11000 rpm for 1 min at room temperature and incubated at room temperature for 3 h 30 min. The T4 DNA Ligase was then inactivated by incubating the mixture for 10 min at 65 °C.

5.2.1.6. Transformation of *E. coli* competent cells

The transformation of competent cells was performed in XL1-Blue competent and in XL1-Blue subcloning competent *E. coli* strains. These strains have different transformation efficiencies, ≥ 1 x 10^8 and ≥ 1 x 10^6 transformants per microgram of DNA, respectively, and are used for gene cloning and manipulation. Additionally, BLR (DE3) competent cells, with an efficiency of ≥ 2 x 10^6 transformants per microgram of DNA, were also transformed for protein expression.

For the transformation of the XL1-Blue competent cells was added 5 µL of the ligation reaction solution to 50 µL of bacteria and 1.7 µL of β-mercaptoethanol in a pre-chilled 14-mL BD Falcon polypropylene round-bottom tube (Stratagene). The solution was incubated in ice for 30 min and then submitted to a thermic shock at 42 °C for 45 s, being after placed in ice for 2 min. Subsequently, 450 µL of pre-heated SOC I medium at 42 °C was added to the cells and the solution was putted in an incubator at 37 °C, 250 rpm for 1 h.

Finally, a volume of 50 µL or 100 µL of cells were platted on petri dishes with LB-Agar medium, supplemented with kanamycin or ampicillin if the ligation was performed using the pD or the p7 vector, respectively. The plates were then incubated overnight at 37 °C.

Some modifications were done when transforming the subcloning and the BLR (DE3) strains. To transform the XL1-Blue subcloning competent cells were only used 10 µL of *E. coli*, 1 µL of ligation reaction solution, the first incubation on ice was for 20 min and the heat-pulse at 42 °C was for 30 s.

To transform the BLR (DE3) competent cells was used 250 µL of cells without β-mercaptoethanol, 400 ng of plasmid DNA and the thermic shock was submitted for 2 min. Additionally, 250 µL of pre-warmed LB medium at 37 °C were used instead of SOC I medium.

5.2.1.7. Plasmid purification from bacteria

The day following *E. coli* strains transformation, the bacteria were incubated overnight in LB medium with the appropriate antibiotic depending on the vector used (kanamycin for the cloning and ampicillin for the expression vector). After, the plasmids were purified using the NucleoSpin® Plasmid kit (Macherey-Nagel) and their concentration and purity were measured

with the Nano Drop 2000c Spectrophotometer (ThermoFisher Scientific), using the NanoDrop2000 software.

After purification of the plasmids and bacterial gene fragments, the samples were sequenced to compare the DNA sequences of the samples with the theoretical sequences. For sequencing the genes cloned in the pD plasmid, were used primers T7 and Sp6 while for genes cloned in the p7 vector, primers T7 and T7ter were employed.

5.2.1.8. Expression screening

After confirmation of the gene sequences cloned in the p7 vector, BLR (DE3) cells harboring the p7 :: ELRs constructs were grown in expression medium (55.85 g/L TB medium, 8 mL/L glycerol and 100 µL of defoamer, 5 mL of the expression medium in a 50 mL falcon) with 5 µL of ampicillin at 37 °C and 250 rpm overnight. The negative control consisted in BLR (DE3) cells harboring the p7 :: ELRs constructs grown in 5 mL of TB medium and 5 µL of ampicillin.

5.2.1.9. Sodium dodecyl sulfate polyacrylamide gel electrophoresis (SDS-PAGE)

To assess if the ELRs proteins were expressed, their expression pattern was analyzed by sodium dodecyl sulfate polyacrylamide gel electrophoresis (SDS-PAGE) with a 10 % resolving gel.

Samples were prepared by adding 20 µL of cells previously centrifuged at 11000 rpm for 1 min and 5 µL protein loading buffer 5X to an Eppendorf tube. The samples were then boiled for 5 min at 100 °C and were then centrifuged for 5 min at 13400 rpm. The samples and the protein weight marker (Unstained Protein Molecular Weight Marker (ThermoFisher Scientific) in **Figure 5-3**) were loaded into the polyacrylamide gel and the electrophoresis was ran in a "MiniVe vertical electrophoresis system" from Hoefer (Amersham Pharmacia Biotech) using the following conditions: 300 V (variable) and 25 mA (constant) for 80 – 120 min.

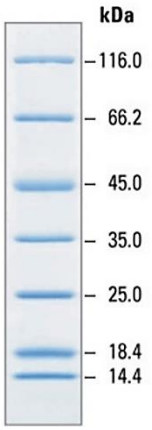

Figure 5-3 — Unstained Protein Molecular Weight Marker. Adapted from [106].

To form the resolving gel, the total percentage of acrylamide (% T) was chosen according to the molecular weight of the ELRs to be separated, as shown in **Table 5-4**.

Table 5-4 — Correspondence between target size range and percentage in separation gel

Target size range (kDa)	% T in separation gel
24 - 205	7.5
14 - 205	10
14 - 66	12.5
14 - 45	15

Furthermore, the resolving and stacking gel compositions are illustrated in **Table 5-5**.

Table 5-5 — SDS-PAGE resolving and stacking gel composition (one gel)

One gel	Resolving gel				Stacking gel
	7,5 %	**10 %**	**12 %**	**15 %**	**4 %**
Type I H_2O	4.10 mL	3.63 mL	3.25 mL	2.69 mL	1.585 mL
Tris 1.5 M (pH = 8.8)	1.88 mL	1.88 mL	1.88 mL	1.88 mL	-
Tris 0.5 M (pH = 6.8)	-	-	-	-	0.625 mL
Acrylamide 40 %	1.40 mL	1.875 mL	2.25 mL	2.81 mL	250 µL
SDS 10 %	75 µL	75 µL	75 µL	75 µL	18.75 µL
APS 10 %	37.5 µL	37.5 µL	37.5 µL	37.5 µL	18.75 µL
TEMED	3.75 µL	3.75 µL	3.75 µL	3.75 µL	2.35 µL
Total Volume	**7.5 mL**	**7.5 mL**	**7.5 mL**	**7.5 mL**	**2.5 mL**

The resolution gel used was 10 % since the SKS-IKVAV protein is 75946 kDa and the SKS-PPFLM protein is 76980 kDa.

Following the termination of SDS-PAGE, the gel was stained with copper chloride solution (0.3 M) for 10 min with constant agitation to visualize the proteins and the expression pattern (protein bands) was visualized on a Bio-Rad Gel Doc EZ Imager, using the Image Lab™ software.

5.2.1.10. Glycerol stock preparation

After analyzing the expression screening results, the clones that best expressed the ELRs of interest were selected and conserved by preparing glycerol stocks.

The positive colony was grown in 5 mL LB medium supplemented with 1 % glucose and 1 % of ampicillin at 37 °C and 250 rpm until reaching an optical density at a wavelength of 600 nm (OD_{600nm}) of 0.6 – 0.8. Subsequently, 0.9 mL of these bacterial suspensions and 0.1 mL of 80 % sterile glycerol were added to a cryovial. The glycerol stock was then conserved at – 80 °C to ensure total preservation.

5.2.2. Bioproduction of SKS-IKVAV and SKS-PPFLM polymers

The polymer ELRs were bioproduced using two distinct methods. The SKS-IKVAV protein was produced in Erlenmeyer flasks, while the SKS-PPFLM protein was produced in a fermenter.

Initially two pre-inoculums were prepared, each in 5 mL of LB medium supplemented with ampicillin, 250 µL of glucose 20 %, and the corresponding transformed cells were grown at 37 °C overnight with constant agitation (250 rpm). After this period, two subcultures were prepared using 30 mL of LB medium, 30 µL of ampicillin, 1.5 mL of glucose 20 % and 100 µL of corresponding pre-inoculum in each. Then, each inoculum was prepared in two 2 L Erlenmeyer flasks, each with 15 mL of subculture, 500 mL of LB-Agar medium, 1 % antibiotic and 1 % glucose. The inoculums were then grown at 37 °C with constant agitation (250 rpm) for 2 h.

After the 2 h incubation period, the SKS-IKVAV inoculum was used to inoculate 2 L Erlenmeyer flasks, each with 500 mL of fermenter medium (final volume of 8 L).

The SKS-PPFLM protein was produced using a 20 L bioreactor (Applicon bioreactor (ADI 1025, ADI 1032, ADI 1010, USA)). After the 2 h incubation period, the SKS-PPFLM inoculum was used to inoculate the fermenter, which had 10 L of TB medium with glycerol and defoamer and 4 L of LB medium (final volume of 15 L). The higher volume of TB medium in the fermenter medium was justified due to the TB richer nutritional composition when compared to the LB medium.

To prepare the negative controls, the inoculums were grown each in 5 mL of TB medium supplemented with ampicillin at 37 °C with constant agitation (250 rpm) overnight.

The optimal culture conditions used for SKS-IKVAV protein expression was 37 °C and 250 rpm and for SKS-PPFLM was 37 °C, 500 rpm, 20 L/min air flow and pH 7.0, having both productions been left overnight to induce the maximum of protein expression.

The bacterial growth in the fermenter and Erlenmeyer flasks was monitored through absorbance measurements. If the peak of absorbance (600 nm) was reached (two contiguous measurements with similar OD_{600nm} values or the second measure was lower than the first), the bioproduction was immediately stopped.

5.3. Results and discussion

The first part of this dissertation, developed at TPNBT, was focused on the synthesis of SKS-IKVAV and SKS-PPFLM genes. After gene synthesis, the expression of these proteins was tested.

5.3.1. Genetic engineering of SKS-IKVAV and SKS-PPFLM genes

The synthesis of the recombinant SKS-IKVAV and SKS-PPFLM genes was carried out in parallel at each step of the process in order to optimize resources.

5.3.1.1. Cloning vector pDrive All

Initially it was necessary to obtain cloning plasmids to insert the first SKS-IKVAV/SKS-PPFLM gene fragment. For this purpose, pD plasmids were inserted in XL1-Blue subcloning competent cells and the concentration and purity of pD plasmid samples were analyzed after their purification from bacteria (**Table 5-6**).

Table 5-6 – Concentration (ng/µL) and degree of purity of pD plasmids after purification

Sample	Concentration (ng/µL)	Purity (260nm/280nm)
pD 1	1175.9	1.88
pD 2	1200.3	1.89
pD 3	493.5	1.89

All samples presented high DNA concentration and purity. However, for the first insertion of the gene fragments, the sample pD 2 was selected due to its higher DNA concentration.

Afterwards, pD 1, 2 and 3 underwent a fast digestion with the *Ear* I endonuclease and an analytical agarose gel (1 %) electrophoresis was performed to verify if the characteristics bands of the plasmid were obtained after *Ear* I digestion. The experimental result (**Figure 5-4 A)**) were

compared with the theoretical restriction map of the pD vector obtained with the *Ear* I restriction enzyme (**Figure 5-4 B)**).

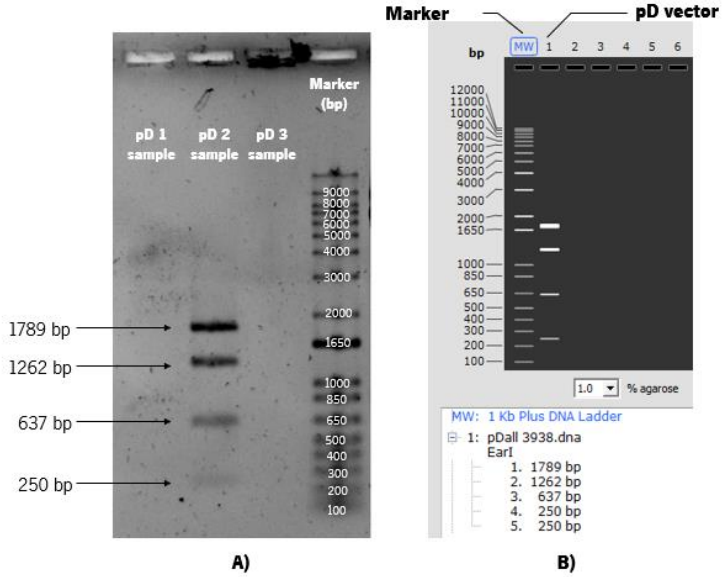

Figure 5-4 — A) Analytical agarose gel (1 %) electrophoresis of pD 1, pD2 and pD3 vectors digested with *Ear* I endonuclease (Image Lab™). **B)** Theoretical restriction map of pD vector digested with *Ear* I (SnapGene®).

Analyzing the results of the electrophoresis, no bands were detected after digestion with the *Ear* I enzyme for samples pD 1 and pD 3. These results were most likely related with pipetting problems on the agarose gel (the volume of sample used was not enough for the bands to be noticeable). However, since the use of sample 2 was foreseen (higher DNA concentration) and the restriction map obtained for this sample agreed with the bands expected, the experiment was not repeated for pD1 and pD3 samples.

The three samples (pD 1, pD 2, and pD 3) were sequenced with the appropriate primers of pD vector (T7 and Sp6) and the results were analyzed with the SnapGene® software, having been concluded that, due to the irrelevant quantity of mismatches and gaps presented in their sequence, the three samples would be suitable for use in future experiments. Since a confidentiality agreement has been signed with TPNBT, the sequenced samples were not presented in this master dissertation.

The pD 2 plasmid was linearized using *Sap* I endonuclease (**Figure 5-5 A)**). The digestion of the plasmid was compared to the theoretical restriction map obtained using the SnapGene

software. After confirmation of vector linearization, the band corresponding to the linearized pD vector was excised (**Figure 5-5 B)**).

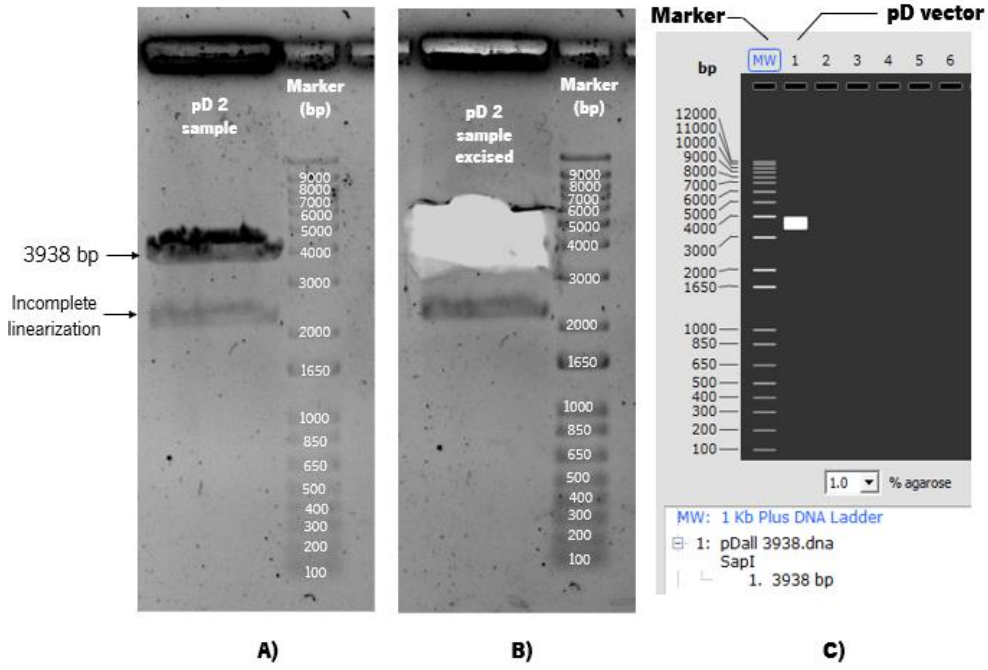

Figure 5-5 — A) Preparative agarose gel (1 %) electrophoresis of pD 2 vector digested with *Sap* I endonuclease (Image Lab™). **B)** Excision of the band corresponding to the linearized pD2 vector (Image Lab™). **C)** Theoretical restriction map of pD vector digested with *Sap* I (SnapGene®).

Despite the band corresponding to the linearized pD vector was present in the experimental agarose gel, another band was observed between 2000 – 3000 bp. This band indicated that the linearization was not complete, corresponding to one of the isoforms of the non-linearized vector. Since a good concentration of linearized vector was obtained, the restriction with *Sap* I enzyme was not repeated. After DNA purification, the DNA concentration and purity of the sample were determined (**Table 5-7**).

Table 5-7 – Concentration (ng/µL) and degree of purity of linearized pD 2 vector

Sample	Concentration (ng/µL)	Purity (260nm/280nm)
pD 2	47.7	1.67

It is important to note that the purity (260nm/280nm = 1.67) of the plasmid was not within the reference values (1.8 - 2.00). However, previous laboratory experience indicated that this value was not reliable for DNA obtained after a purification from an agarose gel. Moreover, data

showed that this degree of purity did not affect the ligation and cloning steps of SKS-IKVAV and SKS-PPFLM gene fragments. Thereafter, the plasmid pD 2 underwent a DNA dephosphorylation and was further used for cloning purposes.

5.3.1.2. SKS-IKVAV and SKS-PPFLM inserts

The linearized pD 2 plasmid was then used to clone the SKS-IKVAV and SKS-PPFLM DNA inserts previously obtained with *Ear* I endonuclease. The cloning strategy was based on compatible sticky ends obtained by using the *Sap* I enzyme for the pD plasmid and the *Ear* I for the ELRs inserts.

For the preparation of the ELRs inserts, XL1-Blue subcloning competent cells were transformed with the commercial plasmids containing one insert of the SKS-IKVAV or with one insert of the SKS-PPFLM gene. Afterwards, four positive transformants of each ELR were selected, the plasmids were purified, and their concentration and purity were assessed (**Table 5-8**).

Table 5-8 — Concentration (ng/µL) and degree of purity of commercial plasmids with the SKS-IKVAV or SKS-PPFLM insert

Sample	Concentration (ng/µL)	Purity (260nm/280nm)
Commercial plasmid :: SKS-IKVAV 1	576.1	1.89
Commercial plasmid :: SKS-IKVAV 2	820.2	1.89
Commercial plasmid :: SKS-IKVAV 3	658.9	1.86
Commercial plasmid :: SKS-IKVAV 4	595.2	1.89
Commercial plasmid :: SKS-PPFLM 1	738.6	1.89
Commercial plasmid :: SKS-PPFLM 2	626.1	1.86
Commercial plasmid :: SKS-PPFLM 3	5.6	2.47
Commercial plasmid :: SKS-PPFLM 4	288.0	1.90

All samples presented good purity and DNA concentration with the exception of sample commercial plasmid :: SKS-PPFLM 3. Commercial plasmid :: SKS-IKVAV 2 and commercial plasmid::SKS-PPFLM 1 were selected for ELR insert purification.

The plasmids containing the SKS-IKVAV and SKS-PPFLM genes were digested with the *Sap* I endonuclease to obtain the inserts for cloning into the linearized pD vector. Samples were run in an agarose (1 %) preparative gel (**Figure 5-6**).

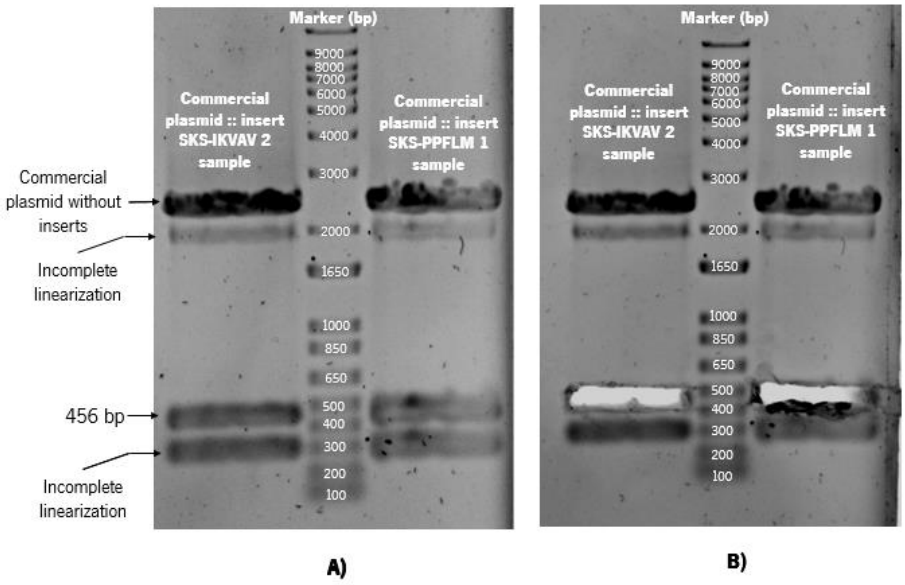

Figure 5-6 — A) Preparative agarose gel (1 %) electrophoresis of commercial plasmid :: SKS-IKVAV 2 and commercial plasmid :: SKS-PPFLM 1 digested with *Sap* I endonuclease (Image Lab™). **B)** Excision of the bands corresponding to the linearized SKS-IKVAV and SKS-PPFLM inserts (Image Lab™).

After digestion of the commercial plasmids harboring the SKS-IKVAV and the SKS-PPFLM genes with *Sap* I, were obtained different bands, which correspond to the vector without inserts (2710 bp), the gene fragments (456 bp) and to non-digested, or partial digested plasmid. After excised the bands form the gel, the genes were purified, and the concentration and degree of purity were evaluated (**Table 5-9**).

Table 5-9 — Concentration (ng/µL) and degree of purity of SKS-IKVAV and SKS-PPFLM inserts after purification

Sample	Concentration (ng/µL)	Purity (260nm/280nm)
SKS-IKVAV 2	11.7	1.68
SKS-PPFLM 1	8.3	2.25

5.3.1.3. SKS-IKVAV and SKS-PPFLM genes insertion in the pDrive All plasmid

After purification, the SKS-IKVAV and SKS-PPFLM genes were cloned in two distinct ligation reactions, into the linearized pD vectors. After transformation of XL1-Blue competent cells with the pD :: SKS-IKVAV and pD :: SKS-PPFLM ligation reactions, were obtained transformants for both gene constructs.

A screening of positive transformants for each gene was performed after plasmid purification. The cloning strategy here used allowed the insertion of one insert (SKS-IKVAV 1x or SKS-PPFLM 1x) or several inserts (SKS-IKVAV nx or SKS-PPFLM nx). The nomenclature used gives information on the number of inserts cloned into the cloning vector and transformant analyzed. The concentration and purity of the plasmids containing the inserts was evaluated (**Table 5-10**).

Table 5-10 — Concentration (ng/µL) and degree of purity of pD vector harboring the SKS-IKVAV or SKS-PPFLM inserts

Sample	Concentration (ng/µL)	Purity (260nm/280nm)
pD :: SKS-IKVAV 1x 1	758.3	1.89
pD :: SKS-IKVAV 1x 2	711.4	1.90
pD :: SKS-IKVAV 1x 3	736.5	1.90
pD :: SKS-IKVAV 1x 4	688.7	1.91
pD :: SKS-PPFLM 1x 1	604.7	1.88
pD :: SKS-PPFLM 1x 2	596.4	1.89
pD :: SKS-PPFLM 1x 3	735.1	1.92
pD :: SKS-PPFLM 1x 4	705.8	1.90

All DNA samples presented good DNA concentrations and high purity degree. The pD :: SKS-IKVAV 1x 1 and the pD :: SKS-PPFLM 1x 3 plasmids were selected for the next cloning steps (gene size amplification – number of repetitions) as they presented the highest DNA concentrations.

An analytical agarose (1 %) gel was performed to verify if the pD plasmids had the SKS-IKVAV or the SKS-PPFLM inserts, and the numbers of inserts cloned. The DNA samples were digested with *Ear* I and *EcoR* I and were analyzed (**Figure 5-7**).

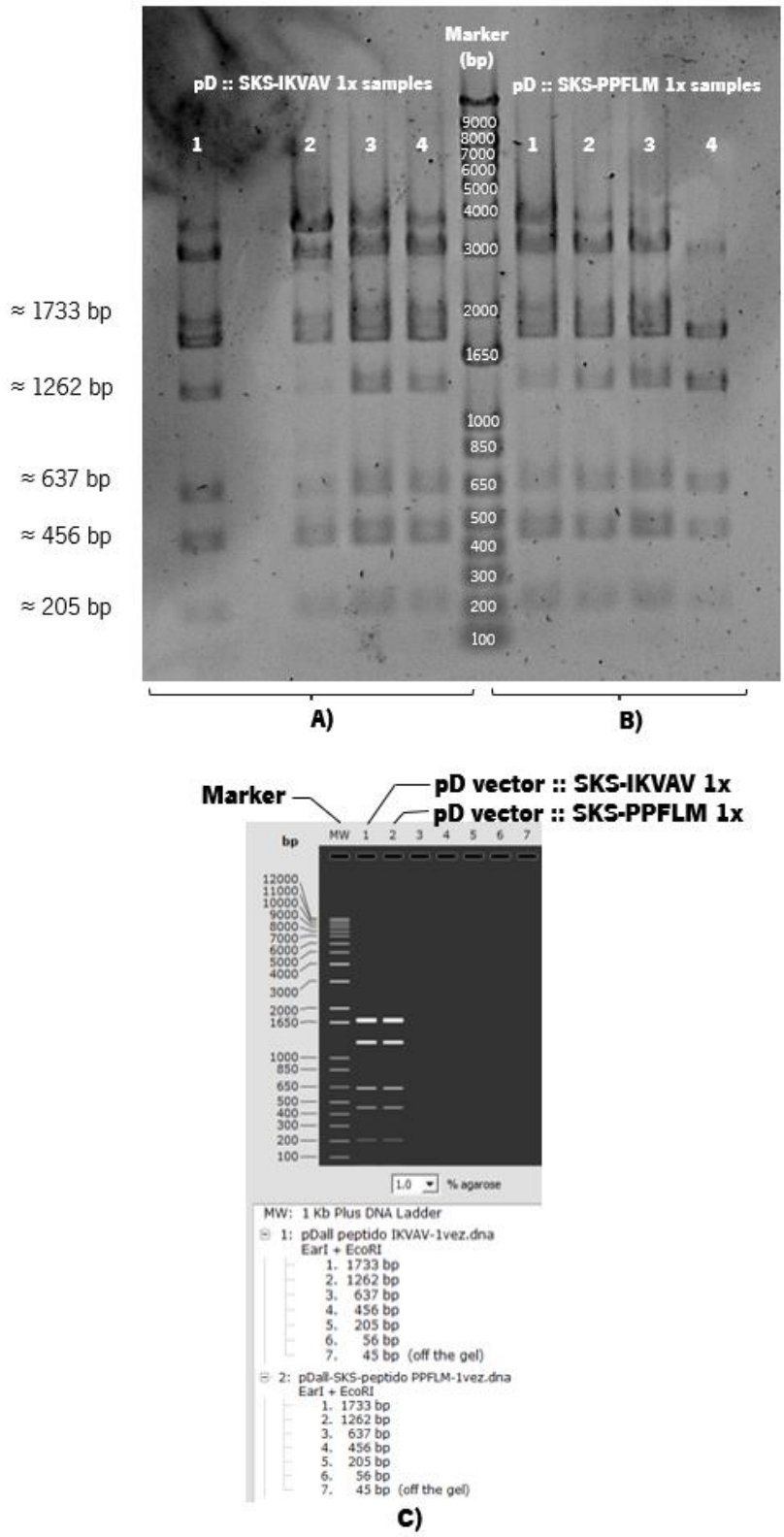

Figure 5-7 — Analytical agarose gel (1 %) electrophoresis of **A)** pD :: SKS-IKVAV 1x and **B)** pD :: SKS-PPFLM 1x. The DNA samples were digested with *Ear* I and *EcoR* I endonucleases (Image Lab™). **C)** Theoretical restriction map of pD :: SKS-IKVAV 1x and pD :: SKS-PPFLM 1X vectors digested with *Ear* I and *EcoR* I (SnapGene®).

Analyzing the results, the electrophoretic pattern observed was different from the theoretical. Despite the bands corresponding to one repetition of the SKS-IKVAV or the SKS-PPFLM (456 bp) genes and the bands from the digestion of the plasmid with the *Ear* I (1733 bp, 1262 bp, 637 bp and 205 bp) were observed, other bands higher than 2000 bp were also found. These bands might correspond to non-linearized plasmid. The plasmids with the genes were sequenced (data not shown) and the results confirmed the correct insertion of the SKS-IKVAV and SKS-PPFLM genes into the pD vector.

After successfully cloning the SKS-IKVAV and SKS-PPFLM genes in the pD vector, the size of the genes was increased by increasing the number of repetitions until six repetitions (SKS-IKVAV 6x and SKS-PPFLM 6x) using the iterative/recursive approach.

To confirm the correct insertion of the inserts, the pD :: SKS-IKVAV 6x and pD :: SKS-PPFLM 6x samples underwent a fast digestion with the *EcoR* I and *Ssp* I enzymes and an analytical agarose gel (1 %) electrophoresis was performed (**Figure 5-8**).

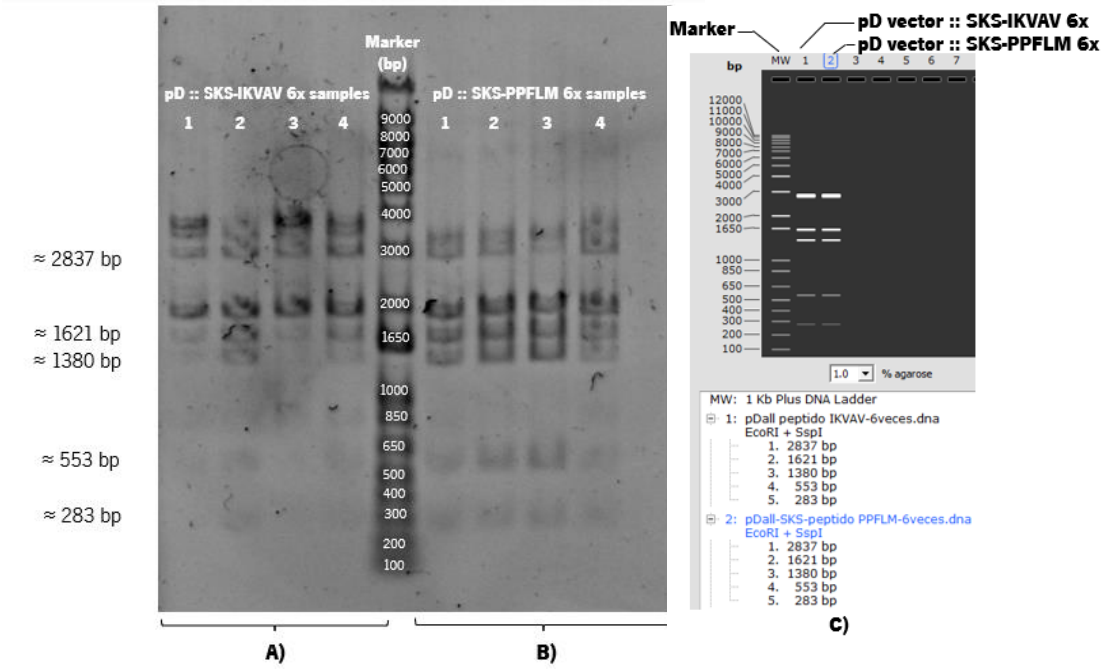

Figure 5-8 — Analytical agarose gel (1 %) electrophoresis of **A)** pD :: SKS-IKVAV 6x and **B)** pD :: SKS-PPFLM 6x. The DNA samples were digested with *EcoR* I and *Ssp* I endonucleases (Image Lab™). **C)** Theoretical restriction map of pD :: SKS-IKVAV 6x and pD::SKS-PPFLM 6x vectors digested with *EcoR* I and *Ssp* I (SnapGene®).

Analyzing the results obtained in the experimental agarose gel, two bands (around 2000 bp and between 3000 and 4000 bp) were identified in addition to the theoretical pattern. These additional bands might correspond to non-linearized isoforms of the samples. The selected plasmids were further sequenced and the genetic sequences of the SKS-IKVAV 6x and SKS-PPFLM 6x genes were confirmed.

5.3.1.4. SKS-IKVAV and SKS-PPFLM genes insertion in the p7RARE plasmid

After confirmation of SKS-IKVAV and SKS-PPFLM genes sequences with six repetitions, the inserts were cloned into the p7RARE plasmid using the strategy previously used for the cloning in the pD plasmid. The p7, pD :: SKS-IKVAV and pD :: SKS-PPFLM plasmids were purified from XL1-Blue transformants and their concentration and degree of purity were analyzed (**Table 5-11**).

Table 5-11 — Concentration (ng/µL) and degree of purity of p7, pD :: SKS-IKVAV and pD :: SKS-PPFLM plasmids after purification

Sample	Concentration (ng/µL)	Purity (260nm/280nm)
p7 1	103.6	1.90
p7 2	103.2	1.92
p7 3	99.9	1.89
pD :: SKS-IKVAV 1	327.3	1.91
pD :: SKS-IKVAV 2	323.3	1.90
pD :: SKS-PPFLM 1	479.2	1.92
pD :: SKS-PPFLM 2	465.2	1.92

After purification, the p7 samples were digested with the *Sap* I endonuclease to linearize the vector, and the pD :: SKS-IKVAV 1 and pD :: SKS-PPFLM 1 samples were digested with *Ear* I to obtain the genes. The samples were run in an agarose gel (1 %), the bands corresponding to the linearized p7 plasmid, to the SKS-IKVAV 6x and SKS-PPFLM 6x genes were excised from the gel (**Figure 5-9**) and were further purified and characterized regarding their concentration and degree of purity (**Table 5-12**).

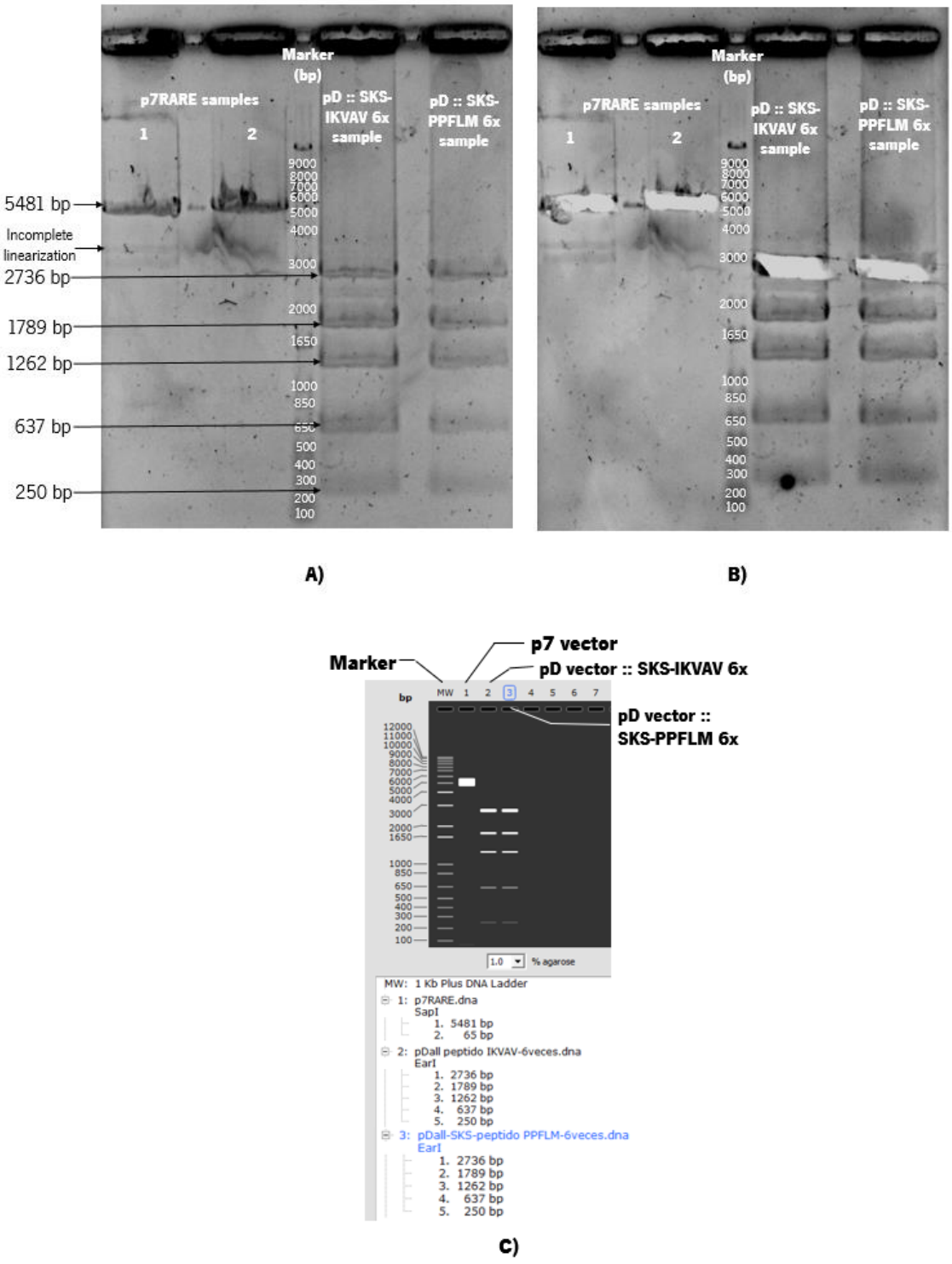

Figure 5-9 — A) Preparative agarose gel (1 %) electrophoresis of p7 vector digested with *Sap* I endonuclease and pD :: SKS-IKVAV 6x 1 plasmid and pD :: SKS-PPFLM 6x 3 plasmids digested with *Ear* I endonuclease (Image Lab™). **B)** Excision of the bands corresponding to the linearized p7 vectors, SKS-IKVAV and SKS-PPFLM inserts (Image Lab™). **C)** Theoretical restriction map of p7 vector and pD :: SKS-IKVAV/SKS-PPFLM plasmids digested with *Sap* I and *Ear* I, respectively (SnapGene®).

Table 5-12 — Concentration (ng/µL) and degree of purity of p7 plasmid, SKS-IKVAV 6x and SKS-PPFLM 6x genes after purification

Sample	Concentration (ng/µL)	Purity (260nm/280nm)
p7 1	32.2	1.75
p7 2	19.5	1.53
SKS-IKVAV 6x gene	14.9	1.77
SKS-PFLM 6x gene	17.4	1.99

After cloning of the SKS-IKVAV 6x and SKS-PPFLM 6x genes into the expression plasmids, several positive transformants of XL1-Blue competent cells were obtained for both genes and were analyzed by analytical agarose gel (1 %) electrophoresis after a fast digestion with the *EcoR*I and *Nde* I enzymes (**Figure 5-10**).

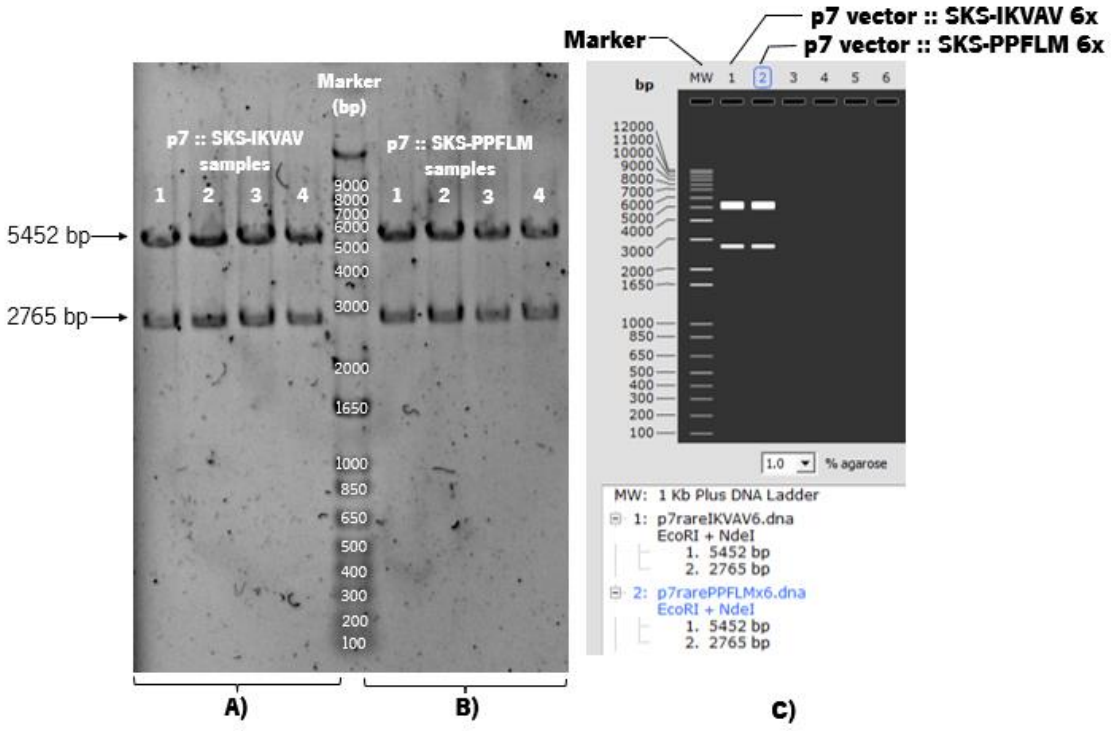

Figure 5-10 — Analytical agarose gel (1 %) electrophoresis of **A)** p7 :: SKS-IKVAV 6x and **B)** p7 :: SKS-PPFLM 6x. The DNA samples were digested with *EcoR*I and *Nde* I endonucleases (Image Lab™). **C)** Theoretical restriction map of p7 :: SKS-IKVAV 6x and p7::SKS-PPFLM 6x vectors digested with *EcoR*I and *Nde* I (SnapGene®).

The results obtained in **Figure 5-10** confirmed the successful cloning of the SKS-IKVAV 6x and SKS-PPFLM 6x genes in the p7 expression vector. The gene sequences were further confirmed (data not shown) and the plasmids were used to transform *E. coli* strain suitable for protein expression.

5.3.2. Bioproduction of SKS-IKVAV and SKS-PPFLM polymers

The expression strain *E. coli* BLR (DE3) was transformed with the p7 vectors harboring the SKS-IKVAV 6x and the SKS-PPFLM 6x ELRs genes. Four transformants of each gene were selected and the expression of the two proteins was performed in expression medium. The expression of SKS-IKVAV 6x (75946 Da) and SKS-PPFLM 6x (76980 Da) proteins was further evaluated in a SDS-Page (10 %) proteins (**Figure 5-11**).

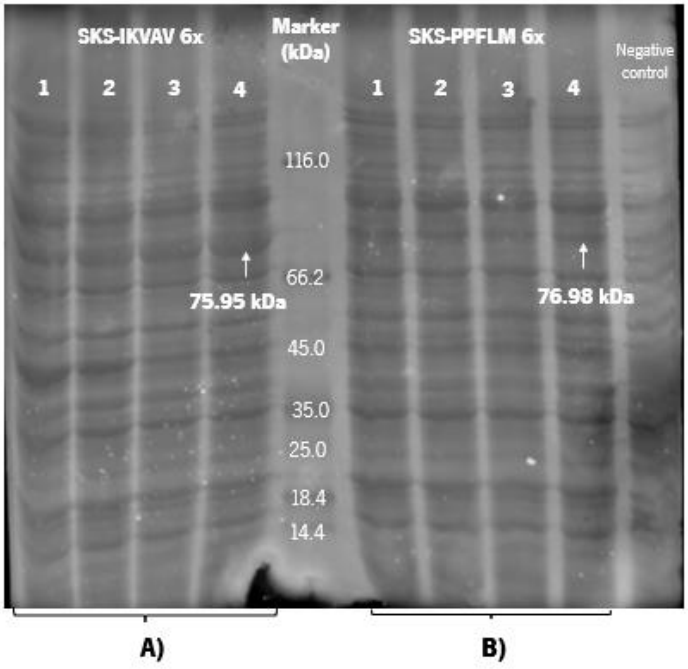

Figure 5-11 — SDS-Page (10 %) of SKS-IKVAV and SKS-PPFLM proteins (expression screening). The gel was stained with cooper chloride solution (0.3 M) for visualization (Image Lab™). The inoculum grown overnight in TB medium and ampicillin served as the negative control.

Analyzing the results, both proteins were expressed. A band near the theoretical molecular weight (75.95 kDa for SKS-IKVAV 6x and 76.98 kDa for SKS-PPFLM 6x) was observed for all the tested transformants. However, the transformant for the two proteins that presented a higher expression level was further selected for the production of the SKS-IKVAV and SKS-PPFLM.

To reduce the time required to obtain the recombinant polymers, the SKS-IKVAV protein was produced in Erlenmeyer flasks and the SKS-PPFLM protein was produced in a fermenter.

The bioproduction of SKS-IKVAV was terminated after the decrease of the $OD6_{00nm}$ from 13.48 to 10.91. The **Table 5-13** presents the fermentation conditions for the SKS-PPFLM.

Table 5-13 — Fermentation conditions for the SKS-PPFLM protein

Production samples	pH	Temperature (°C)	Agitation (rpm)	Base added (mL)	OD_{600nm} SKS-PPFLM
1st	7	37	499	13 mL	9,05
2nd	7	37	499	-	11,596
3rd	7	37	499	-	13,21
4th	7	37	499	-	11,746

After to confirm the success of the bioproduction, SDS-Pages (10 %, **Figure 5-12** and **5-13**) were performed with the samples collected over time and heated after production. The latter correspond to samples in which purification based on the *Tt* of the ELRs produced was attempted.

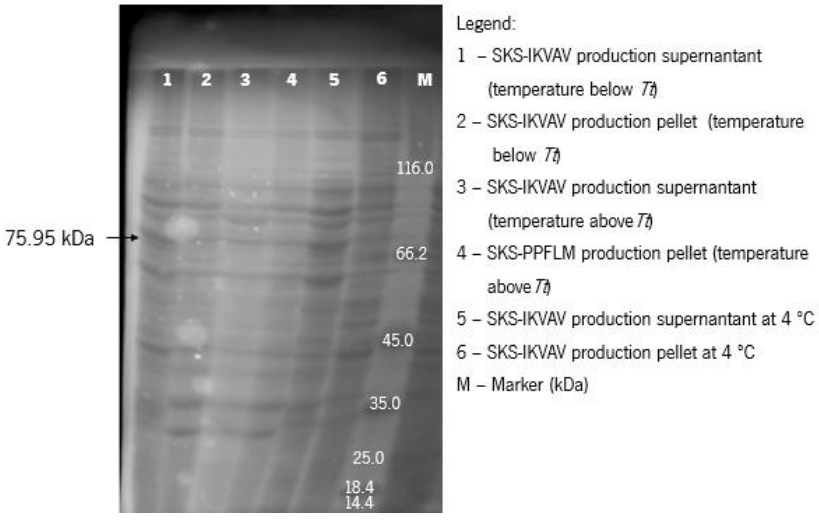

Figure 5-12 — SDS-Page (10 %) of SKS-IKVAV protein after purification. The gel was stained with cooper chloride solution (0.3 M) for visualization (Image Lab™).

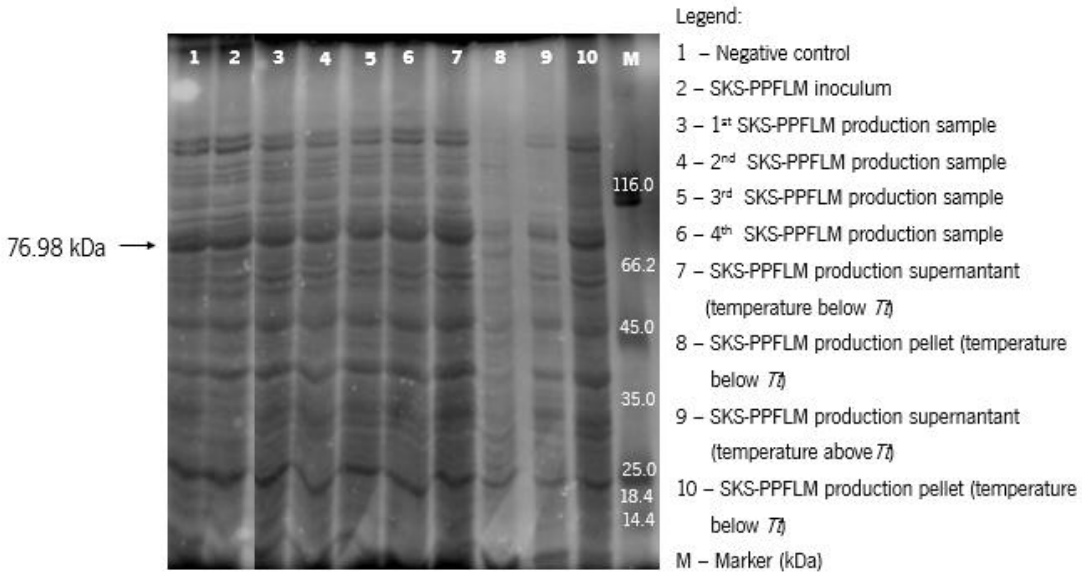

Figure 5-13 — SDS-Page (10 %) of SKS-PPFLM protein production in the fermenter and purification. The gel was stained with cooper chloride solution (0.3 M) for visualization (Image Lab™). The inoculum grown overnight in TB medium and ampicillin served as the negative control.

Since no SDS-Page was performed on the SKS-IKVAV samples after production, it is not possible to determine which method produced the greater concentration of protein. Nonetheless, due to the noticeable width of the band corresponding to the SKS-PPFLM protein in the gel in the previous figure, it is denoted that the fermenter protocol is suitable for the production of this specific protein.

It is expected that if the solution containing the ELRs is heated to a temperature above the *Tt*, the recombinamer will be present in the pellet; otherwise, if the solution is chilled below the *Tt*, the protein will be dissolved in the supernatant.

At temperatures below *Tt*, the SKS-IKVAV protein is observed in the supernatant but not in the pellet. Furthermore, at 4 °C, the protein is more noticeable in the solution's supernatant while remaining absent from the pellet. In both the supernatant and the pellet, the SKS-IKVAV protein is undetectable at temperatures above *Tt*.

The previously reported smart behavior was also observed for the SKS-PPFLM protein, this polymer presented in the solution supernatant at temperatures below *Tt* and not in the pellet. Similarly, the protein was present in the pellet of the heated solution above *Tt*, and it was also present, although in lower concentration, in the heated supernatant.

5.4. Conclusions

Regarding the genetic engineering tools used in this section of the dissertation project, it is concluded that the development of the recombinant SKS-IKVAV and SKS-PPFLM genes was successful since the iterative-recursive method allowed for easy clustering of inserts to create the final genes.

It is proposed in future projects to optimize the production of both ELRs and, although the promising results, the complete purification of the two ELRs produced was not possible during my ERASMUS. Therefore, it is imperative to develop an optimized purification protocol for each recombinant protein to obtain the ELRs polymers and proceed with their characterization, scaffold manufacturing, and ultimately conclude their utility as biomaterials for skin TE solutions. It is recommended that the purification protocol be based on the *Tt* of the ELRs polymers, with the protein solubility being altered by varying the salt concentration, acidity, and temperature of the solution, due to the promising results obtained.

6. EXPLORING STAR PROTEIN FOR SKIN TISSUE ENGINEERING

The use of STAR protein in the second part of this dissertation for the development of skin TE applications is based on its similarity with proteins from the ELR family.

Since the genetic engineering process involved in the development of the STAR protein was already developed and the expression confirmed, this section of the dissertation was focused on the optimization of STAR expression and in the development and characterization of STAR-based films for skin TE applications.

6.1. Materials

The materials used for the production and purification of the STAR polymer and for the preparation and characterization of STAR-based films are below. The aa composition of STAR will not be disclosed in this dissertation for the sake of intellectual property protection.

6.1.1. Chemical reagents

The chemical reagents employed are listed in **Table 6-1**.

Table 6-1 — List of chemical reagents employed

Reagent and Abbreviation	Brand
Acetic acid	Sigma Aldrich
Acrylamide	Plus one
Ammonium sulphate	Sigma
APS	Biorad
Coomassie Brilliant Blue G-250	Merck
Dialysis membrane with a 14 kDa cutoff	Sigma Aldrich
Dimethyl sulfoxide (DMSO)	Sigma
Distilled water	

D - glucose	Sigma
DTT	Sigma
Dulbecco's modified Eagle's medium (DMEM)	Sigma Aldrich
D(+) Lactose monohydrate	Panreac
Ethanol	Merck
EDTA	Sigma
Fetal bovine serum (FBS) 5 %	Sigma Aldrich
Glycerol	Fisher Bioreagents
Hydrochloric acid	Fisher Scientific
Hygromycin	Sigma Aldrich
Kanamycin	Fisher Chemical
L - glutamine	Sigma
Medium 199	Sigma Aldrich
Methanol	Carlo Erba
Penicillin	Sigma Aldrich
Phenylmethylsulfonyl fluoride	Sigma
Phosphate buffered saline (PBS)	Biochrom
Potassium phosphate dibasic trihydrate	Sigma
Potassium dihydrogen phosphate	Panreac
Potassium phosphate dibasic	Sigma
Sodium bicarbonate	Aldrich
SDS	Biorad
Sodium hydroxide	Sigma
Streptomycin	Sigma Aldrich
TEMED	Biorad
Tris	Panreac
Trypan Blue	Sigma
Trypsin	Aldrich
Tryptone	Grisp
Type I water	
Yeast extract	Grisp
β-Mercaptoethanol	Sigma Aldrich

6.1.2. Culture media for *E. coli* growth

The culture media used for *E. coli* growth include Luria-Broth (LB) (Lennox, Grisp) 20 g/L and Terrific Broth Autoinduction medium (TB AIM) (Grisp) 35 g/L.

The TB manual medium consisted of yeast extract (24 g/L), tryptone (12 g/L), glycerol (5.04 g/L) and 1X solution of K_2HPO_4 (12.54 g/L) and KH_2PO_4 (2.31 g/L) dissolved in 1 L distilled water.

6.1.3. *In vitro* culture medium for immortalized human fibroblasts

The BJ-5ta cell line (normal human skin fibroblasts immortalized by overexpression of telomerase) was maintained according to American Type Culture Collection (ATCC) recommendations, i.e., four parts of DMEM (powder) containing 4 mmol/L-glutamine, D-glucose, 4.5 g/L sodium bicarbonate and 1 part of medium 199, supplemented with 5 % (v/v) of FBS, 10 μg/mL hygromycin and 1 % (v/v) of penicillin/streptomycin solution.

The cell viability assay was performed with the MTS (3-(4,5-dimethylthiazol-2-yl)-2,5-diphenyltetrazoliumbromide) cell assay kit (Promega).

6.1.4. Buffer solutions

The buffer solutions used are listed in **Table 6-2**.

Table 6-2 – List of buffer solutions

Buffer solution	Composition or supplier
Protein loading buffer 5X	0.3 M tris pH 6.5, 10 % (w/v) SDS, 50 % (v/v) glycerol, 25 % (v/v) β-mercaptoethanol, 2 % (v/v) BPB
SDS-PAGE running buffer	25 mM tris-base pH 8.3, 192 mM glycine and 0.1 % (w/v) SDS
Tris-EDTA (TEDTA)	50 mM tris pH 8, 1 mM EDTA

6.2. Methods

The methods used in this section of the dissertation are described further below.

6.2.1. Optimization of STAR polymer production

The STAR protein was produced using several media and culture conditions in order to optimize protein expression. Previously, *E. coli* BLR (DE3) cells transformed with the expression plasmid containing the STAR recombinant gene were incubated for 8 h in 10 mL of LB medium supplemented with 10 µL of kanamycin at 37 °C and 180 rpm. Then, LB medium was added to a final volume of 100 mL and the bacteria were incubated overnight at 25 °C at 180 rpm.

The pre-inoculum was centrifuged at 6000 rpm, 4 °C for 10 min and the cell pellet was resuspended in 20 mL of TB manual medium.

The cell suspension was then used to inoculate different culture media to an OD_{600nm} of 0.1, and the cells were incubated for 24 h at 37 °C with constant agitation to induce the expression of STAR protein (**Table 6-3**). The OD_{600nm} of the samples of each condition was measured at specific fermentation time-points (elapsed fermentation time, EFT) in order to assess the growth of *E. coli*.

Table 6-3 — Inoculum media and conditions tested to assess the optimal protocol for the production of Star protein

Type of media	Agitation of incubation (rpm)	Ratio (flask capacity/culture media volume)	Induction
TB AIM	180	1:5	Autoinduction
LB	180	1:5	Lactose induction at an OD_{600nm} 0.6 – 1.5
TB manual	180	1:5	Lactose induction at an OD_{600nm} 0.6 – 1.5
LB	250	1:10	Lactose induction after 8 h EFT
TB manual	250	1:10	Lactose induction after 8 h EFT
TB manual	250	1:5	Lactose induction after 8 h EFT
TB AIM	250	1:10	Autoinduction

6.2.2. STAR polymer purification

The STAR polymer was purified using the salting-out effect, which is the precipitation of a protein due to a decrease in its solubility caused by the addition of high concentrations of salt. Ammonium sulfate was used as the salt because it is a preferred reagent for salting-out due to its much higher solubility than any of the phosphate salts [107].

After fermentation, the cells were harvested by centrifugation at 6500 rpm for 10 min at 4 °C and the pellet was resupended in 55 mL of TEDTA with 1 % of protease inhibitor (phenylmethylsulfonyl fluoride). Then, the cell suspension was sonicated (30 min with 3 s ON, 9 s OFF cycles) and placed at 4 °C overnight.

The next day, the lysate was centrifuged at 8000 rpm for 20 min at 4 °C and the soluble and the insoluble fractions were collected separately. The soluble fraction was incubated in ice with constant agitation (250 rpm) and ammonium sulphate was added to a final concentration of 30 % to promote protein precipitation. The suspension was then centrifuged at 8000 rpm for 20 min at 4 °C and the pellet was resuspended in cold distilled water at 4 °C overnight.

The protein solution was dialyzed against distilled water for 4 days using a dialysis membrane with a 14 kDa cutoff. The pure STAR protein was then freeze dried for 6 days and kept in an exsiccator until further use.

6.2.2.1. Sodium dodecyl sulfate polyacrylamide gel electrophoresis (SDS-PAGE)

The expression of the STAR protein was verified by SDS-PAGE with a running gel of 12.5 % and stacking gel of 4 %.

The samples were prepared with 5X loading buffer, denatured at 100 °C for 5 min, and were loaded onto the gel. The samples were run with variable voltage and constant amperage (20 mA per gel).

The gels were stained with Coomassie Blue solution (methanol 50 % (v/v), acetic acid 10 % (v/v), Coomassie Brilliant Blue G-250 2.5 g/L) for 40 min followed by an incubation in distaining solution (methanol 15 % (v/v), acetic acid 10% (v/v)) for 1.5 h.

6.2.3. STAR-based films preparation

The STAR-based films were prepared with the solvent casting method [108]. The freeze-dried STAR polymer was dissolved in water with constant agitation (250 rpm) in ice and the protein solution (3 % (w/v) or 5 %(w/v)) was casted into circular Teflon molds (100 µL volume/mold). Some protein samples were also prepared with DTT (3 mM) since it reduces the disulfide bonds of proteins and peptides, preventing the formation of intramolecular and intermolecular disulfide bonds between cysteine residues of proteins [109]. After casting, the Teflon molds with the protein solutions were kept for 48 h at room temperature or for 24 h with extraction (fume hood) for the samples containing the reducing agent.

The films were then retrieved from the mold with a tweezers and kept at room temperature protect from light until further use.

To promote the films insolubility, some of the STAR-based films were exposed to a methanol saturated atmosphere for 48 h.

The various formulations of the STAR-based films developed are shown in **Table 6-4**.

Table 6-4 — List of the STAR-based films prepared

STAR-based films	Composition
3 %	3 % (w/v) STAR polymer dissolved in water to a final volume of 100 µL
3 % DTT	3 % (w/v) STAR polymer and 3 mM of DTT dissolved in water to a final volume of 100 µL
3 % methanol	3 % (w/v) STAR polymer dissolved in water to a final volume of 100 µL. After gelation, the film was physically crosslinked in a saturated atmosphere of methanol.
3 % DTT methanol	3 % (w/v) STAR polymer and 3 mM of DTT dissolved in water to a final volume of 100 µL. After gelation, the film was physically crosslinked in a saturated atmosphere of methanol.
5 %	5 % (w/v) STAR polymer dissolved in water to a final volume of 100 µL
5 % DTT	5 % (w/v) STAR polymer and 3 mM of DTT dissolved in water to a final volume of 100 µL
5 % methanol	5 % (w/v) STAR polymer dissolved in water to a final volume of 100 µL. After gelation, the film was physically crosslinked in a saturated atmosphere of methanol.

5 % DTT methanol	5 % (w/v) STAR polymer and 3 mM of DTT dissolved in water to a final volume of 100 µL. After gelation, the film was physically crosslinked in a saturated atmosphere of methanol.

6.2.4. STAR-based films characterization

The characterization of the STAR-based films involved several techniques, in order to assess the influence that the protein content, presence of DTT and physical crosslinking with methanol had on the chemical and physical properties of the films.

6.2.4.1. Thickness measurements

Thickness measurements were performed with the MPO Dualscope Thickness Gauge (Fischer). For each film condition analyzed, three different samples were used and at least five measurements were performed on each sample at different locations of the film. The thickness of the films was expressed as the average of the measurements recorded for each condition.

Data are presented as average standard deviation (SD), n = 15 and statistical comparisons were performed by one-way ANOVA with GraphPad Prism 5.0 software (La Jolla, CA, U.S.A.). Tukey's posthoc test was used to compare all the results between them and a P-value of < 0.05 was considered to be statistically significant.

6.2.4.2. Contact angle

Contact angle measurements were performed with a sessile drop in dynamic mode at room temperature using the DataPhysics OCA 20 device and type I water as test liquid. Contact angles were measured by analyzing the deposition of 0.5 µL type I water droplets on the sample surface with SCA 20 software.

For each film condition analyzed (3 % methanol, 3 % DTT methanol, 5 % methanol, and 5 % DTT methanol), four different samples were used and at least two measurements were performed on each sample at different locations on the film surface.

Data are presented as average SD, n = 4 and statistical comparisons were performed by one-way ANOVA with GraphPad Prism 5.0 software (La Jolla, CA, U.S.A.). Tukey's posthoc test was used to compare all the results between them and a P-value of < 0.05 was considered to be statistically significant.

6.2.4.3. Swelling degree and *in vitro* degradation

The swelling degree was assessed by measuring the difference in weight between dry and swollen samples. The dry films were immersed in distilled water or culture media for BJ-5ta cells at 37 °C for 24 h. After removal of excess fluid, the wet weight of the films was determined.

To determine the *in vitro* degradation expressed as percentage of mass loss, the films incubated in water were dried at 37 °C for 24 h after swelling experiment.

The swelling degree was calculated according to **Equation 6-1**:

Equation 6-1 $$Swelling\ degree\ (\%) = \frac{Ws - Wd}{Wd} \times 100$$

where Ws is the mass of the swollen material and Wd is the initial dry mass.

The *in vitro* degradation was calculated according to **Equation 6-2**:

Equation 6-2 $$Weight\ loss\ (\%) = \frac{mi - mf}{mi} \times 100$$

where mi is the initial dry mass and mf is the final dry mass.

Data are presented as average SD for swelling degree in distilled water and *in vitro* degradation, n = 2 and statistical comparisons were performed by one-way ANOVA with GraphPad Prism 5.0 software (La Jolla, CA, U.S.A.). Tukey's posthoc test was used to compare all the results between them and a P-value of < 0.05 was considered to be statistically significant.

6.2.4.4. Microstructural morphology

The microstructural morphology of the STAR-based films was performed in a desktop scanning electron microscope (SEM) (Phenom ProX, Netherlands) at 5 Kv with a spot size of 3.3 or at 15 kv with a spot size of 4.3. Prior analysis, samples were placed in aluminum pin stubs and fixed with electrically conductive carbon adhesive tape (PELCO Tabs™) and coated with 25 Å of gold.

The resulting images were acquired using the ProSuite software v.3.0.

To evaluate the chemical composition of the films (in particular to elucidate the composition of some crystals present on the surface of the 3 % DTT methanol films), the samples were characterized using a desktop SEM (15 kV and spot size of 5.1) coupled with energy-dispersive X-ray spectroscopy (EDS) analysis (Phenom ProX with EDS detector, Phenom-World BV, Netherlands). The results acquired with the ProSuite software integrated with Phenom Element Identification software allowed the identification and respective quantification of the elements present in the samples, expressed in either weight or in atomic concentration.

6.2.4.5. FTIR and secondary structure analysis of STAR polymer and STAR-based films

The secondary structure of the STAR protein and the effect of film formation on protein structure were evaluated by Fourier-transform infrared spectroscopy (FTIR).

The spectra were acquired at room temperature by Opus 8.22.28 software using Bruker Alpha II (Massachusetts, USA). Samples were mounted directly on the crystal and spectra were acquired after 64 scans, between 400 – 4000 cm^{-1} wavenumbers, and with a resolution of 4 cm^{-1}.

The derived FTIR convoluted curves corresponding to the amide I spectral range of 1600 - 1700 cm^{-1} were processed in the “Feat Peaks (Pro)” procedure of the “Peak Analyzer” menu in OriginPro software, v.8.5.0. (OriginLab Corporation, USA). No smoothing was performed prior to fitting for each deconvoluted curve. The baseline subtraction was followed by a multi-pass fit and an integrated Second Derivative method was used to identify discrete starting peak spectral locations for fitting.

The resulting secondary conformational data from individual peaks were derived based on the reported peak assignments [110].

6.2.4.6. Cell culture

BJ-5ta cell line (normal human fibroblasts immortalized by overexpression of telomerase), was cultured in four parts of DMEM (powder), containing L-glutamine, D-glucose, sodium bicarbonate and 1 part medium 199, supplemented with 5 % FBS, 1 % (v/v) penicillin/streptomycin solution and 10 μg/mL hygromycin.

Cellular subcultures were performed when confluence reached values close to 80 – 90 %. BJ-5ta cells were maintained in 25 cm^2 tissue culture flasks in an incubator at 37 °C in a humidified atmosphere with 5 % CO_2. The cell culture medium was renewed two times per week. For subcultures and plating, the adherent cells were detached with trypsin solution 0.05 %, and fresh medium was added in order to neutralize the trypsin. The cell suspension was centrifuged 5 min at 160g. The supernatant was discarded, and fresh medium was added to obtain a new cell suspension. The cell suspension was loaded in a Neubaeur chamber, and the concentration of cells was estimated.

6.2.4.7. Cytotoxicity evaluation

The cytotoxicity of STAR-based films was assessed by indirect contact by exposing BJ-5ta cells to conditioned media containing STAR-based films degradation products and leachable.

Initially, the films were sterilized by exposure to UV radiation for 30 min and the conditioned medium was obtained by incubating the sterilized films in 2 mL of medium at 37 °C in a humidified atmosphere of 5 % CO_2 for 24 h.

Cells were seeded at a density of 10×10^3 cells/100 μL/well in 96-well tissue culture polystyrene (TCPS) plates (TPP, Trasadingen, Switzerland) the day before experiments. The cells were then exposed to the conditioned media in different percentages (100 % conditioned medium, 50 % conditioned medium with 50 % culture media, and 25 % conditioned medium with 75 % culture media) and were further incubated at 37 °C in a humidified atmosphere of 5 % CO_2.

Cells incubated with DMSO (30 % of the total volume) and cells without the addition of the compounds were used as control of death and control of life, respectively. At the end of 24 h and 48 h of contact, cell metabolic activity was assessed by MTS viability assay. The MTS assay protocol was based on the reduction of the MTS tetrazolium compound by viable cells, creating a colored formazan dye soluble in cell culture media. This conversion is carried out by NAD(P)H-dependent dehydrogenase enzymes in metabolically active cells and the formazan dye is quantified by measuring the absorbance at 490 nm [111].

After incubation with samples, 20 µL of a MTS solution was added to each well, and cells were incubated at 37 °C for 2 h. Color was measured with 96-well plate reader at 490 nm in a microplate spectrofluorometer (BioTek Synergy MX). The results were determined relatively to the control of life.

6.3. Results and discussion

The innovation of the work developed in CEB resides in the use of a novel recombinant protein – STAR – with properties similar to ELRs to create protein-based films and assess their potential use in the skin TE area.

6.3.1. Optimization of STAR polymer production

The production of the STAR protein was optimized (higher yields) testing several growth conditions that differed in the culture medium used for the inoculum's incubation, in the flask capacity and culture media ratios, in the angular speed of the incubation, or in the type and time of induction.

It is important to note that the purification protocol was already developed specifically for the STAR protein.

Since increased protein production is related to increased bacterial growth, the OD_{600nm} of the samples for each condition was measured at defined EFT points (**Figure 6-1**).

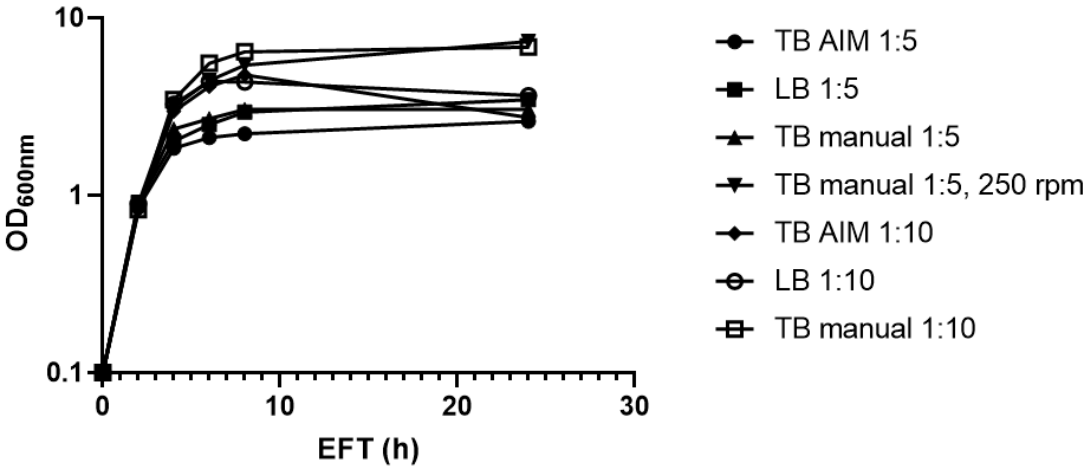

Figure 6-1 — Optical density (600 nm) measured for specific elapsed fermentation time-points for the culture conditions evaluated.

After 2 h of incubation, there were no perceptible differences in *E. coli* growth. However, after 4 and 6 h of incubation, the TB manual 1:10 had the highest OD_{600nm} values (3.46, 5.55), followed by LB 1:10 (3.27, 4.40) and TB manual 1:5, 250 rpm (3.17, 4.44), respectively.

After the incubation, the TB manual 1:5 medium, 250 rpm sample presented the highest OD_{600nm} value (7.37). Generally, the culture medias that presented higher *E. coli* growth throughout the incubation period were TB manual 1:5, 250 rpm and TB manual 1:10.

Samples collected after 8 h (before induction; LB 1:5 and TB manual 1:5 at 4 h) and 24 h of inoculum incubation were analyzed by SDS-Page (12.5%, **Figure 6-2**) to confirm the correlation between bacterial growth and protein production.

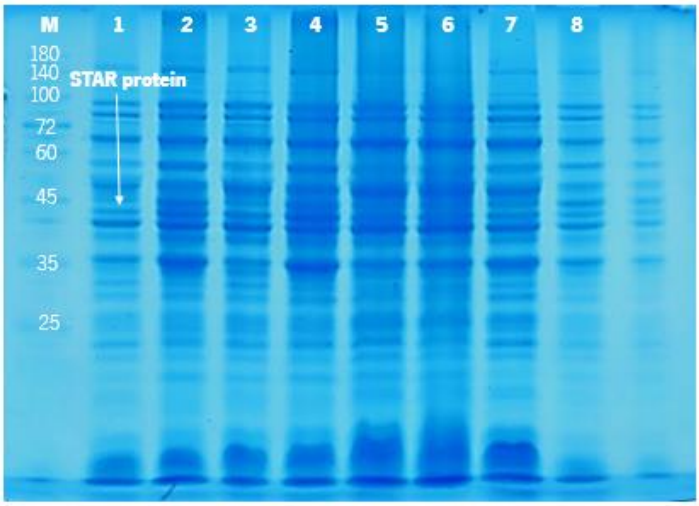

Legend:
M – Marker (kDa)
1 – TB AIM 1:5, 8 h
2 – TB manual 1:10, 8 h
3 – TB manual 1:5, 8 h
4 – TB manual 1:5 250 rpm, 8 h
5 – LB 1:5, 8 h
6 – LB 1:10, 8 h
7 – TB AIM 1:10, 8 h
8 – TB manual 1:5, 4 h

A)

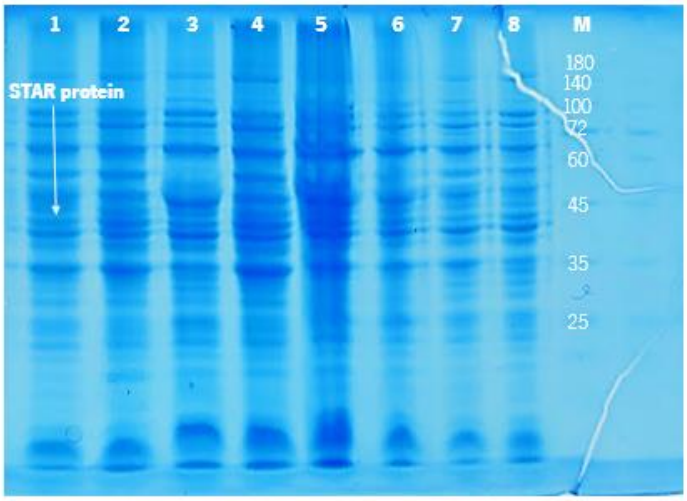

Legend:
1 – TB AIM 1:5, 24 h
2 – TB manual 1:10, 24 h
3 – TB manual 1:5, 24 h
4 – TB manual 1:5 250 rpm, 24 h
5 – LB 1:5, 24 h
6 – LB 1:10, 24 h
7 – TB AIM 1:10, 24 h
8 – LB 1:5, 4 h
M – Marker (kDa)

B)

Figure 6-2 – SDS-Page (12.5 %) of STAR protein expression samples **A)** after 8 h of inoculum's incubation and TB manual 1:5 after induction and **B)** after 24 h of inoculum's incubation and TB manual 1:5 after induction. Gel stained with Coomassie Blue.

Given that the STAR protein has a molecular weight at around 41000 Da, it was observable that the LB 1:5 and the TB manual 1:5 conditions did not produce STAR protein after 4 h of incubation, which was expected since the induction had not yet happened. However, after 8 h (**Figure 6-2 A)**), the referred conditions produced STAR protein due to the lactose induction initiated at EFT = 4 h. The highest productions were verified after 8 h and 24 h of production in TB manual 1:5, 250 rpm, and TB manual 1:10 conditions.

Comparing the highest bacterial productions and the conditions that allowed for higher protein expression, the TB manual 1:5, 250 rpm, was selected for express the STAR protein.

6.3.2. STAR-based films

The STAR-based films were obtained by solvent casting of STAR solutions in circular Teflon molds. DTT was added to some solutions to prevent the formation of intramolecular and intermolecular disulfide bonds between cysteine residues of this protein, helping in the filming properties of STAR [109]. Afterwards, some of the films obtained were exposed to a saturated methanol atmosphere to promote their insolubility.

The effect of protein concentration, presence of DTT and insolubilization with methanol on the macroscopic properties of the STAR-based films were evaluated (**Figure 6-3**).

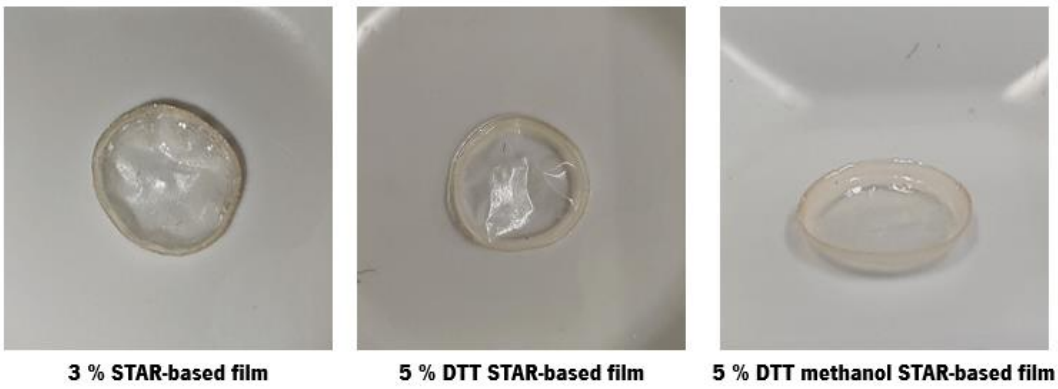

Figure 6-3 – Macroscopical image of a 3 % STAR-based film, a 5 % DTT STAR-based film and a 5 % DTT methanol STAR-based film.

Regardless of the condition, all the films were macroscopically translucent, with opaque regions on the periphery of the film. This could be due to the presence of some impurities in the solution and was more noticeable for the highest concentrations of STAR protein (5 %).

Therefore, the protein content of the films was the property that most influenced their macroscopic appearance because the film after being physically crosslinked with methanol maintained the same macroscopic structure. In addition, due to the low concentration of DTT, the reducing agent had no influence on the macroscopic structure of the films.

6.3.3. STAR-based films characterization

The developed STAR-based films were characterized in terms of their physical and chemical properties, morphology, and cytotoxic potential.

6.3.3.1. Thickness measurements

The macroscopic structure of a TE device (films, scaffolds...) affect both the mechanical properties and the cell response [112]. Thus, the thickness of the STAR-based films was measured (**Table 6-5**) to conclude the effect of the different compositions on the films' three-dimensional structure.

Table 6-5 — Thickness measurements of the STAR-based films with the MPO Dualscope Thickness Gauge (Fischer).

STAR-based films	Thickness (µm)
3 %	3.9 ± 2.3
3 % DTT	5.7 ± 3.4
3 % methanol	10.3 ± 1.6
3 % DTT methanol	7.7 ± 2.6
5 % *	7.8 ± 2.9
5 % DTT *	16.3 ± 7.1
5 % methanol *	308.0 ± 259.7
5 % DTT methanol *	170.5 ± 224.6

*P<0.05

The difference in thickness between 3 % and 5 % films was expected based on the higher protein concentration in the latter. In contrast, the increase of the films thickness after methanol physical cross-liking was not predicted. Furthermore, with the addition of DTT, there was an increase in thickness, which could be attributed to a change in the chemical structure of the films.

Comparing the unmodified films with those with DTT or physically crosslinked with methanol, only statistically significant differences existed between the films 5 % vs. 5 % methanol,

5 % vs. 5 % DTT methanol, 5 % DTT vs. 5 % DTT methanol, and 5 % methanol vs. 5 % DTT methanol. As a result, for the 5 % films, the addition of DTT or physical cross-liking with methanol causes a significant increase in film thickness.

The increase in SD values across the table reflects the increasing difficulty encountered during thickness measurement in keeping the films' surface flat, which was related to the concave surface that the films presented due to the extraction process of the films from the respective molds. Furthermore, the surface of the films had a limited diameter in comparison to the thickness gauge, making thickness measurement in different areas of the surface challenging.

6.3.3.2. Contact angle

The surface wettability of a material is determined by its surface roughness and chemical composition, and the study of this property determines whether the material is suitable for a particular application. Because differential adsorption is dependent on surface hydrophobicity in TE applications, adequate wettability allows for optimal adhesion or cell release, ensuring the material's biofunctionality [113-115]. Because contact angle is the main parameter used to determine the wettability of a surface [113], the surface wettability of the STAR-based films was measured. Only the films physically crosslinked with methanol were assessed (**Table 6-6**), as the others dissolved in contact with type I water.

Table 6-6 — Contact angle of the STAR-based films performed at room temperature with type I water as test liquid

STAR-based films	0''	15''	30''	45''	1'
3 % methanol	(93.3 ± 7.4) °	(101.8 ± 11.8) °	(104.9 ± 10.7) °	(115.2 ± 4.6) °	(113.6 ± 9.3) °
3 % DTT methanol	(111.5 ± 14.6) °	(126.6 ± 19.8) °	–	–	–
5 % methanol	(102.8 ± 32.4) °	(129.4 ± 25.4) °	(128.9 ± 26.3) °	(99.7 ± 0.0) °	(99.7 ± 0.0) °
5 % DTT methanol	(101.3 ± 5.7) °	(101.7 ± 7.8) °	(106.8 ± 9.2) °	(111.6 ± 14.8) °	(111.2 ± 18.5) °

Since all contact angles obtained are greater than 90 °, it can be stated that the STAR-based films physically crosslinked with methanol had a hydrophobic surface [116]. The surface hydrophobicity of the 3 % methanol and 5 % methanol films increased in the first 15'' and 45''

after droplet deposition, respectively, and decreased until 60''. Furthermore, the contact angle values for the 5 % methanol films were very similar at 0'' and 60''.

Moreover, the hydrophobicity of the 3 % and 5 % DTT methanol films increased over time.

The changes in contact angle values over time were most likely caused by structural rearrangement of the molecules in the films in contact with water.

Because the 3 % and 5 % films were physically crosslinked with methanol under the same conditions, the higher hydrophobic character of the 5 % samples might be related with the higher STAR content.

The addition of DTT to the 3 % STAR-based films resulted in an increase in hydrophobicity. However, the opposite was observed for the 5 % films, even though the increase in the hydrophilic character with the addition of DTT could be disregarded as it is not statistically significant.

6.3.3.3. Swelling degree and *in vitro* degradation

The swelling of materials in the presence of fluids is essential to enable absorption and transfer of nutrients or metabolites throughout the film structure in a physiological environment and can be measured through the swelling degree [117].

The ability of a structure to absorb a specific fluid, which is primarily determined by its hydrophobicity and microstructure, influences cell adhesion and proliferation, as well as its mechanical integrity and properties, because biomaterials used in TE are biodegradable. In addition, as water is the primary constituent of human body fluids, it is critical to assess the degradation of a biomaterial caused by contact with water – *in vitro* degradation [117].

The swelling degree and the *in vitro* degradation of STAR-based-crosslinked with methanol are shown in **Table 6-7**. The swelling degree was evaluated at 37 °C using distilled water or culture media, and the *in vitro* degradation was determined with the samples used to evaluate the swelling degree in distilled water.

Table 6-7 — Swelling degree performed at 37 °C for 24 h with distilled water and culture media and *in vitro* degradation of the STAR-based films

STAR-based films	Swelling degree (%)		*In vitro* degradation
	Distilled water	Culture medium	(weight loss %)
3 % methanol	174.4 ± 24.0	60.0	13.7 ± 14.7
3 % DTT methanol	137.6 ± 1.3	47.6	17.7 ± 2.0
5 % methanol	94.4 ± 7.9	82.6	12.4 ± 1.3
5 % DTT methanol	84.7 ± 27.3	53.3	5.9 ± 0.2

The swelling degree and the *in vitro* degradation were only determined for the samples incubated in methanol because all the other samples dissolved when incubated in water.

Comparing the swelling degree results in distilled water, the highest value was obtained for the 3 % films. This was related with the lower protein content of these films, which led to a less compaction in the polymeric matrix during the methanol physical crosslinking, resulting in a higher capacity to absorb water. The 3 % methanol films also exhibited the highest degradation profiles.

When the STAR-based films were incubated in cell culture medium a decrease on the swelling degree was observed for all the conditions. This might have been due to the presence of proteins and other bioactive substance in the culture media.

6.3.3.4. Microstructural morphology

The microstructural morphology of TE solutions is primarily responsible for the mechanical properties of a TE solution. Thus, it should resemble the native tissue to be regenerated in order to meet physiological mechanical needs and ensure a favorable environment for cell adhesion, proliferation, and differentiation [118].

SEM was used to examine the microstructural morphology of the STAR-based films at surface and cross-sections (**Figures 6-4** and **6-5**).

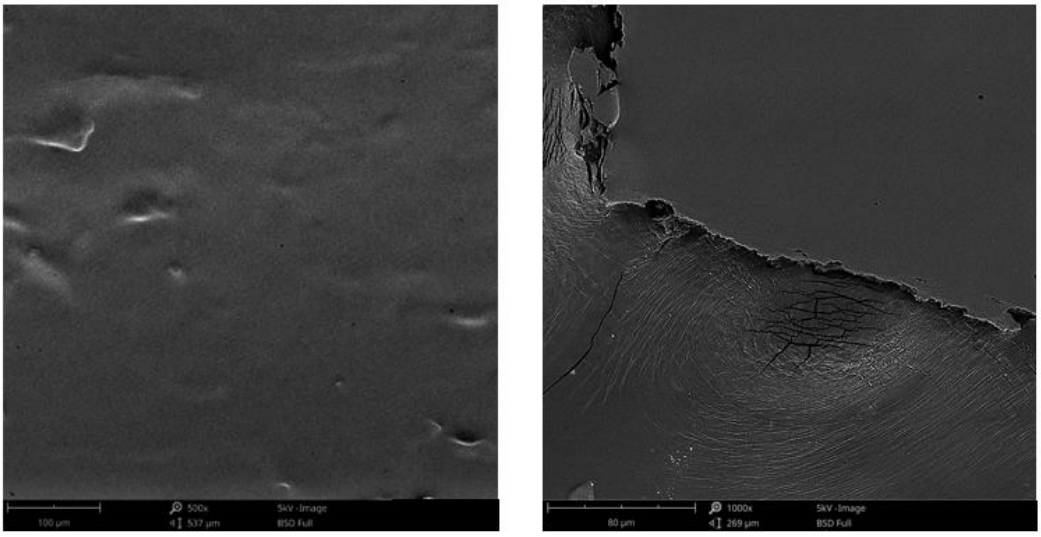

A) B)

Figure 6-5 — SEM micrographs of 3 % STAR-based films: **A)** general view of the film surface and **B)** cross-section view.

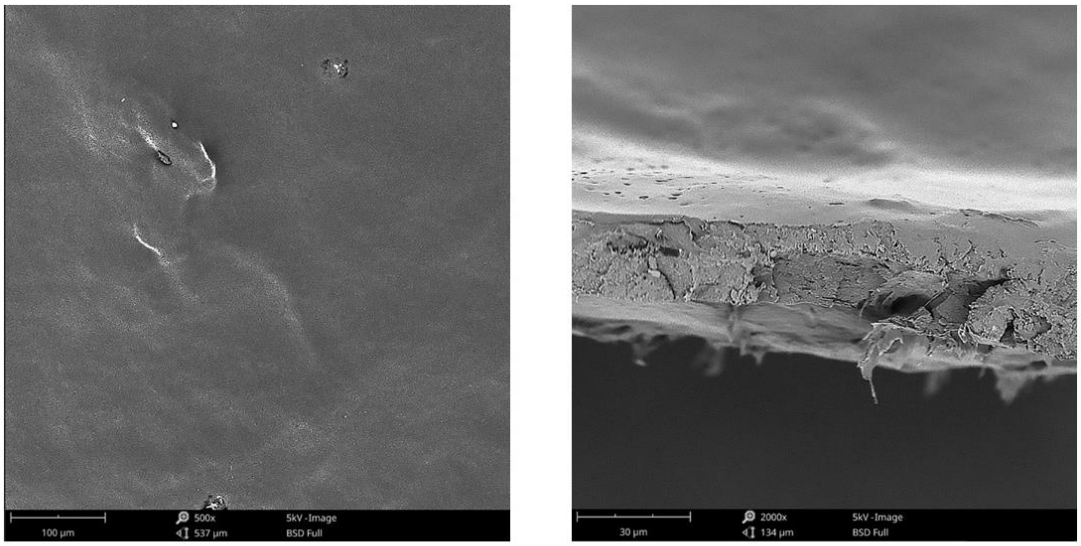

A) B)

Figure 6-4 — SEM micrographs of 5 % STAR-based films: **A)** general view of the film surface and **B)** cross-section view.

The 3 % STAR-based films presented more surface irregularities than the 5 % STAR-based films.

Figures 6-6 and **6-7** show the microstructural morphology of the 3 % DTT and 5 % DTT films.

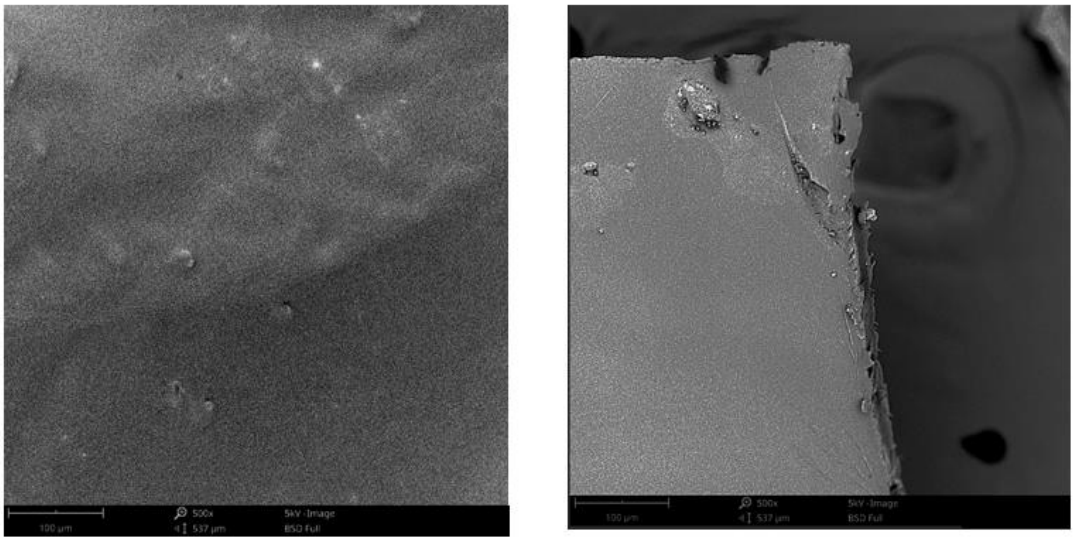

A) B)

Figure 6-7 — SEM micrographs of 3 % DTT STAR-based films: **A)** general view of the film surface and **B)** cross-section view.

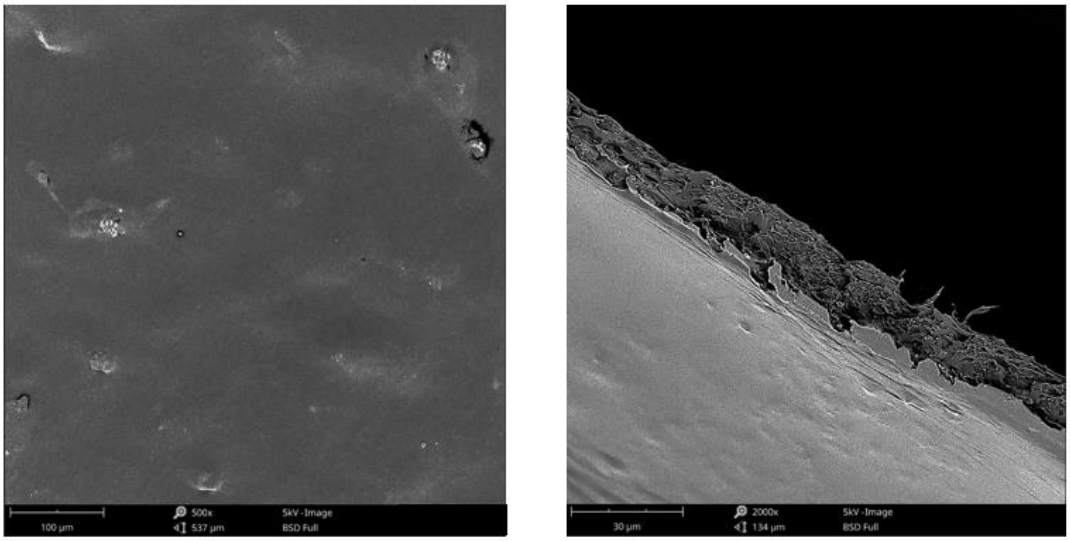

A) B)

Figure 6-6 — SEM micrographs of 5 % DTT STAR-based films: **A)** general view of the film surface and **B)** cross-section view.

Although the surface roughness of the 5 % films increased slightly with the addition of DTT, the surface of the 3 % DTT presented more clusters of protein aggregates and less clefts. Nonetheless, the addition of DTT did not considerably alter the microstructure of the films.

The surface of the films crosslinked with methanol are presented in **Figures 6-8** and **6-9**.

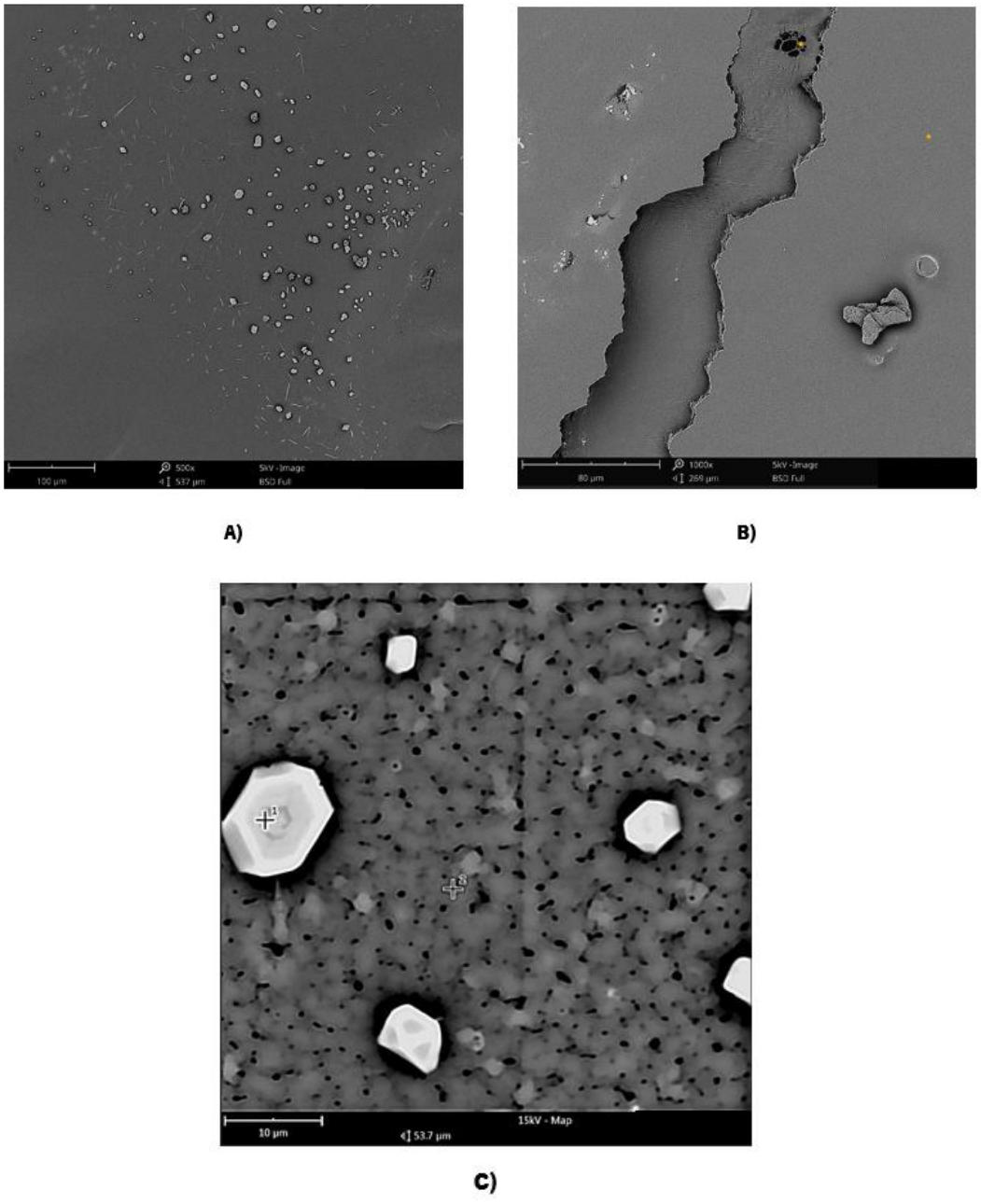

Figure 6-8 — SEM micrographs of 3 % methanol STAR-based films: **A)** general view of the film surface, **B)** cross-section view and **C)** EDS image highlighting the crystals formed on the film's surface.

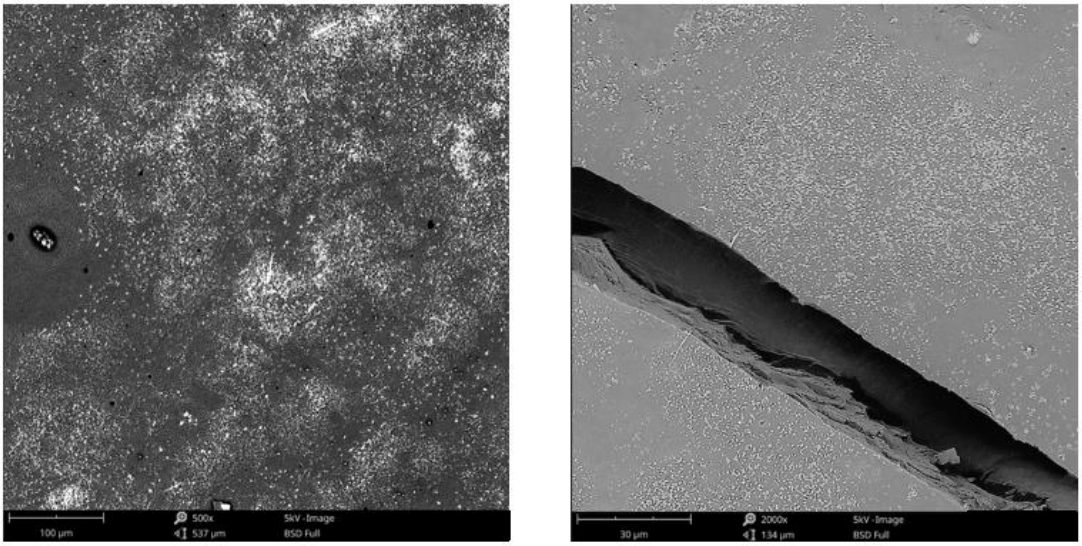

A) B)

Figure 6-9 — SEM micrographs of 5 % methanol STAR-based films: **A)** general view of the film surface and **B)** cross-section view.

As observed, the films modified with methanol showed crystals in their microstructure. Therefore, an EDS analysis was performed, which indicated the presence of the substances present in **Table 6-8** for the crystals analyzed.

Table 6-8 — Substances present in the 3 % methanol film's crystals and their atomic concentration

Substance	Atomic concentration (%)
Gold	5.26
Carbon	68.60
Oxygen	15.33
Sulfur	5.24
Sodium	5.07
Chlorine	0.27
Phosphorus	0.23

The EDS analysis allowed to conclude that the crystals contained carbon, oxygen, sulfur, sodium, and trace amounts of chlorine and phosphorus. This composition is consistent with the composition of the STAR protein (data not shown) and the physical crosslinking with methanol.

Figures 6-10 and **6-11** demonstrate the micro-scale morphology of the methanol physically crosslinked DTT films.

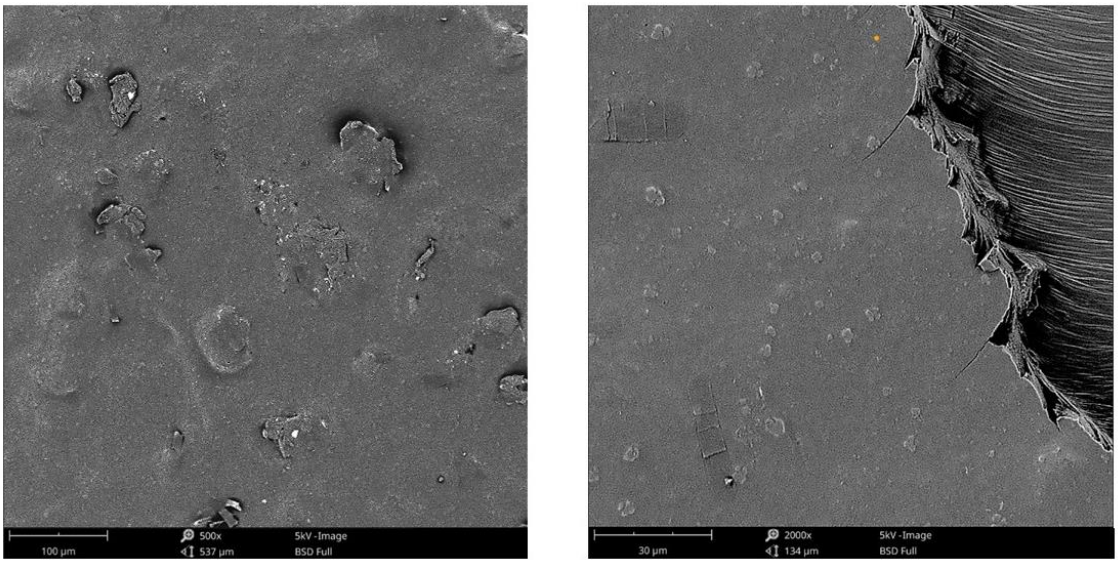

A) B)

Figure 6-10 — SEM micrographs of 3 % DTT methanol STAR-based films: **A)** general view of the film surface and **B)** cross-section view.

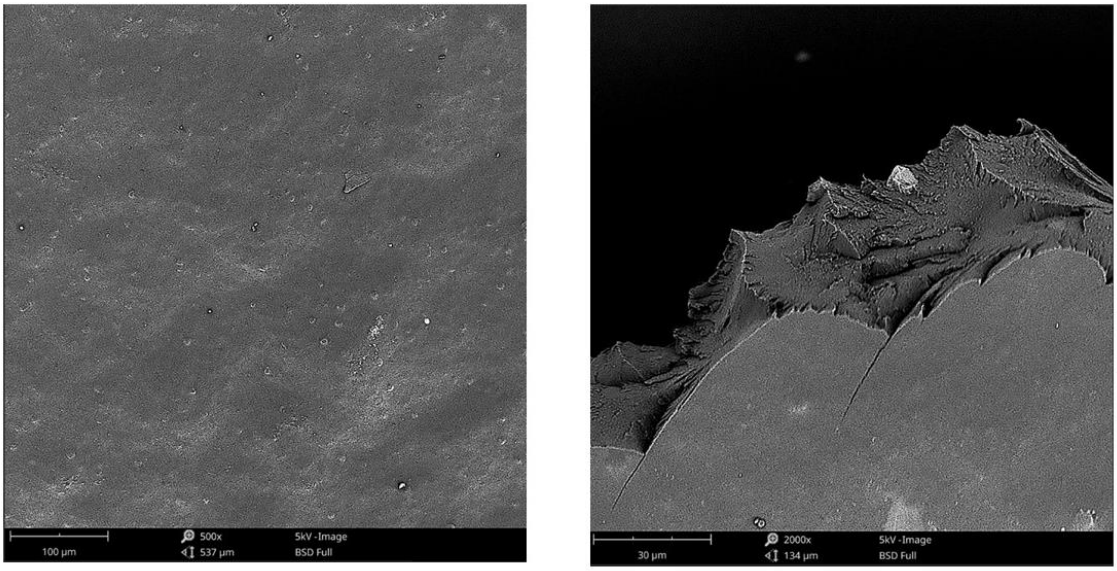

A) B)

Figure 6-11 — SEM micrograph of 5 % DTT methanol STAR-based films: **A)** general view of the film surface and **B)** cross-section view.

The surface of the films containing DTT and cross-linked with methanol did not demonstrate the crystals previously observed for the films physically cross-linked with methanol without DTT. The roughness and appearance of fractures was shown to be more prominent in the 3 % films.

6.3.3.5. FTIR and secondary structures analysis of STAR protein and STAR-based films

The FTIR spectra (**Figure 6-12**) were examined to determine the intermolecular composition of the STAR protein and STAR-based films.

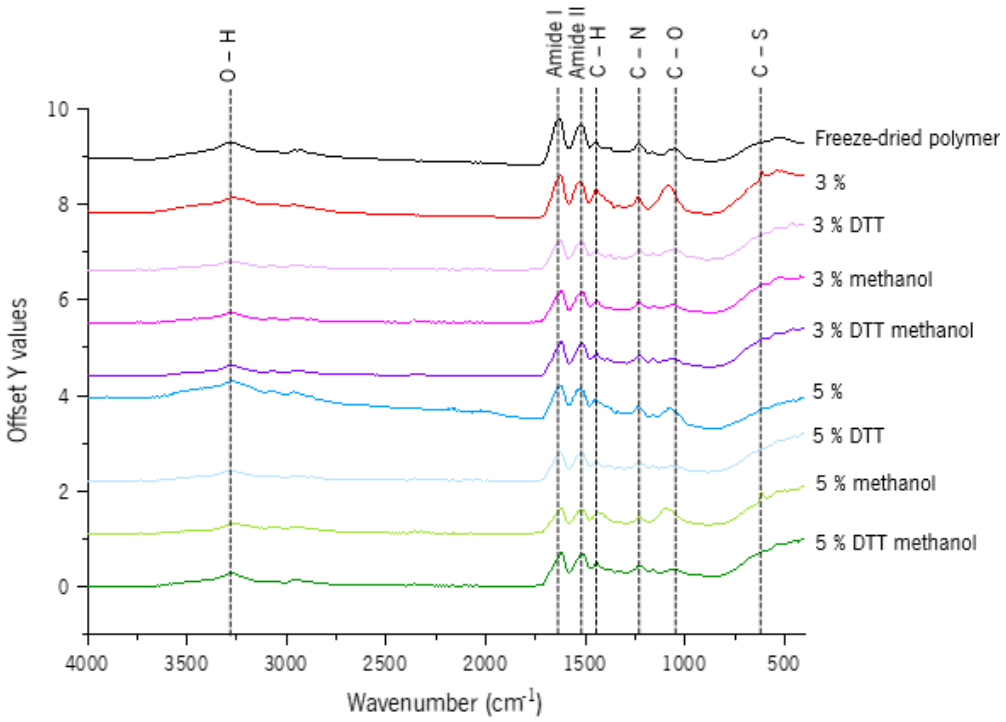

Figure 6-12 – FTIR spectra of STAR protein and STAR-based films.

The spectra of the STAR protein and STAR-based films showed the characteristic vibrational bands of proteins, corresponding to the amide I and amide II (mainly C=O stretching vibrations) [119].

The amide I and the amide II bands in the freeze-dried polymer appeared at 1628 cm^{-1} and 1523 cm^{-1}, respectively. A shift on the amide I band (1624 cm^{-1}) was observed for the 3 %, 5 %, 3 % DTT, and 5 % DTT when compared to the pristine protein. This shift was even more noticeable for the 3 % methanol, 5 % methanol, 3 % DTT methanol, and 5 % DTT methanol films with a value of 1620 cm^{-1}.

A shift on amide II bands was also observed for 5 % DTT (1521 cm^{-1}), 5 % methanol (1519 cm^{-1}), 3 % DTT methanol (1517 cm^{-1}), 5 % DTT methanol (1517 cm^{-1}), 3 % (1527 cm^{-1}), 3 % methanol (1509 cm^{-1}) and 3 % DTT (1509 cm^{-1}).

The shift observed for amide I and amide II bands were related with possible rearrangement of proteins' structure during film formation.

Other bands were observed for STAR proteins and STAR-based films. The bands at 3290 – 3260 cm^{-1} were attributed to the O–H stretching of carboxylic acid, at 1450 – 1430 cm^{-1} were due to the C–H bending of alkane methyl group, at 1235 – 1225 cm^{-1} corresponded to the C–N stretching of amine, at 1085 – 1050 cm^{-1} were attributed to the C–O stretching of primary alcohol, and at 630 – 620 cm^{-1} were due to the C–S bonds present in cystine [120,121].

The vibrational spectra of the amide I is frequently used to determine the secondary structures of any protein, because it indicates the type of secondary structures present in the samples with great sensitivity [122].

The deconvoluted data obtained from the amide I spectra of the STAR protein and STAR-based films are presented in **Table 6-9** and **Figure 6-13**, with the discrete peaks and their respective contributions in the FTIR-derived curves, as well as the structural assignment of the bands according to Kong [110]. To clarify the terminology used in **Table 6-9**, random refers to an unordered conformation, -sheet refers to the dense hydrophobic structure of β-sheets, and β-turns are associated with β-sheets folding centers.

Table 6-9 — Resulting discrete peaks, respective contribution to the FTIR-derived curves and corresponding structural assignments of STAR polymer and STAR-based films

Sample	Deconvoluted data		Deconvoluted data assignment				
	Peak center (cm^{-1})	Area occupied (%)	β-sheet	β-turn	Helical 3_{10}	Helical α	Random
STAR polymer	1606	4.6	+				
	1622	28.2	+				
	1646	51.1					+
	1671	10.3		+			
	1685	4.2		+			
	1695	1.5	+				
3 %	1622	47.7	+				
	1647	25.3					+
	1651	5.6					+
	1668	14.5		+			
	1679	1.6		+			

	1688	5.2		+			
	1604	6.2	+				
	1620	29.0	+				
3 % DTT	1647	51.7					+
	1674	7.8		+			
	1685	3.3		+			
	1696	2.1	+				
	1602	4.8	+				
	1619	34.4	+				
3 % methanol	1647	49.2					+
	1670	2.5		+			
	1684	6.9		+			
	1699	2.2	+				
3 % DTT	1618	37.6	+				
methanol	1649	58.4					+
	1696	4.0	+				
	1605	7.6	+				
	1626	49.6	+				
	1639	3.5	+				
5 %	1648	9.0					+
	1655	1.8				+	
	1660	11.0			+		
	1671	3.8		+			
	1681	13.6		+			
	1603	6.9	+				
	1620	31.5	+				
	1642	33.0	+				
5 % DTT	1652	2.7					+
	1667	19.8		+			
	1685	4.9		+			
	1696	1.2	+				
	1618	39.7	+				
5 % methanol	1649	55.5					+
	1691	4.8	+				
5 % DTT	1618	34.0	+				
methanol	1644	66.0					+

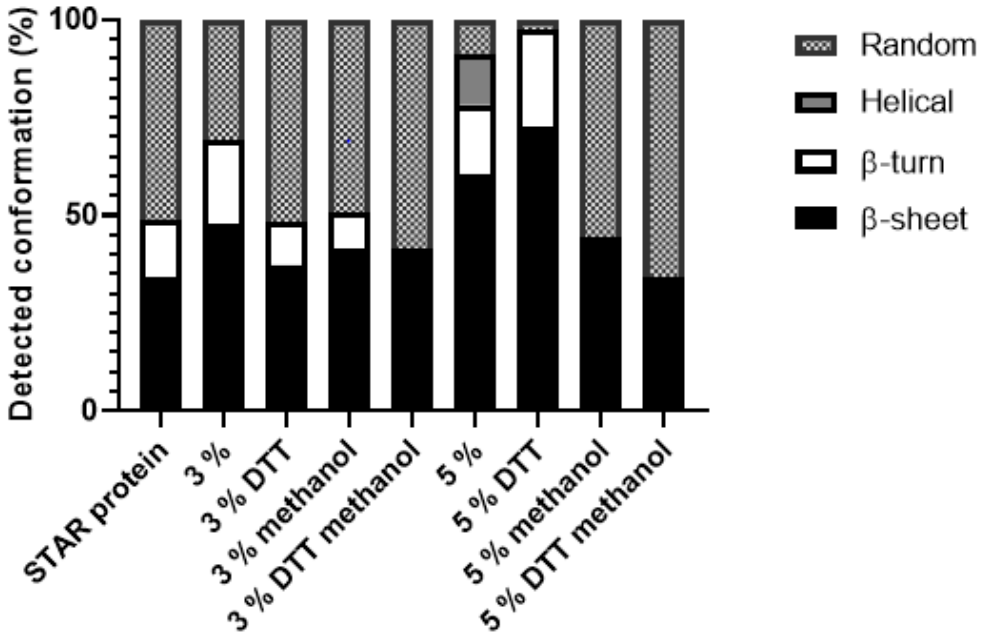

Figure 6-13 — Secondary structural conformations of the STAR-based films elucidated by deconvolution of amide I spectral region. STAR protein corresponds to the control. The 3_{10} and α-helix are referred as helical.

Figure 6-13 shows that the 3 % and 5 % films had more β-sheets and β-turns when compared with the freeze-dried STAR polymer. This indicates a crystallization of the protein during film formation.

6.3.3.6. Cytotoxicity evaluation

Biocompatibility is key parameter when developing a TE device/solution. The films, coated/functionalized surfaces and scaffolds should not display any toxicity towards cells and must not contain toxic degradation products in order to elicit an appropriate response in a host in a specific application [80].

The preliminary biocompatibility study was conducted via indirect contact assay to evaluate the cytotoxicity of STAR-based films degradation products and leachable in human immortalized fibroblasts (BJ-ta5) cells. The cells were exposed for 24 h (**Figure 6-14**) and 48 h (**Figure 6-15**) to undiluted and diluted (50 % and 75 %) culture medium pre-conditioned by contact with the films for 24 h, at 37 °C, 5 % CO_2.

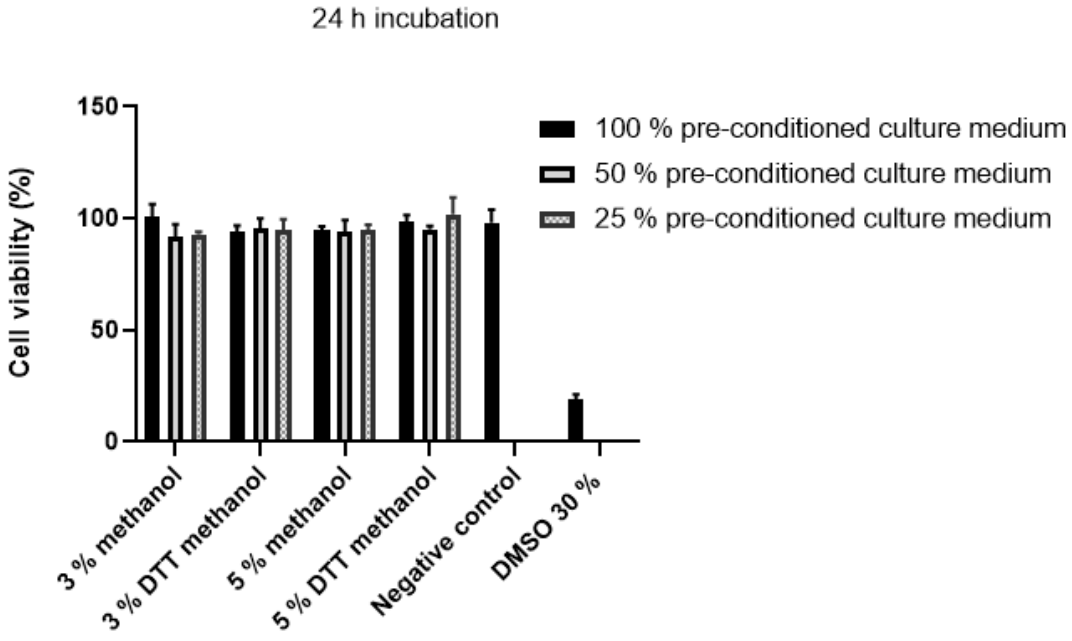

Figure 6-15 — BJ-5ta cell viability at 24 h of incubation with pre-conditioned culture media.

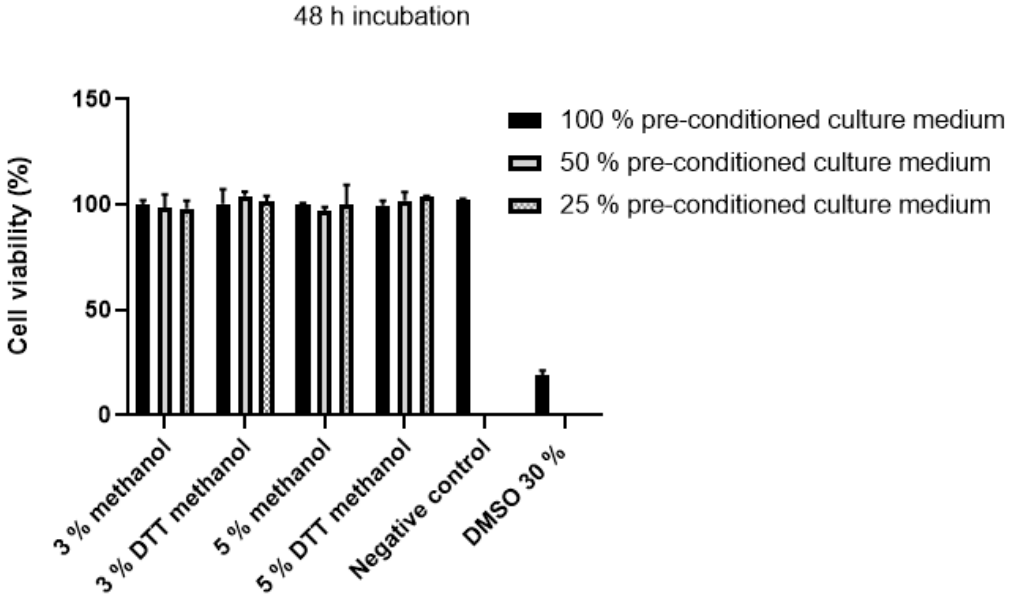

Figure 6-14 — BJ-5ta cell viability at 48 h of incubation with pre-conditioned culture media.

Analyzing the previous graphs, it was concluded that the degradation products and leachable of the STAR-based films did not interfere with the viability of the BJ-5ta cells. The minimal decrease of cells observed after 48 h of incubation in were due to the build-up of toxic

metabolites and decrease of nutrients and oxygen. In addition, the increase denoted in some STAR-based films conditioned media corresponded to the characteristic growth of the used cells.

As a result, the indirect contact assay allowed the assessment of the degradation products and leachable of the films as inert to BJ-ta5 cells.

6.4. Conclusions

The optimization of STAR protein expression and the development and characterization of STAR-based films as a new approach for the development of skin TE applications was successfully achieved in the second part of this dissertation.

The expression of STAR protein was increased using the following conditions: TB manual medium with a 1:5 flask capacity/culture media volume ration, constant agitation (250 rpm), 37 °C for 24 h.

Two sets of STAR-based films were obtained using different protein concentrations (3 % and 5 %). The films were translucent and fragile, particularly the samples with 3 % of protein content, and presented a concave curvature caused by the demolding process. The influence of DTT and methanol on film formation and film properties was evaluated. The amount of protein and the incubation with methanol influenced the thickness of the films. The films with 5 % presented greater thickness when compared to the 3 % films, and the same was observed for the films incubated with methanol when compared with the films without methanol.

After measuring the wettability, the films proved to be mainly hydrophobic with contact angles higher than 93.3 ± 7.4 °. Despite the ideal contact angle value for skin TE applications in not yet disclosed, the literature indicates that surfaces with contact angles ranging between 60 ° to 80 ° promote cell adhesion and growth [114]. However, the contact angle measured *in vivo* on the skin in areas with low sebaceous lipids is between 91 ° and 102 °, which is comparable to the values obtained for the STAR-based films. Hence, although hydrophilic surface materials are generally preferred, since skin contact angles range from 57 ° to 102 °, hydrophobic films can also be advantageous for skin TE applications in anatomical areas with lower sebaceous lipid content [123].

In terms of microstructure, the samples revealed a rough surface, which was most noticeable in the 3 % samples. The presence of irregularities was reduced with the addition of

DTT, and the physical crosslinking with methanol revealed crystalline clusters on the surface of the films. It should be noted that the roughness displayed by all of the analyzed films is a promising feature when considering a cell-based application, as it provides a favorable environment for cell adhesion.

The evaluation of the cytotoxic potential of STAR-based films degradation products and leachable revealed that all the films could be considered as safe for cells.

7. INTEGRATED CONCLUSIONS AND FUTURE PROSPECTS

The goal of this dissertation was to create scaffolds for Tissue Engineering and Regenerative Medicine in the context of skin regeneration using ELRs. To that end, two synthetic genes were created that corresponded to different recombinant proteins based on the natural sequence of elastin, SKS-IKVAV and SKS-PPFLM.

The ELRs were produced, however, the scaffolds were not obtained because the purification protocols for the proteins were not developed due to the limited time of the ERASMUS internship. Because of the high potential of the proteins developed to serve as biomaterials for skin regeneration, the development of purification protocols to assess the properties of SKS-IKVAV and SKS-PPFLM scaffolds is of paramount importance to continue this project.

The second part of this dissertation was dedicated to the production optimization of the STAR polymer, a protein with properties similar to the ELRs, and the development of STAR-based films for skin TE. As the genetic engineering process involved in the development of the STAR protein had already been developed and its expression confirmed, an optimized process for producing the protein was developed.

The creation of STAR-based films was a proof of concept of the potential of this protein to be used in the formation of biodegradable films with some properties ideal for Tissue Engineering applications. Since the STAR-based films proved to be fragile when handled, the design of scaffolds with this protein could expand its application in the tissue engineering field. Additional, cell adhesion and proliferation assays should be performed to confirm the potential of STAR-based films for skin tissue engineering applications.

Because of the skin's complex biomechanics, an in-depth study of the rheology of the developed materials is also required. Furthermore, since chronic wounds are commonly caused by prolonged inflammation and/or infection, the films should be modified to include antibacterial, antioxidant, and/or anti-inflammatory properties, as well as growth factors, which have been shown to aid in skin regeneration.

REFERENCES

[1] A. Dehdashtian, T. P. Stringer, A. J. Warren, E. W. Mu, B. Amirlak, and L. Shahabi, "Anatomy and physiology of the skin," *Melanoma A Mod. Multidiscip. Approach*, pp. 15–26, 2018, doi: 10.1007/978-3-319-78310-9_2.

[2] W. Montagna, "Comparative Anatomy and Physiology of the Skin," *Arch. Dermatol.*, vol. 96, no. 4, pp. 357–363, 1967, doi: 10.1001/ARCHDERM.1967.01610040007003.

[3] H. Sorg, D. J. Tilkorn, S. Hager, J. Hauser, and U. Mirastschijski, "Skin Wound Healing: An Update on the Current Knowledge and Concepts," *Eur. Surg. Res.*, vol. 58, no. 1–2, pp. 81–94, 2017, doi: 10.1159/000454919.

[4] A. C. O. Gonzalez, Z. A. Andrade, T. F. Costa, and A. R. A. P. Medrado, "Wound healing – A literature review," *Anais brasileiros de dermatologia*, vol. 91, no. 5, pp. 614-620, 2016, doi: 10.1590/ABD1806-4841.20164741.

[5] P. Beldon, "Basic science of wound healing," *Surgery*, vol. 28, no. 9. pp. 409–412, 2010, doi: 10.1016/J.MPSUR.2010.05.007.

[6] S. Gupta *et al.*, "Chronic wounds: magnitude, socioeconomic burden and consequences Chronic," *Wounds Asia*, vol. 4, no. 1, pp. 8–14, 2021.

[7] B. Blanco-Fernandez, O. Castaño, M. Á. Mateos-Timoneda, E. Engel, and S. Pérez-Amodio, "Nanotechnology Approaches in Chronic Wound Healing," *Adv. Wound Care*, vol. 10, no. 5, pp. 234–256, 2021, doi: 10.1089/WOUND.2019.1094.

[8] P. X. Ma, "Scaffolds for tissue fabrication," *Materials Today*, vol. 7, no. 5. pp. 30–40, 2004, doi: 10.1016/S1369-7021(04)00233-0.

[9] S. K. Min, S. C. Lee, S. D. Hong, C. P. Chung, W. H. Park, and B. M. Min, "The effect of a laminin-5-derived peptide coated onto chitin microfibers on re-epithelialization in early-stage wound healing," *Biomaterials*, vol. 31, no. 17, pp. 4725–4730, 2010, doi: 10.1016/J.BIOMATERIALS.2010.02.045.

[10] A. Pandit, G. Damodaran, R. Collighan, and M. Griffin, "Tethering a laminin peptide to a crosslinked collagen scaffold for biofunctionality," *J. Biomed. Mater. Res. - Part A*, vol. 89, no. 4, pp. 1001–1010, 2009, doi: 10.1002/JBM.A.32045.

[11] X. Tang *et al.*, *Polymeric Biomaterials in Tissue Engineering and Regenerative Medicine*. Elsevier Inc., 2014.

[12] M. M. Farajollahi, S. Hamzehlou, A. Mehdipour, and A. Samadikuchaksaraei, "Recombinant proteins: Hopes for tissue engineering," *BioImpacts*, vol. 2, no. 3. pp. 123–125, 2012, doi: 10.5681/BI.2012.010.

[13] K. A. X. Furtado, P. Infante, A. Sobral, P. Gaspar, G. Eliseu, and M. Lopes, "Prevalence of acute and chronic wounds – with emphasis on pressure ulcers – in integrated continuing care units in Alentejo, Portugal," *Int. Wound J.*, vol. 17, no. 4, pp. 1002–1010, 2020, doi: 10.1111/IWJ.13364.

[14] M. C. F. Simões, J. J. S. Sousa, and A. A. C. C. Pais, "Skin cancer and new treatment perspectives: A review", *Cancer Letters*, vol. 357, no. 1, pp. 8–42, 2015, doi: 10.1016/J.CANLET.2014.11.001.

[15] J. R. Yu *et al.*, "Current and Future Perspectives on Skin Tissue Engineering: Key Features of Biomedical Research, Translational Assessment, and Clinical Application," *Adv. Healthc. Mater.*, vol. 8, no. 5, 2019, doi: 10.1002/ADHM.201801471.

[16] J. Koller, "Effects of radiation on the integrity and functionality of amnion and skin grafts, in *Sterilisation of Tissues Using Ionising Radiations* in *Biomaterials*, J. F. Kennedy, G. O. Phillips, P. A. Williams, Eds. Woodhead Publishing, 2005, pp. 197-220, doi: 10.1533/9781845690779.3.197.

[17] H. Shahin, M. Elmasry, I. Steinvall, F. Söberg, and A. El-Serafi, "Vascularization is the next challenge for skin tissue engineering as a solution for burn management," *Burn. Trauma*, vol. 8, 2020, doi: 10.1093/BURNST/TKAA022.

[18] R. F. Pereira and P. J. Bártolo, "Traditional Therapies for Skin Wound Healing," *Adv. Wound Care*, vol. 5, no. 5, pp. 208–229, 2016, doi: 10.1089/WOUND.2013.0506.

[19] R. Wang, Y. Peng, Y. Jiang, and J. Gu, "Managing chronic wounds during novel coronavirus pneumonia outbreak", *Burns & trauma,* vol. 8. 2020, doi: 10.1093/BURNST/TKAA016.

[20] J. Ho, C. Walsh, D. Yue, A. Dardik, and U. Cheema, "Current Advancements and Strategies in Tissue Engineering for Wound Healing: A Comprehensive Review," *Advances in Wound Care*, vol. 6, no. 6, pp. 191–209, 2017, doi: 10.1089/WOUND.2016.0723.

[21] J. C. Rodríguez-Cabello, I. G. De Torre, S. Acosta, S. Salinas, and M. Herrero, *Elastin-like proteins: Molecular design for self-assembling*. Elsevier Ltd., 2018.

[22] A. Girotti, A. Fernández-Colino, I. M. López, J. C. Rodríguez-Cabello, and F. J. Arias, "Elastin-like recombinamers: Biosynthetic strategies and biotechnological applications," *Biotechnol. J.*, vol. 6, no. 10, pp. 1174–1186, 2011, doi: 10.1002/BIOT.201100116.

[23] "*Values"*, Technical Proteins Nanobiotechnology, 2021. Accessed on: November 13, 2021. [Online]. Available: https://www.tpnbt.com/values/#.

[24] "*About"*, Centre of Biological Engineering, 2021. Accessed on: November 13, 2021. [Online]. Available: https://www.ceb.uminho.pt/About.

[25] "*About"*, Bioprocess and Bionanotechnology Research Group, 2021. Accessed on: November 13, 2021. [Online]. Available: https://www.ceb.uminho.pt/bbrg/About.

[26] M. Venus, J. Waterman, and I. McNab, "Basic physiology of the skin," *Surgery*, vol. 28, no. 10, pp. 469–472, 2010, doi: 10.1016/J.MPSUR.2010.07.011.

[27] S. Lawton, "Skin 1: the structure and functions of the skin," *Nursing Times* [online], vol. 115, no. 12, p. 30-33, 2019.

[28] S. Kusuma, R. K. Vuthoori, M. Piliang, and J. E. Zin, "Skin Anatomy and Physiology" in *Plastic and Reconstructive Surgery*, M. Z. Siemionow, M. Eisenmann-Klein, Eds. Springer, 2010, pp. 161-171, doi:10.1007/978-1-84882-513-0.

[29] "*Skin*", Cleveland Clinic, October 13, 2021. Accessed on: December 29, 2021. [Online]. Available: https://my.clevelandclinic.org/health/articles/10978-skin.

[30] E. McLafferty, C. Hendry, and F. Alistair, "The integumentary system: anatomy, physiology and function of skin.," *Nurs. Stand.*, vol. 27, no. 3, pp. 35–42, 2012, doi: 10.7748/ns2012.09.27.3.35.c9299.

[31] P. Agache, T. Lihoreau, S. Mac-mary, and P. Humbert, Measuring the Skin. 2016.

[32] J.S. Barbieri, K. Wanat, J. Seykora, "Skin: Basic Structure and Function" in *Pathobiology of Human Disease*, L. M. McManus, R. N. Mitchell, Eds. Academic Press, 2014, pp. 1134-1144, doi: 10.1016/B978-0-12-386456-7.03501-2.

[33] H. Yousef, M. Alhajj, and S. Sharma, "Anatomy, Skin (Integument), Epidermis" in StatPearls [Internet]. Treasure Island (FL): StatPearls Publishing, 2021 Jan-. Available: https://www.ncbi.nlm.nih.gov/books/NBK470464/.

[34] "*Epidermis*", istockphoto, June 8, 2019. Acessed on: January 2, 2022. [Online]. Available: https://www.istockphoto.com/es/vector/capas-de-epidermis-c%C3%A9lulas-epiteliales-gm1154464788-313960624.

[35] J.A. McGrath, and J. Uitto, "Structure and Function of the Skin" in *Rook's Textbook of Dermatology*, Ninth Edition, J. Barker, T. Bleiker, R. Chalmers and D. Creamer, Eds. C.E.M. Griffiths, 2016 pp. 1-34, doi: 10.1002/9781118441213.rtd0002.

[36] B.Brodsky, and A.V. Persikov, "Molecular structure of the collagen triple helix", *Advances in protein chemistry*, vol. 70, pp. 301-339, 2005, doi: 10.1016/S0065-3233(05)70009-7.

[37] D. J.S. Hulmes, "Building Collagen Molecules, Fibrils, and Suprafibrillar Structures," *Journal of Structural Biology*, vol.137, no.1-2, pp. 2-10, 2002, doi: 10.1006/jsbi.2002.4450.

[38] S. M. Mithieux, and A. S. Weiss, "Elastin," *Advances in protein chemistry*, vol. 70, pp. 437–461, 2005, doi:10.1016/S0065-3233(05)70013-9.

[39] "*Skin structure diagram vectors material 01*", freedesignfile, 2022. Acessed on: January 5, 2022. [Online]. Available: https://freedesignfile.com/151805-skin-structure-diagram-vectors-material-01/.

[40] S. G. Wise, *et al.*, "Tropoelastin: a versatile, bioactive assembly module," *Acta biomaterialia*, vol. 10, no. 4, pp. 1532–1541, 2014, doi:10.1016/j.actbio.2013.08.003.

[41] D. V. Bax, U. R. Rodgers, M. M. Bilek, and A. S. Weiss, "Cell adhesion to tropoelastin is mediated via the C-terminal GRKRK motif and integrin alphaVbeta3", *The Journal of biological chemistry*, vol. 284, no.42, pp. 28616–28623, 2009, doi: 10.1074/jbc.M109.017525.

[42] S. Rauscher, S. Baud, M. Miao, F. W. Keeley, an R. Pomès, "Proline and glycine control protein self-organization into elastomeric or amyloid fibrils," *Structure (London, England : 1993)*, vol. 14, no.11, pp. 1667–1676, 2006, doi: 10.1016/j.str.2006.09.008.

[43] A. Ibáñez-Fonseca, T. Flora, S. Acosta, and J. C. Rodríguez-Cabello, "Trends in the design and use of elastin-like recombinamers as biomaterials," *Matrix biology : journal of the International Society for Matrix Biology*, vol. 84, pp. 111–126, 2019, doi: 10.1016/j.matbio.2019.07.003.

[44] J. E. Wagenseil, and R. P. Mecham, "New insights into elastic fiber assembly," *Birth defects research. Part C, Embryo today : reviews*, vol. 81, no.4, pp. 229–240, 2007, doi: 10.1002/bdrc.20111.

[45] S. Rauscher, and R. Pomès, "Structural disorder and protein elasticity," *Advances in experimental medicine and biology*, vol. 725, pp. 159–183, 2012, doi: 10.1007/978-1-4614-0659-4_10.

[46] J. H.Miner, and P. D. Yurchenco, "Laminin functions in tissue morphogenesis," *Annual review of cell and developmental biology*, vol. 20, pp. 255–284, 2004, doi: 10.1146/annurev.cellbio.20.010403.094555.

[47] A.M. Mercurio, and L.M. Shaw, "Laminin binding proteins," *Bioessays*, vol. 13, pp. 469-473, 1991, doi:10.1002/bies.950130907.

[48] T. Nishiyama, S. Amano, M. Tsunenaga, K. Kadoya, A. Takeda, E. Adachi, and R. E. Burgeson, "The importance of laminin 5 in the dermo-epidermal basement membrane,"

Journal of dermatological science, vol.24, no. 1, S51–S59, 2000, doi: 10.1016/s0923-1811(00)00142-0.

[49] L.A. Davidson, R. Keller, and D.W. DeSimone, "Assembly and remodeling of the fibrillar fibronectin extracellular matrix during gastrulation and neurulation in Xenopus laevis," *Developmental dynamics: an official publication of the American Association of Anatomists*, vol. 231, no.4, pp. 888-895, 2004.

[50] M.Larsen, C. Wei, and K.M. Yamada, "Cell and fibronectin dynamics during branching morphogenesis," *Journal of cell science*, vol.119, no.16, pp. 3376-3384, 2006.

[51] J.Qin, O. Vinogradova, and E. F. Plow, "Integrin bidirectional signaling: a molecular view," *PLoS biology*, vol. 2, no.6, e169, 2004, doi: 10.1371/journal.pbio.0020169.

[52] J.E. Schwarzbauer, and D.W. DeSimone, "Fibronectins, their fibrillogenesis, and in vivo functions," *Cold Spring Harbor perspectives in biology*, vol. 3, no.7, pp. a005041, 2011.

[53] R.Pankov, and K. M. Yamada, "Fibronectin at a glance," *Journal of cell science*, vol. 115, Pt 20, pp. 3861–3863, 2002, doi: 10.1242/jcs.00059.

[54] "*Integumentary System*", Socratic Q&A, July 21, 2016. Accessed: January 6, 2022. [Online]. Available: https://socratic.org/questions/in-the-skin-what-is-the-function-of-the-papillary-layer.

[55] "*The Immune system and immunity in swine: skin*", pig333, March 29, 2018. Accessed: January 6, 2022. [Online]. Available: https://www.pig333.com/articles/the-immune-system-and-immunity-in-swine-skin_13496/.

[56] "*Subcutaneous layer*", shutterstock, 2022. Accessed: January 6, 2022. [Online]. Available: https://www.shutterstock.com/es/search/subcutaneous+layer.

[57] A. Ní Annaidh, K. Bruyère, M. Destrade, M. D. Gilchrist, and M. Otténio, "Characterization of the anisotropic mechanical properties of excised human skin," *Journal of the Mechanical Behavior of Biomedical Materials*, vol. 5, no. 1. pp. 139–148, 2012, doi: 10.1016/j.jmbbm.2011.08.016.

[58] K. A and L. A, “Mechanical Behaviour of Skin: A Review,” *J. Mater. Sci. Eng.*, vol. 5, no. 4, 2016, doi: 10.4172/2169-0022.1000254.

[59] Dhivya, S., Padma, V. V., & Santhini, E. (2015). Wound dressings - a review. *BioMedicine*, 5(4), 22. https://doi.org/10.7603/s40681-015-0022-9

[60] S. Guo and L. A. DiPietro, “Critical review in oral biology & medicine: Factors affecting wound healing,” *J. Dent. Res.*, vol. 89, no. 3, pp. 219–229, 2010, doi: 10.1177/0022034509359125.

[61] T. Brocke, J. Barr, “The History of Wound Healing,” *Surgical Clinics of North America*, vol. 100, no. 4, pp. 787-806, 2020, doi: 10.1016/j.suc.2020.04.004.

[62] R. D. Forrest, “Early history of wound treatment”, in *Journal of the Royal Society of Medicine,* vol. 75, no. 3, pp. 198–205, 1982.

[63] J. B. Shah, “The history of wound care,” *The journal of the American College of Certified Wound Specialists*, vol. 3, no.3, pp. 65–66, 2011, doi: 10.1016/j.jcws.2012.04.002.

[64] G. Broughton 2nd, J. E. Janis, and C. E. Attinger, “A brief history of wound care,” *Plastic and reconstructive surgery*, vol. 117, 7 Suppl, 6S–11S, 2006, doi: 10.1097/01.prs.0000225429.76355.dd.

[65] Swaim, F. Steven, “Skin Grafts,” *Veterinary Clinics of North America: Small Animal Practice*, vol. 20, no.1, pp. 147–175, 1990, doi:10.1016/S0195-5616(90)50008-X.

[66] R. L. Reis and J. S. Román, Biodegradable in *TISSUE ENGINEERING and REGENERATIVE MEDICINE*, 2005.

[67] Q. Zeng, *et al.*, “Skin Tissue Engineering,” *Comprehensive Biomaterials*, vol. 5, pp. 467-499, 2011, doi: 10.1016/B978-0-08-055294-1.00186-0.

[68] “*Epicel Product - Cea Cultured Epithelial Autograft*”, kindpng, 2022. Accessed: January 6, 2022. [Online]. Available: https://www.kindpng.com/imgv/hwohxwh_epicel-product-cea-cultured-epithelial-autograft-hd-png/.

[69] "*Integra Skin Graft: Uses, Side Effects, Procedure, Results*", very well health, 2022. Accessed: January 6, 2022. [Online]. Available https://www.verywellhealth.com/integra-skin-graft-4796663.

[70] F. Peinemann, and S. Sauerland, "Negative-pressure wound therapy: systematic review of randomized controlled trials," *Deutsches Arzteblatt international,* vol. 108, no. 22, pp. 381–389, 2011, doi: 10.3238/arztebl.2011.0381.

[71] S. P. Zhong, Y. Z. Zhang, and C. T. Lim, "Tissue scaffolds for skin wound healing and dermal reconstruction," *Wiley Interdisciplinary Reviews: Nanomedicine and Nanobiotechnology*, vol. 2, no. 5. pp. 510–525, 2010, doi: 10.1002/WNAN.100.

[72] R. Scott Ward, "Chapter 31 – Burns" in *Physical Rehabilitation*, M. H. Cameron, L. G. Monroe, Eds. W.B. Saunders, 2007, pp. 828-843, doi: 10.1016/B978-072160361-2.50034-X.

[73] B. J. Larson, A. Nauta, K. Kawai, M. T. Longaker, and H. P. Lorenz, "Scarring and scarless wound healing," *Adv. Wound Repair Ther.*, pp. 77–111, 2011, doi: 10.1533/9780857093301.1.77.

[74] P. V. Pham, "Chapter 19 - Medical Biotechnology: Techniques and Applications," in *Omics Technologies and Bio-Engineering*, D. Barh, V. Azevedo, Eds. Academic Press, pp. 449-469, 2018, doi: 10.1016/B978-0-12-804659-3.00019-1.

[75] E. M. Tottoli, R. Dorati, I. Genta, E. Chiesa, S. Pisani, and B. Conti, "Skin wound healing process and new emerging technologies for skin wound care and regeneration," *Pharmaceutics*, vol. 12, no. 8. pp. 1–30, 2020, doi: 10.3390/pharmaceutics12080735.

[76] L. Liverani, V. Guarino, V. L. Carrubba, and Aldo R. Boccaccini, "Porous Biomaterials and Scaffolds for Tissue Engineering," *Encyclopedia of Biomedical Engineering*, R. Narayan, Eds. Elsevier, pp. 188-202, 2019, doi: 10.1016/B978-0-12-801238-3.99872-6.

[77] H. Walles, T. Walles, "2.220 - Extracellular Matrix as Biomimetic Biomaterial: Biological Matrices for Tissue Regeneration," *Comprehensive Biomaterials*, P. Ducheyne, Eds. Elsevier, pp. 361-367, 2011, doi: 10.1016/B978-0-08-055294-1.00077-5.

[78] J. P. Vacanti and C. A. Vacanti, *The History and Scope of Tissue Engineering*, Fourth Edition. Elsevier, 2013.

[79] M. Mabrouk, H. H. Beherei, and D. B. Das, "Recent progress in the fabrication techniques of 3D scaffolds for tissue engineering," *Materials Science and Engineering C*, vol. 110. 2020, doi: 10.1016/j.msec.2020.110716.

[80] A. M. Testera *et al.*, "Biocompatible elastin-like click gels: design, synthesis and characterization," *Journal of Materials Science: Materials in Medicine*, vol. 26, no. 2. 2015, doi: 10.1007/s10856-015-5435-1.

[81] Donaruma, L.G. "Definitions in biomaterials" in *J. Polym. Sci. C Polym. Lett.*, D. F. Williams, Eds. Elsevier, Amsterdam, vol. 72, no.26, pp. 414-414, 1988, doi: 10.1002/pol.1988.140260910.

[82] B. Love, "Chapter 9 - Polymeric Biomaterials," *Biomaterials*, B. Love, Eds. Academic Press, pp. 205-238, 2017, doi:10.1016/B978-0-12-809478-5.00009-2.

[83] A. Shrivastava, "1 - Introduction to Plastics Engineering," In *Plastics Design Library*, A. Shrivastava, Eds. William Andrew Publishing, pp. 1-16, 2018, doi:10.1016/B978-0-323-39500-7.00001-0.

[84] S. Acosta, L. Quintanilla-Sierra, L. Mbundi, V. Reboto, and J. C. Rodríguez-Cabello, "Elastin-Like Recombinamers: Deconstructing and Recapitulating the Functionality of Extracellular Matrix Proteins Using Recombinant Protein Polymers," *Advanced Functional Materials*, 1909050, 2020, doi:10.1002/adfm.201909050.

[85] J. Kaur, and D. P. Reinhardt, "Chapter 3 - Extracellular Matrix (ECM) Molecules," in *Stem Cell Biology and Tissue Engineering in Dental Sciences*, A. Vishwakarma, P. Sharpe, S. Shi, M. Ramalingam, Eds. Academic Press, pp. 25-45, 2015, doi: 10.1016/B978-0-12-397157-9.00003-5.

[86] J. C. Rodríguez-Cabello, F. J. Arias, M. Alonso Rodrigo, A. Girotti, "Elastin-like polypeptides in drug delivery," *Advanced Drug Delivery Reviews*, vol. 97, pp. 85-100, 2016, doi: 10.1016/j.addr.2015.12.007.

[87] S. M. Staubli *et al.*, "Control of angiogenesis and host response by modulating the cell adhesion properties of an Elastin-Like Recombinamer-based hydrogel," *Biomaterials*, vol. 135, pp. 30–41, 2017, doi: 10.1016/j.biomaterials.2017.04.047.

[88] L. Quintanilla-Sierra, C. García-Arévalo, and J.C. Rodriguez-Cabello, "Self-assembly in elastin-like recombinamers: a mechanism to mimic natural complexity," *Materials Today Bio*, vol. 2, pp. 1000072019.

[89] Gray, W. R., Sandberg, L. B., & Foster, J. A. (1973). Molecular model for elastin structure and function. *Nature*, 246(5434), 461–466. https://doi.org/10.1038/246461a0.

[90] Urry, D. W., Cunningham, W. D., & Ohnishi, T. (1974). Studies on the conformation and interactions of elastin. Proton magnetic resonance of the repeating pentapeptide. *Biochemistry*, 13(3), 609–616. https://doi.org/10.1021/bi00700a032.

[91] A. Yeboah, R.I. Cohen, C. Rabolli, M.L. Yarmush, and F. Berthiaume, "Elastin-like polypeptides: A strategic fusion partner for biologics," *Biotechnol. Bioeng.*, vol. 113, pp. 1617-1627, 2016, doi:10.1002/bit.25998.

[92] N. K. Li, F. García Quiroz, C. K. Hall, A. Chilkoti, and Y. G. Yingling, "Molecular description of the LCST behavior of an elastin-like polypeptide," *Biomacromolecules*, vol. 15, no.10, pp. 3522–3530, 2014, doi: 10.1021/bm500658w.

[93] S. Salinas-Fernández, M. Santos, M. Alonso, L. Quintanilla, and J. C. Rodríguez-Cabello, "Genetically engineered elastin-like recombinamers with sequence-based molecular stabilization as advanced bioinks for 3D bioprinting," *Appl. Mater. Today*, vol. 18, p. 100500, 2020, doi: 10.1016/j.apmt.2019.100500.

[94] D.W. Urry T.M. Parker, M.C. Reid, and D.C. Gowda, *Journal of Bioactive and Compatible Polymers*, vol. 6, pp. 263-282, 1991.

[95] J.C. Rodríguez-Cabello, L. Martín, M. Alonso, F.J. Arias, A.M. Testera, "Recombinamers" as advanced materials for the post-oil age, *Polymer*, vol. 50, no. 22, 2009, pp. 5159-5169.

[96] A. Ibáñez-Fonseca, T. Flora, S. Acosta, and J. C. Rodríguez-Cabello, "Trends in the design and use of elastin-like recombinamers as biomaterials," *Matrix Biol.*, vol. 84, pp. 111–126, 2019, doi: 10.1016/j.matbio.2019.07.003.

[97] Huang, W., Rollett, A., & Kaplan, D. L., "Silk-elastin-like protein biomaterials for the controlled delivery of therapeutics," *Expert opinion on drug delivery*, vol. 12, no. 5, pp. 779–791, 2015, https://doi.org/10.1517/17425247.2015.989830.

[98] G. Damodaran, W.H.C. Tiong, R. Collighan, M. Griffin, H. Navsaria, A. Pandit, "In vivo effects of tailored laminin-332a3 conjugated scaffolds enhances wound healing: A histomorphometric analysis," *J Biomed Mater Res Part* A2013:101, pp. 2788–2795, 2013.

[99] Abdalla E., Gaoyan Z., Ameen M., "Scaffold Techniques and Designs in Tissue Engineering Functions and Purposes: A Review", *Advances in Materials Science and Engineering*, vol. 2019, Article ID 3429527, 13 pages, 2019, https://doi.org/10.1155/2019/3429527.

[100] Mbundi, L., & Carlos, J., "Trends in the Development of Tailored Elastin-Like Recombinamer–Based Porous Biomaterials for Soft and Hard Tissue Applications," *Frontiers in Materials*, 2021, https://doi.org/10.3389/fmats.2020.601795.

[101] M. González-Pérez, I. González de Torre, M. Alonso, and J. C. Rodríguez-Cabello, "Controlled Production of Elastin-like Recombinamer Polymer-Based Membranes at a Liquid-Liquid Interface by Click Chemistry," *Biomacromolecules,* vol. 21, no. 10, pp. 4149–4158, 2020, doi: 10.1021/acs.biomac.0c00939.

[102] C. J. Huang, *Advanced surface modification technologies for biosensors*. Elsevier Inc., 2019.

[103] Rosano, G. L., Morales, E. S., & Ceccarelli, E. A., "New tools for recombinant protein production in Escherichia coli: A 5-year update," *Protein science: a publication of the*

Protein Society, vol. 28, no. 8, pp. 1412–1422, 2019, https://doi.org/10.1002/pro.3668.

[104] J. C. Rodríguez-Cabello, A. Girotti, A. Ribeiro, and F. J. Arias, "Synthesis of genetically engineered protein polymers (recombinamers) as an example of advanced self-assembled smart materials," *Methods in molecular biology (Clifton, N.J.)*, vol. 811, pp. 17–38, 2012, doi: 10.1007/978-1-61779-388-2_2.

[105] Meyer, D.E. and A. Chilkoti, "Genetically Encoded Synthesis of Protein-Based Polymers with Precisely Specified Molecular Weight and Sequence by Recursive Directional Ligation: Examples from the Elastin-like Polypeptide System," *Biomacromolecules*, vol. 3, no.2, pp. 357-367, 2002.

[106] U. K. Laemmli, "Cleavage of structural proteins during the assembly of the head of bacteriophage T4", *Nature*, vol. 227, pp. 680-685, 1970.

[107] Wingfield P., "Protein precipitation using ammonium sulfate," *Current protocols in protein science*, Appendix 3, Appendix–3F, 2001, https://doi.org/10.1002/0471140864.psa03fs137.

[108] Meyer, D.E. and A. Chilkoti, "Genetically Encoded Synthesis of Protein-Based Polymers with Precisely Specified Molecular Weight and Sequence by Recursive Directional Ligation: Examples from the Elastin-like Polypeptide System," *Biomacromolecules*, vol. 3, no.2, pp. 357-367, 2002.

[109] Alliegro M. C., "Effects of dithiothreitol on protein activity unrelated to thiol-disulfide exchange: for consideration in the analysis of protein function with Cleland's reagent," *Analytical biochemistry*, vol. 282, no.1, pp. 102–106, 2000, https://doi.org/10.1006/abio.2000.4557.

[110] Kong J., Yu S., "Fourrier transform infrared spectroscopic analysis of protein secondary structures," *Acta Biochim. Biophys.*, Sin. 39, no. 8, pp. 549–559, 2007.

[111] "*MTS Assay Kit (Cell Proliferation) (Colorimetric) (ab197010)*", abcam, 2022. Accessed: June 24, 2022. [Online]. Available: https://www.abcam.com/mts-assay-kit-cell-proliferation-colorimetric-ab197010.html.

[112] Borzacchiello, A., Mayol, L., Ramires, P. A., Pastorello, A., Bartolo, C. D., Ambrosio, L., & Milella, E., "Structural and rheological characterization of hyaluronic acid-based scaffolds for adipose tissue engineering." *Biomaterials*, vol. 28, no. 30, pp. 4399-4408, 2007, https://doi.org/10.1016/j.biomaterials.2007.06.007.

[113] Kasalkova, N. S. , Slepicka, P., & Svorcik, Z. K. a., "Wettability and Other Surface Properties of Modified Polymers," In (Ed.), *Wetting and Wettability*. IntechOpen, 2015, https://doi.org/10.5772/60824.

[114] Ribeiro, A., Volkov, V., Oliveira, M. B., Padrão, J., Mano, J. F., Gomes, A. C., & Cavaco-Paulo, A. (2016). BSA/HSA ratio modulates the properties of Ca2+-induced cold gelation scaffolds. *International Journal of Biological Macromolecules*, 89, 535-544. https://doi.org/10.1016/j.ijbiomac.2016.05.012.

[115] Riveiro, A., Maçon, A. L., del Val, J., Comesaña, R., & Pou, J. (2018). Laser Surface Texturing of Polymers for Biomedical Applications. *Frontiers in Physics*. https://doi.org/10.3389/fphy.2018.00016.

[116] Lingyu Sun, Jiahui Guo, Hanxu Chen, Dagan Zhang, Luoran Shang, Bing Zhang, Yuanjin Zhao, "Tailoring Materials with Specific Wettability in Biomedical Engineering," *Advanced Science*, 2021, doi:10.1002/advs.202100126.

[117] X. Feng, R. Pelton, "Carboxymethyl cellulose: polyvinylamine complex hydrogel swelling," *Macromolecules*, vol. 40, pp. 1624–1630, 2007.

[118] Carotenuto, F., Politi, S., Ul Haq, A., De Matteis, F., Tamburri, E., Terranova, M.L., Teodori, L., Pasquo, A., Di Nardo, P., "From Soft to Hard Biomimetic Materials: Tuning Micro/Nano-Architecture of Scaffolds for Tissue Regeneration," *Micromachines*, vol. 13, no. 780, 2022, https:// doi.org/10.3390/mi13050780.

[119] Vasconcelos, A., Freddi, G., & Cavaco-Paulo, A., "Biodegradable materials based on silk fibroin and keratin," *Biomacromolecules*, vol. 9, no. 4, pp. 1299–1305, 2008, https://doi.org/10.1021/bm7012789.

[120] Tinoco, A., Gonçalves, F., Costa, A. F., Freitas, D. S., Cavaco-Paulo, A., & Ribeiro, A., "Keratin:Zein particles as vehicles for fragrance release on hair," *Industrial Crops and Products*, vol. 159, no. 113067, 2021, https://doi.org/10.1016/j.indcrop.2020.113067.

[121] "*Infrared Spectroscopy Absorption Table*", Chemistry LibreTexts, 2022. Accessed: September 17, 2022. [Online]. Available: https://chem.libretexts.org/Ancillary_Materials/Reference/Reference_Tables/Spectroscopic_Reference_Tables/Infrared_Spectroscopy_Absorption_Table.

[122] A. Barth, C. Zscherp, "What vibrations tell us about proteins," *Q. Rev. Biophys*, vol. 35, no. 4, pp. 369–430, 2002.

[123] Elkhyat, Ahmed, "Skin Wettability and Friction", 2004.

ANNEX I

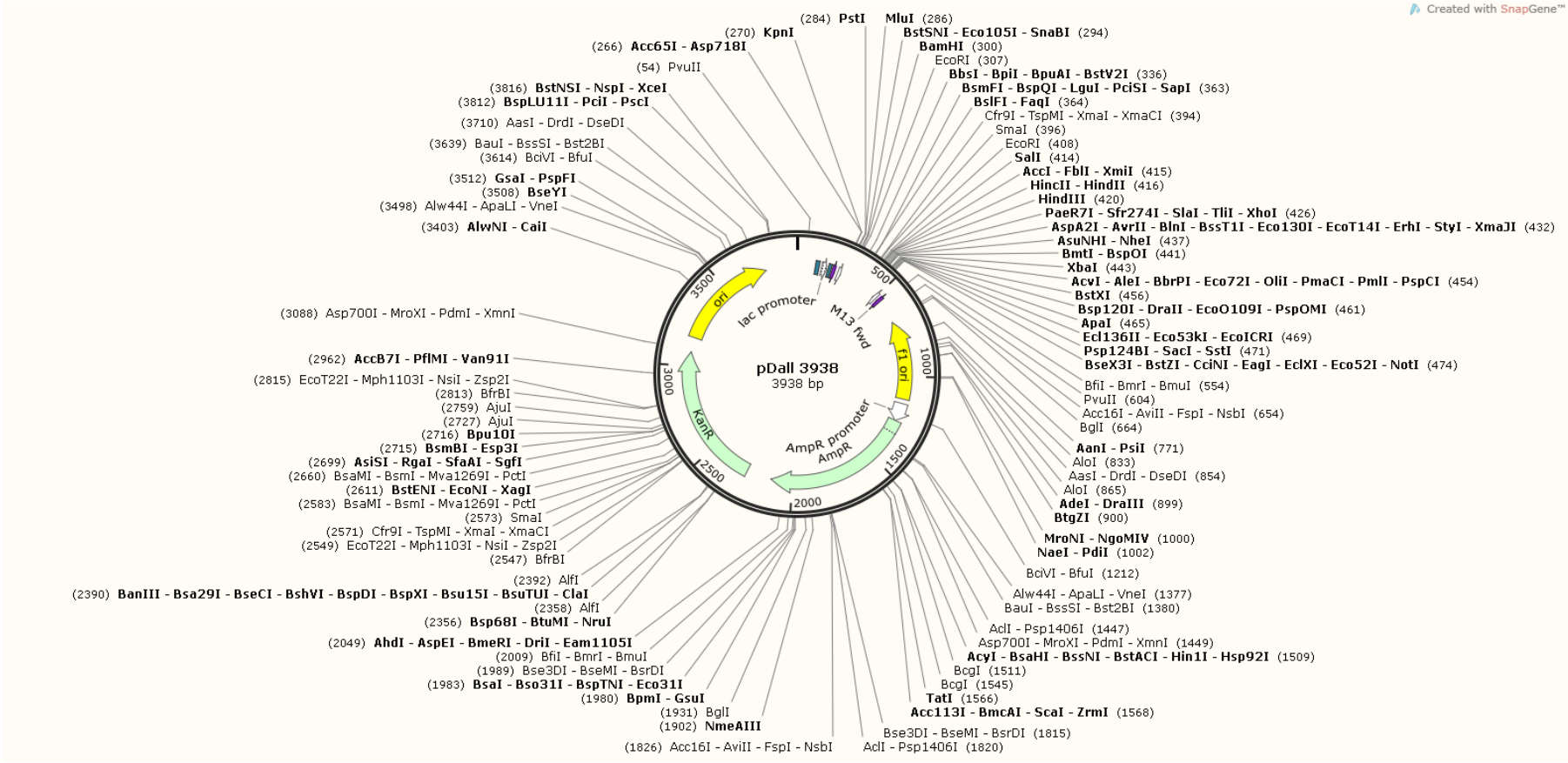

Figure Annex I-1 — Cloning plasmid pDrive All map. Created with SnapGene® software.

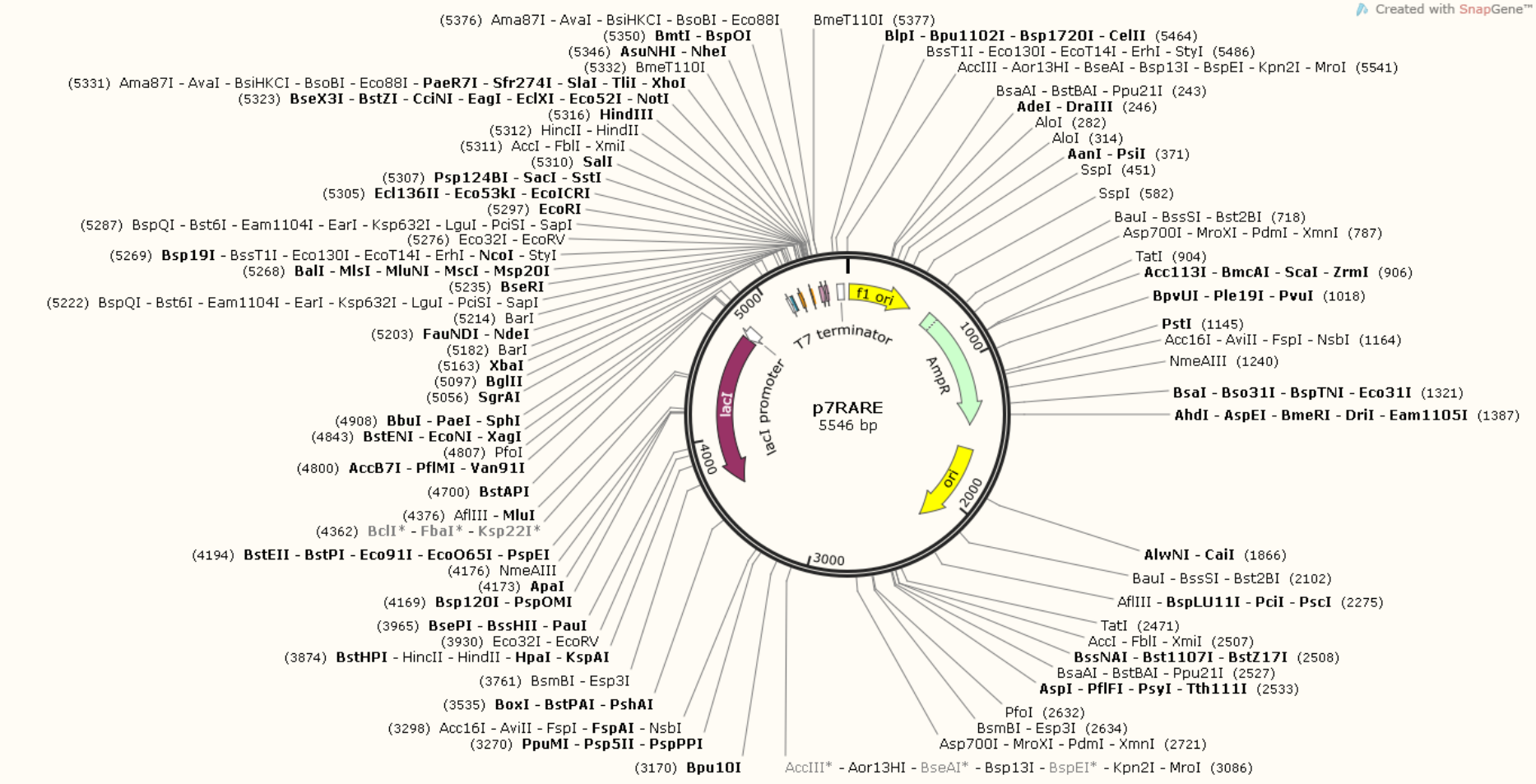

Figure Annex I-2 — Expression plasmid p7RARE map. Created with SnapGene® software.